INTERFEROMETRIC STUDY OF POROUS METAL BEARINGS

by

KWAN – MING YUNG

A thesis submitted for the degree of

DOCTOR OF PHILOSOPHY

of the University of London

and also for the

DIPLOMA OF MEMBERSHIP of the IMPERIAL COLLEGE

MAY 1977

Lubrication Laboratory, Department of Mechanical Engineering,
Imperial College of Science and Technology,
London, SW7 2BX.

ABSTRACT

The mechanism of lubrication of porous metal bearings is investigated by means of optical interferometry. It is found that at the contact surface a dam of oil builds up in front of most of the metal lands and a cavitation zone develops immediately after the lands. This system of 'dam-land-cavity' eventually turns the lands into miniature 'tilting thrust pads'. These are formed by thermoelastic effects and so permit hydrodynamic lubrication films to be established. Based on this model a theoretical relationship linking the oil film thickness with the sliding speed, the load and the land size has been derived and confirmed semi-quantitatively by experiment. The model is further supported by the discovery of wedge-shaped sulphur layers deposited on the rear part of each land. The sulphur being provided by the additives in the lubricant.

The recirculation of the oil in the porous matrix is also studied. Several observations indicate that there are three ways by which the oil can arrive at the working surface: wettability (or capillarity), pumping and suction. When the system is starved of oil, however, only the first continues to function.

Additional experiments are performed to illustrate the effect of the presence of graphite particles in the metal matrix, of the influence of sulphur films, as well as of wear and metal smearing both during the running-in period and at the on-set of bearing failure.

ACKNOWLEDGEMENTS

I would like to express my sincere thanks to the following:

Professor A. Cameron for his kind supervision and encouragement during the course of this research.

Mr. V.T. Morgan of GKN Bound Brook Ltd. for his continuous support and supply for the test samples.

Mr. R. Dobson for his valuable aid in the Laboratory.

Mr. J. Sherwood for passing on his knowledge.

Professor W.T. Welford of Applied Optics Section of Physics Department for his permission to use their facilities.

Mr. P.L. Bird and Mr. P.R. Monk of Analytical Service of Metallurgy Department for their assistance in using the Electron Probe Microanalyser.

Mr. R. Woodward of GKN Bound Brook Ltd. for performing the running-in test of the bearings in Chapter 4.2.

Mr. L.T. Tam for drawing some of the figures.

GKN Powder Met. Ltd., for their financial support of the project and for a research grant enabling me to carry out the work.

CONTENTS

LIST OF FIGURES

Page

NOMENCLATURE

b	length of load carrying zone, direction of motion
B	land length, direction of motion
c	radial clearance in journal bearing
C	reducing factor
D	bore diameter of journal bearing
e	eccentricity
f	porosity
h	oil film thickness
h_0	exit oil film thickness
h_1	inlet oil film thickness
H	wall thickness of bearing
I	Intensity of light
K_p	tilting factor = $\frac{h_1 - h_0}{h_0}$
ℓ	width of load carrying zone at right angles to motion
L	land width at right angles to motion
L	width of journal bearing
m	order of interference
M	number of lands along the running direction
n	refractive index
N	number of lands traverse the running direction
PV	pressure (lb/in^2) x velocity (ft/min)
P	pressure
Q	oil flow per unit volume through the porous matrix
R_1	bearing radius
R_2	shaft radius

S side leakage factor

t time

U surface velocity in x direction

V visibility of fringes

W load

α separation of lands at right angles to motion

β separation of lands, direction of motion

γ complex degree of coherence

δ phase change on reflection

$\frac{1}{\Delta}$ Sommerfeld reciprocal for journal bearing

$$= \frac{U\eta}{W/L} \times \frac{R^2}{c^2}$$

ε eccentricity ratio $= \frac{e}{c}$

η absolute viscosity

Θ angular coordinate from max. film thickness

λ wavelength of light

$\Delta\lambda$ width of spectrum

ρ density

σ surface tension

Φ permeability

Ψ permeability parameter $= \frac{H\Phi}{c^3}$

CHAPTER ONE

INTRODUCTION AND SURVEY

1.1. Introduction

One of the practical problems in bearing design is the supply of a sufficient amount of lubricant to the assembly in order to maintain its satisfactory operation. Where a continuous supply is not required for cooling purposes, the usual solution is to add a prescribed quantity of oil to the bearing, or to employ automatic oil supply units. These arrangements are not always convenient from both economical and practical considerations. An alternative way of solving the oil supply problem is to use porous metal as the bearing material, so that the oil stored within the porous matrix can provide adequate lubrication for the entire bearing life. The behaviour of this type of bearing has been widely studied, but most of the previous work has concentrated on the theoretical analysis. Very little experimental work has been done to validate the proposed theories. Above all, the analysis is found to use assumptions which are completely unreal in many practical cases. The work presented in this thesis is designed to discover the actual lubrication mechanism by which porous bearings operate. This is done by direct observation using optical interferometry. The thesis is laid out as follows.

Some basic properties of the bearing and a literature survey of previous papers are discussed in Chapter 1. Chapter 2 deals with the instrumentation of the experiments, whilst Chapter 3 explains the principle of optical interferometry. The other chapters describe the results. Numerous new observations were found in the work, most of them had not been mentioned before. Fortunately, they can be satisfactorily interpretted and explained with the classical lubrication theories which have already been developed. When these phenomena are pieced together the lubrication mechanism of porous metal bearings becomes clear. Owing to the large number of phenomena involved, the presentation is arranged in a special way, in which each phenomenon, its corresponding discussion and conclusions are treated separately. The final discussion and conclusions are given in Chapter 8.

1.2. General Properties

Porous bearings first appeared at the beginning of this century. In 1909 the use of porous metallo-ceramic products for filters and bearings was suggested. However, it was not until 1924[1] that porous bronze bearings began to be used on a commercial scale, and porous iron bearings appeared later in about 1935. One special feature of porous metal bearings is their ability for self-lubrication. At installation the bearing is endowed with a certain amount of oil which is stored within the porous matrix, and this quantity of oil can be sufficient

to serve the bearing throughout its entire life. In general porous metal bearings are used in the form of journal and thrust washers, but there are also many other shapes such as ball seats, plugs, closed-end bearings, etc., which can be made.

1.2.1. Powder Metallurgy

Porous metal bearings are produced by the powder metallurgy technique. The procedures for which are discussed briefly as follows:-

First, fine metal powder of either copper (50 to 150 microns diameter) and tin (10 to 50 microns), or of iron (50 to 150 microns) in appropriate proportions are mixed together in a cone mixer for ½ to 2 hours. A small quantity of solid lubricants such as graphite is usually added. The cold working action associated with this mixing process may also be used to control the bulk density of the powder mix to a particular figure. Secondly, this evenly mixed powder is compressed in precision tools to produce a compact of the required shape, using a pressure of between 10 and 35 tons per square inch. This compacting process increases the strength and the contact area between the metal particles, as it decreases the porosity of the powder body. Thirdly, the compressed powder bodies are sintered in a reducing atmosphere to a temperature which is about 80% of the absolute melting point of the metal. In this way the metal particles are welded together to produce a strong, coherent yet porous body. Fourthly,

the sintered parts are re-pressed in precision tools, to correct for distortion and any slight change of dimensions produced during the sintering operation. At this stage the bearing is composed of myriads of interconnecting channels and reservoirs, just like a sponge made from metal. Finally, the bearings undergo a vacuum impregnation process in which more than 90% of the voids and pores are filled with oil.

1.2.2. Porous Bronze Bearings

Porous Bronze is the most popular type of porous metal bearings. It consists of 90% of copper and 10% of tin and usually has about 1% of added graphite. Tin has a low atomic affinity for iron[2] and its presence reduces the tendancy for weld formation between the bearing surface and the iron based shaft. It also increases the tendency of the bearing surface to absorb polar compounds from the oil. Furthermore it strengthens and increases the hardness of the copper, thereby reducing the wear rate under unlubricated conditions. The addition of graphite assists lubrication during the compacting and recompacting procedures. It tends to reduce bearing noise, and to prevent seizure in start-stop conditions of service, when direct metal contact is difficult to avoid. In some cases about 50% or more of the copper and tin is replaced by iron powder, to reduce cost and to increase maximum load carrying capacity. Iron powder is cheaper to produce and has a thermal conductivity which is higher than bronze, about

1.5 times. However, iron has poor corrosion resistance so that the application of porous iron bearing is limited to specific cases.

1.2.3. Advantages and Disadvantages

Conventional sleeve bearings usually require oil grooves and oil supply pipe lines for their satisfactory operation. In contrast, porous metal bearings do not need grooves or an external supply of lubricant. They are therefore most applicable in inaccessible positions or where the bearing housing also moves. They are also suitable for rotating loads since all the circumference of the bearing is the same with respect to the loading direction. However, the presence of the porosity reduces the compressive strength in comparison with that of solid metal bearings. Thus under static or impact loads the running clearance would be increased if the yield point of the porous metal was exceeded. For example, the static load for a standard porous bronze bearing with a porosity of 30% should not exceed 7,000 lb/in^2 of projected area. Porosity also causes a decrease in the thermal conductivity and can result in a higher running temperature. Another limitation of porous metal bearings is that their size, shape and composition is restricted to those which can be produced by the powder metallurgy techniques, e.g., the shape should have axial symmetry and the size should not be much smaller than 1/16" or much larger than 3".

1.2.4. Porosity

Porosity is a measure of the quantity of voidage in the porous material, and is defined as $f=1-\frac{\rho}{\rho_0}$ where ρ is the density of the porous metal and ρ_0 is the density of the non-porous metal. This value is controlled by the degree of compaction during manufacture. For most porous metal bearings the value of 'f' ranges from 20% to 40%, with a corresponding tensile strength of about $\frac{1}{2}$ to $\frac{1}{4}$ of solid metal respectively. This reduction of strength is due to the loss of metal and to the high local stress which is concentrated at the welds between particles. Porosity plays an important role in the lubrication of porous bearings. It acts as the oil reservoirs which store almost all of the oil for the entire service life of the bearing. Normally, the size of the porosity, which depends upon the fineness of the metal powders, ranges from one micron to 30 microns in diameter. A given porosity can therefore have either a large number of small pores or a smaller number of larger pores. Higher capillary force and a larger resistance to fluid flow, will in principle be obtained by smaller pores. However, this is limted in practice by a greater probability of pore closure by smearing of the surface porosity by the action of the shaft when operating under boundary lubricate conditions. In short, low porosity is accompanied by high mechanical properties, high thermal conductivity, but low oil holding capacity, and vice versa. Therefore, the choice of porosity is a compromise between these conflicting characteristics.

1.2.5. Permeability

When a pressure gradient is applied across a porous material, with the assumption that the flow is fully viscous or lamina and the inertia effect of the oil is negligible, the flow of fluid through the porous matrix obeys Darcy's law, which states:

$$Q = -\frac{\Phi}{\eta} \nabla P$$

where Q is the flow rate through the matrix and Φ is defined as the permeability of the porous material. The value of Φ depends on the quantity of porosity, pore size, pore shape, pore tortuosity, etc., but is independent of both the quantity of porous material and the nature of the permeating fluid. Permeability has the dimensions of length^2 and is conveniently expressed in the darcy unit which has the value of 10^{-8}cm^2 or the square micron. Typical porous bearings have a permeability ranging from 0.01 to 0.2 darcys[3].

1.2.6. PV Factor

The allowable duty of porous metal bearings is often expressed for industrial purposes in terms of a 'PV' factor, where 'P' is the bearing pressure in pounds per square inch, based on the projected area of the bearing, and 'V' is the surface velocity of the journal, in feet per minute. Typically porous bronze bearings operate at PV factors between 5,000 and 50,000 psi x ft/min. This factor, multiplied by the coefficient of friction, represents

the rate of heat generation per unit of projected area.

A too high PV value may have a catastrophic effect on the bearing. The reason for this is three fold. First the coefficient of friction in porous bearing is generally high (=0.05 to 0.15). Secondly, the oil does not participate actively in the dissipation of heat away from the bearing surface because no external oil supply is available. Thirdly, porous bearings tend to be fitted with smaller running clearances than non-porous bearings, which helps to minimize the out of balance forces caused by centrifugal loading especially with high speed shafts. Consequently a very high PV value will produce a high running temperature and this can easily cause, by differential thermal expansion, a serious reduction in the running clearance leading to failure. Whether the failure is caused by wear or by seizure depends upon the torque of the power source turning the shaft.

1.2.7. Oil

With proper design, the life of a porous bearing depends entirely upon the life of the oil (in terms of quantity and quality), which in turn dependsupon its chemistry and upon the running temperature. Thus oils with a high oxidation resistance and a low boundary friction will have longer life[4]. Further, the oxidation life of oils generally vary as the antilogarithm of the temperature, e.g. an increase of $10^{o}C$ will approximately reduce the life by half. Another factor governing the bearing's life is the rate of oil loss. The oil is held

in the porosity by capillary forces. Therefore the larger the quantity of oil in the pores the smaller is its capability to re-absorb. The hydrodynamic pressure and the centrifugal action generated by the motion of the shaft have a tendency to draw oil away from the porous bearing. The greater the quantity of oil which is lost from the bearing the greater will be its power of reabsorption. As a result an equilibrium balance of the oil quantity tends to be established. The oil loss rate is thus an exponential function with time. It is found in practice that a porous bearing tends to fail when the oil content drops to below 50% of saturation. There are several ways to increase the storage of oil in the bearing system. The first one is to increase the porosity, but this would be at the expense of reducing the mechanical strength and the static load carrying capacity. The second is to increase the wall thickness of the bearing or to use wool felt or other porous material in contact with the porous metal as a supplementary supply of lubricant.

1.3. Hydrodynamic Lubrication

Whenever two dry surfaces slide upon each other, there is friction. According to the Bowden-Tabor hypothesis[5] the force normal to the metallic surfaces causes plastic deformation of the contact region so that surface films, such as the oxide layer, are broken and result in cold welding. As the surfaces move relatively, the welding is broken. The damage so caused is the wear and the force

required to break the welding is the friction. However, if a viscous fluid exists in the gap between the surfaces, and if the gap is converging in the direction of motion, a hydrodynamic pressure will be generated to separate the surfaces from direct metal to metal contact. The force required to shear the viscous fluid is far less than that for the metallic welding. This is the basic principle of hydrodynamic lubrication. The equation governing its behaviours is called Reynolds Equation, after Osborne Reynolds who derived it in 1886[6]. This equation relates the distribution of hydrodynamic pressure with the thickness of the film "h", the viscosity of the fluid "η" and the velocity of the motion "U". By solving the equation with appropriate boundary conditions, the load capacity and the friction of different contact geometries can be obtained.

1.3.1. Non-porous Journal Bearings

A journal bearing is a device which can support the load of a shaft while the shaft remains rotating freely. It has the form of a hollow cylinder whose bore diameter is slightly larger than that of the shaft. The satisfactory operation of journal bearings depends on the generation of a hydrodynamic pressure when the viscous fluid adhering to the rotating shaft is drawn into the converging clearance. This converging gap is formed by the eccentricity of the two cylindrical surfaces during running. A schematic diagram of the contact geometry is

shown in Fig. 1.1. The oil film thickness can be expressed in terms of the radial clearance "c", the eccentricity ratio "ε", and the angular co-ordinate "θ".

That is: $h = c(1 + \varepsilon \cos \theta)$ ..... (1.1)

Substituting this relationship into Reynolds equation, the load capacity and the coefficient of friction can be obtained by solving the equation with suitable boundary conditions. This analysis produces a basic design parameter $\frac{1}{\Delta}$, called Sommerfeld Reciprocal, which is expressed as

$$\frac{1}{\Delta} = \frac{U\eta}{W/L} \cdot \frac{R^2}{c^2} \qquad \text{..... (1.2)}$$

Where R is the reduced radius of the bearing.

and W/L is the load per unit width. This parameter is a function of the eccentricity ratio, and the value of which indicates the operation situation of the journal bearing. The distribution of hydrodynamic pressure in the bearing is shown in Fig. 1.2. The relevant experimental and theoretical work have been well developed in the last century by Reynolds[6], Tower[7] and Sommerfeld[8].

In more recent times efforts have been made by several authors, such as Christopherson[9], Cameron and Wood[10], to refine the solution in simpler and more convenient ways. It should be noted that in normal conditions there is an external supply of oil being fed constantly into the bearing clearance through an oil pocket or groove located in the unloaded part.

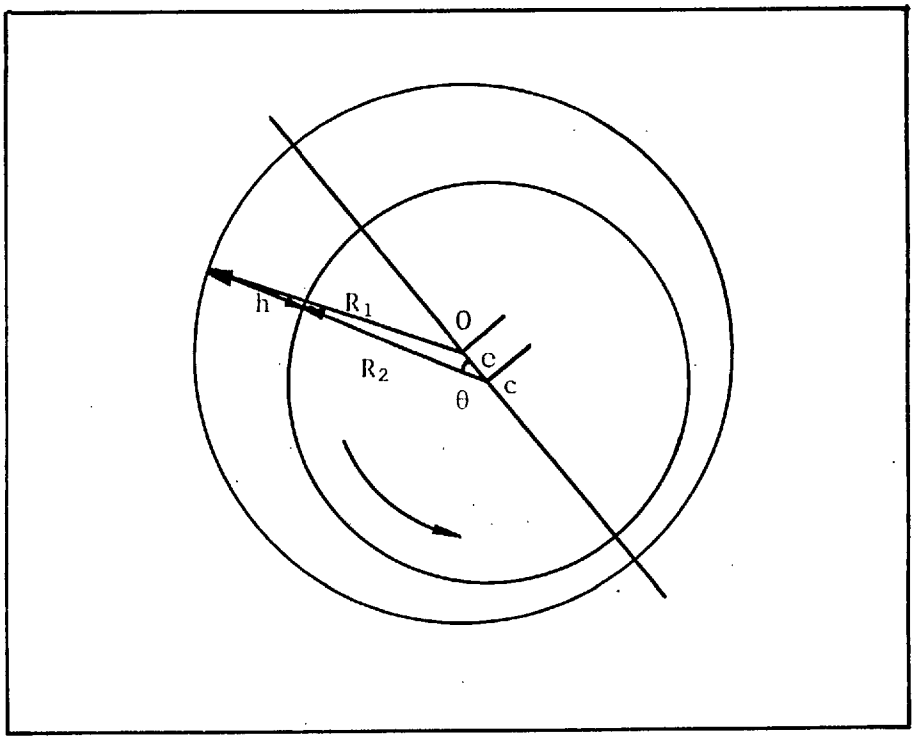

Fig. 1.1 Journal bearing geometry.

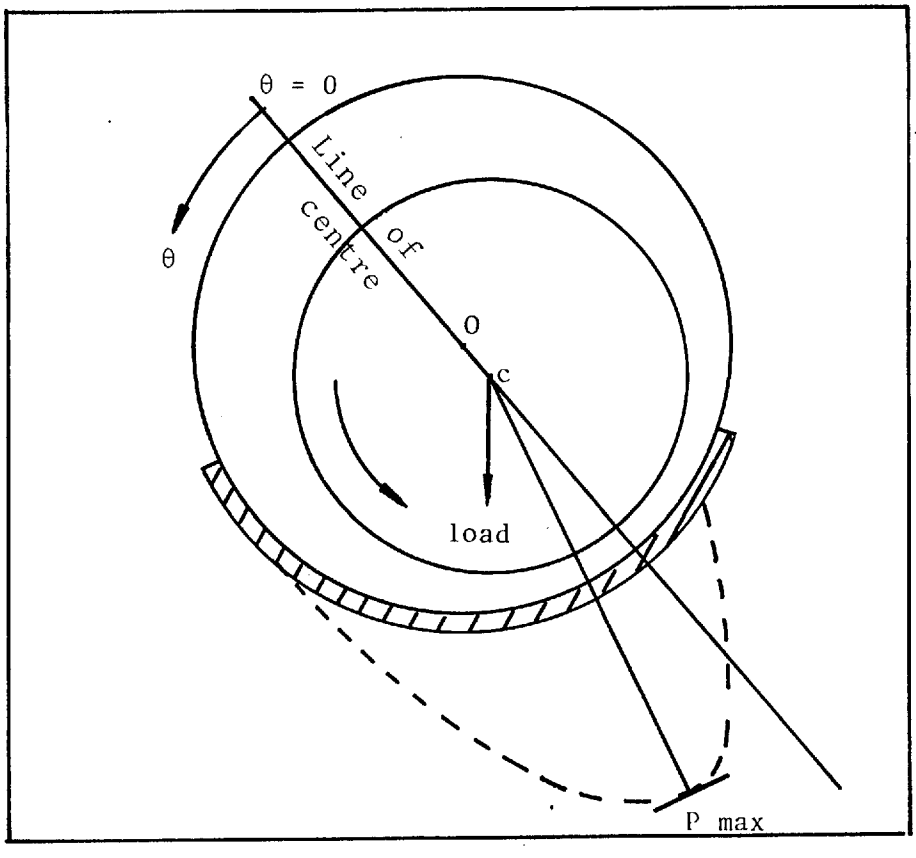

Fig. 1.2. Pressure distribution for journal bearing.

1.3.2. Porous Journal Bearings

The extension of the classical theory to porous bearings was first made by Morgan and Cameron[11] in 1957, more than three decades after the appearance of this form of bearings in a commercial scale. They modified Reynolds' equation by taking into account the entry of lubricant into the bearing material from the gap between the bearing and the journal. In their analysis the pressure of the oil in the film region is governed by Reynolds' equation, whilst that in the porous matrix is governed by the Laplace equation,

$$\nabla^2 P = 0 \qquad \ldots\ldots\ldots\ldots\ldots\ldots \quad (1.3)$$

The latter one is required by the property of continuity of flow. With the help of Darcy's law, which described the flow of fluid in the porous matrix, they obtained an analytical solution by solving the equations simultaneously, while maintaining the continuity of pressure and the normal component of fluid velocity at the film-porous matrix interface. The solution is an approximate one because they have assumed the bearing to be short. Using this assumption leads to the pressure gradient in the matrix varying linearly with distance from the outer boundary of the bearing, where the pressure is set to zero. The short bearing assumption is originated from Ocvick and Dubois[12]. It postulates that the pressure gradient in the circumferential direction is considerably less than the pressure gradient in the length direction. With this assumption the problem is greatly simplified. Morgan and Cameron introduced a non-dimensional

variable Ψ, called the permeability parameter, which described nearly all the behaviour of the bearing's performance, such as coefficient of friction, pressure distribution and load capacity. Ψ is defined as $\Psi = \frac{\Phi H}{C^3}$ where H is the thickness of the bearing wall. This value usually falls between 10^{-3} and 1.0 in practice. When $\Psi < 10^{-3}$ the porous bearing's performance approaches that of a solid bearing in the usual range of Sommerfeld Reciprocal. It was found, as might be expected, that the load capacity decreased and the coefficient of friction increased with increasing values of Ψ. A lower permeability parameter, if achieved by a lower porosity, would mean less ability for self lubrication because of the smaller oil content. The derivation of the theory is given in Appendix I.

Later, Cameron, Morgan and Stainsby[13] evaluated the theory by computation and verified the predicted performance by experiment. They showed that the bearing would operate in the hydrodynamic lubrication regime only if the Sommerfeld Reciprocal excessed a critical value, designated as $\frac{1}{\Delta_c}$, below which the hydrodynamic film failed to exist and boundary lubrication occurred,as shown in Fig. 1.3. One special feature they found was that in the absence of a full fluid film, direct metal to metal contact occurs and causes pore closure, due to metal smearing at the bearing surface. Consequently, the permeability is reduced and hence the critical Sommerfeld Reciprocal is also progressively reduced, causing the bearing to shift

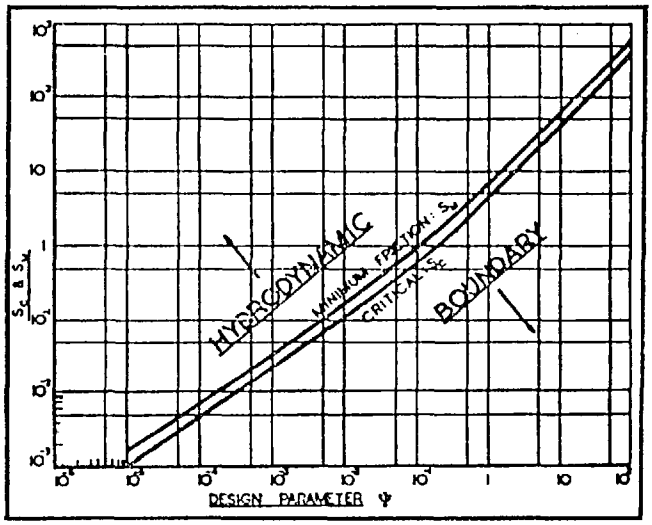

Fig. 1.3. Relation between critical friction and minimum friction conditions for narrow and thin walled porous bearing (after Morgan, Cameron and Stainsby).

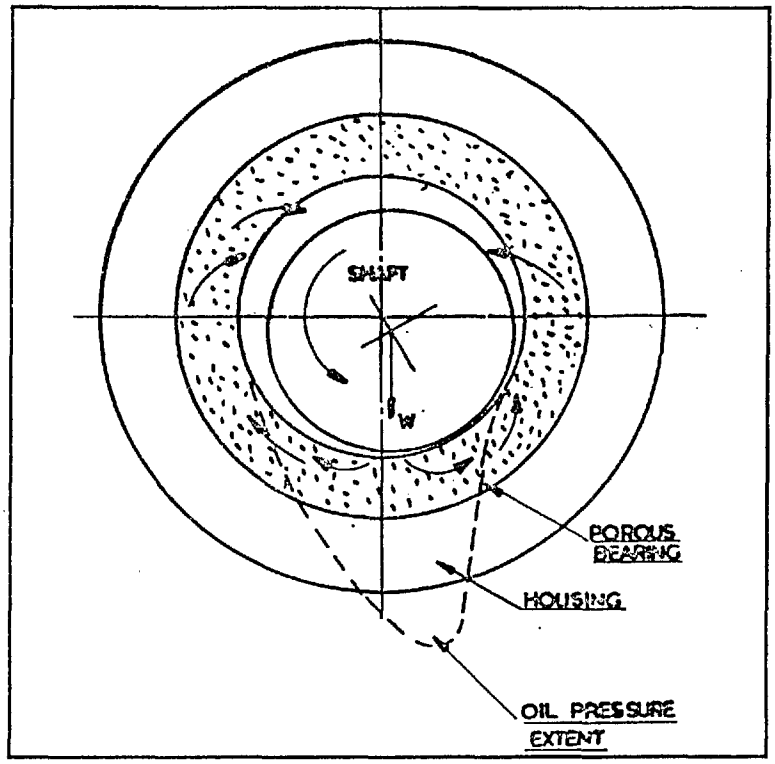

Fig. 1.4. Pressure distribution and circulation of lubricant for a porous bearing (after Morgan).

towards the hydrodynamic regime. Other features they found were that porous bearings operate at a higher eccentricity ratio than a solid bearing, and that in theory porous bearings will have a finite load capacity, e.g. the eccentricity ratio reaches unity at a finite loading defined by the critical Sommerfeld number. This is in contrast with solid bearings which in theory have an infinite load carrying capacity.

Rouleau[14] provided another solution by satisfying an arbitrary boundary condition of zero pressure at the bearing's ends which were exposed to atmosphere. He followed Morgan and Cameron's approach and concluded that, in addition to the permeability parameter, another dimensionless parameter is required to describe the operation of porous bearings. This new parameter is the wall thickness to length ratio H/L, which has a value ranging usually from 0.05 to 0.4 in practice. He found that the load capacity decreased with increasing thickness to length ratio. Rhodes and Rouleau[15] considered the effect of sealing the pores at the ends of the bearing. The idea of the sealing was to prevent the flow of lubricant out into the atmosphere so that a higher pressure is allowed to exist in the bearing matrix. They found that this effect increases the load capacity, with the magnitude of improvement being increased with increasing permeability. Shir and Joseph[16] also improved the earlier solution and presented an analytical solution for the infinitively long bearing. Murti[17] considered the effect of three dimensional flow of lubricant in the

bearing matrix. Carson[18] reviewed the function of all self lubricated bearings.

Morgan[19] gave a comprehensive account of the operation of porous metal bearings and provided guide lines for their successful design and use. In particular he pointed out that the effect of the wall thickness is to control the flow of oil from the pressure wedge to the unloaded side of the bearing. The effectiveness of the control is roughly proportional to the wall thickness when the wall is thin. Therefore, for small value of H/D (say, $H/D < 0.2$), where D is the bore diameter of the bearing, the effect of an increase in the wall thickness is to shift the operation of the bearing away from the hydrodynamic and towards the boundary lubrication regime. This relationship no longer holds when the wall is very thick.

Murti[20] discussed the performance of a narrow bearing with thick wall. He tackled the problem of the wall curvature by using cylindrical co-ordinate to solve the Laplace equation for the pressure of the lubricant on the porous material. However, this is of less practical interest because most porous bearings currently used are thin walled.

Singh[21] considered the stability of a porous bearing with axes skewed, and found that with a slight increase in the skew component, the system became less oscillatory and this improved the load carrying capacity.

Chang-Yi Wang[22] used the Couette flow model to calculate the effect of the porous walls on the heat

generated by viscous dissipation. He showed that when the prandtl number was high there would be a drastic lowering of the maximum temperature due to mass injection through the porous wall. Reason[23] gave a numerical solution for the hydrodynamic lubrication of a finite porous journal bearing. Cusano[24] analysed the finite porous bearing fully charged with oil. Cusano and Phenlan[25] confirmed experimentally that porous bearings operate at a higher eccentricity ratio than solid bearings. They found that the coefficient of friction varied with load and was almost independent of speed for bearings tested under boundary lubrication conditions.

Further analysis of porous metal bearings can be found in Reference 26, 27, 28, 29 and 30.

1.4. Other Aspects of Porous Metal Bearings

There are in fact many parameters involved in the operation of porous bearings. From the above survey we have seen the effects of the permeability, the length to width ratio and the wall thickness on the performance of the bearings. Some other features, concerning the fundamental requirement of fluid mechanics and properties of material, are discussed below.

1.4.1. Slip Flow

So far we have been mainly concerned with the theory which is based on the assumption that no-slip occurs on the film side. According to this assumption, however, the

fluid on travelling from the film into the porous matrix suffers from a discontinuity in the axial and tangential velosity components at the interface. The reason for this is that the velocity of the lubricant is proportional to the pressure gradient on the bearing side, whereas it is dependent on the shaft velocity on the film side. To a first approximation this discontinuity is justified when Darcy's law is applicable, e.g., when the inertia of the oil film is negligible.

Joseph and Tao[31] suggested that it is necessary to improve some requirement on the tangential component of the velocity at the interface. Beaver and Joseph[32] postulated that slip flow took place at the boundary of the permeable material and they verified experimentally that Darcy's law was satisfied in the interior of the permeable material, but not necessarily in the boundary region. They concluded that the effects of viscous shear penetrated into the porous material in the boundary layer region, making the tangential velocity of the fluid at this region much greater than the mean velosity within the porous matrix.

Murti[33] applied this principle to porous bearings. He indicated that the effect of slip is to decrease the resistance of oil flow into the porosity and, as a result the load capacity of the bearing is reduced. This effect is predominant only for low values of permeability, otherwise more fluid flows through the porosity so that the flow of the lubricant in the clearance is not significantly affected and hence the slip flow has less

effect. On the other hand Rouleau and Stainer[34] included the effect of other factors, such as negative pressure and slip flow in the calculation, and came to the conclusion that slip flow had a negligible effect in the usual range of bearing parameters. They also concluded that sealing the axial ends of the bearing had little practical influence in upgrading the load capacity; this is contrary to a conclusion in Rouleau's earlier paper[14] where he found the sealing of bearings' ends improved the load capacity. As will be seen from the results of the present study, his latter conclusion is correct, that sealing the end walls can only prevent the oil in the porous matrix from lossing, but has little effect on the load carrying ability.

1.4.2. Squeeze Film

A 'squeeze film' occurs when there is an unsteady or fluctuating load. With a solid bearing the rotating journal can in theory never touch the bearing surface due to the hydrodynamic pressure, whereas with a porous bearing this contact could occur since there is bleeding of lubricant into the permeable wall. Murti[35] studied analytically the behaviour of squeeze films in a porous circular disk and found that the presence of porosity accelerated the squeezing process. Murti[36] then analysed the squeeze film behaviour in porous journal bearings by modifying Reynolds equation to take account of the mass exchange of the lubricant between the film and the bearing matrix.

He also found[37] that pure squeeze films with a non-rotating journal could have a load capacity only with cyclic loads. Hai Wu[38] analysed the effect of slip flow on the squeeze film between porous rectangular plates. He concluded that the slip velocity further reduced both the load capacity and the response time.

1.4.3. Pore Closure

An attractive feature of porous bearings is that one of the design parameters, the permeability, tends to decrease automatically during operation. The elastic strength of porous material is comparatively low and hence the contact surface may deform under high pressure or sheer stress. Morgan and Cameron[11] observed experimentally pore closure due to metal smearing, which caused a reduction in the permeability of the porous metal. When there is plenty of oil, the effect of pore closure in the high pressure region of the bearing is expected to be beneficial since in this case the oil cannot flow easily into the porous matrix. This argument no longer holds when the quantity of oil available is limited. Cusano and Phenlan[25] reported observation in their experiments that locally reducing the permeability on the loaded side by pore closure induces a rise in both the running temperature and the frictional torque. Their explanation for this was that pore closure causes a loss of oil which in turn gives rise to an increase in temperature. Consequently, the surface tension which holds

the oil within the porous structure decreases and the rate of oil loss by seepage from the bearing is accelerated, leading to oil starvation and making the bearing run under boundary lubrication conditions.

1.4.4. Double Layer Porous Bearings

Youssef and Eudior[39], have provided an alternative way of reducing the permeability without sacrifice of porosity. They reported that by spraying a thin layer of an ultra-fine powder of a nickel alloy on to the bore of a conventional porous bearing, the coefficient of friction is reduced sifnificantly. Marshall and Morgan[40] explained that the small pore size of this layer has a stronger ability to hold the oil, so that it remains fully charged even when oil loss occurs in the bearing. Cusano[41] gave an analytical investigation of such a bearing.

1.5. The Present Problem and the Purpose of the Project

In summary, the conventional theory analysing the lubrication mechanism of porous bearings is based on the permeability being the controlling factor, and imposing this on to the classical theory of hydrodynamic lubrication. According to this theory, the macroscopic wedge between the journal and the bearing forms an oil film in the same way as in a non-porous bearing. The main difference of course is that the oil may escape into the pores and thus reduce the hydrodynamic pressure, as illustrated in Fig. 1.4 [42]. Very little experimental work has been

performed to verify the theory, and also the conclusions from different investigators scattered widely[43]. This was explained to be due to the difficulty in unifying the variable such as permeability, oil content and surface finish, etc., in their studies. In particular the theory was found in some practical cases to be seriously in error[44]. This discrepancy between theoretical and practical results is perhaps not so surprising if one recalls that in the theory the bearing is assumed to be flooded. The reduction in the oil quantity, of paramount importance in the operation of such bearings, was not considered at all. Porous metal bearings are characterized by their ability of self-lubrication without any replenishing of lubricant. Hence the condition of an adequate and full supply of oil cannot be fulfilled except at the beginning of the bearing's life, or running submerged in oil. In fact, porous bearings spend most of their life operating under conditions of partial oil starvation, with the pores filled with a mixture of oil and air. In such conditions the simple theory, using the analysis for journal bearings, Darcy's law and the Laplace equation, is no longer valid. Clearly a new study of the actual mechanism of lubrication for porous bearings is required. Morgan[44] postulated that the porous surface should be regarded as being made up of many micro-thrust pads, the so called metal lands, upon which the load is carried, and that the porosity between the lands served only to supply the oil to the lands. However, no experimental confirmation of this postulate has been made.

The purpose of this project is to investigate what actually happens at the shaft-bearing interface and to identify the fundamental mechanism by which porous bearings are lubricated. The following questions need answering:-

1. How is the hydrodynamic oil film created when the quantity of oil is limited to that contained in the pores?

2. How does the size, shape and smoothness of the lands between the pores affect the creation of these oil films?

3. What is the load capacity of the oil film, expressed in terms of surface speed, oil viscosity,etc.?

4. What is the effect of pore closure during the process of running-in and during the normal running life, and how does it signal the onset of eventual failure of the bearing?

CHAPTER TWO

MECHANICAL SYSTEM

2.1. Introduction

The apparatus employed in this project can be divided into two categories, namely, the mechanical system and optical system. The former reproduces in a realistic manner the operating conditions found in a bearing. The latter provides the observations and measurements. In this chapter the mechanical system only will be described while the optical system is described in the next.

The general view of the experimental set up is shown in Fig. 2.1 and the schematic diagram of the mechanical system in Fig. 2.2.

2.2. Porous Bearing

An analogous method was used in the experiments, in which the journal and the bearing were simulated by the contact between a flat glass plate and a porous thrust bearing whose surface had been domed cylindrically during manufacture. The porous sample was made of bronze (90% Cu and 10% Sn) and was 0.5" thick and 0.5" diameter, as shown in Fig. 2.3. The radius of curvature of the cylindrical surface was about 20ft. When it was loaded against the flat glass plate the gap was equivalent to a 1" diameter journal running with a radial clearance of about 0.001". The justification of this analogy is that

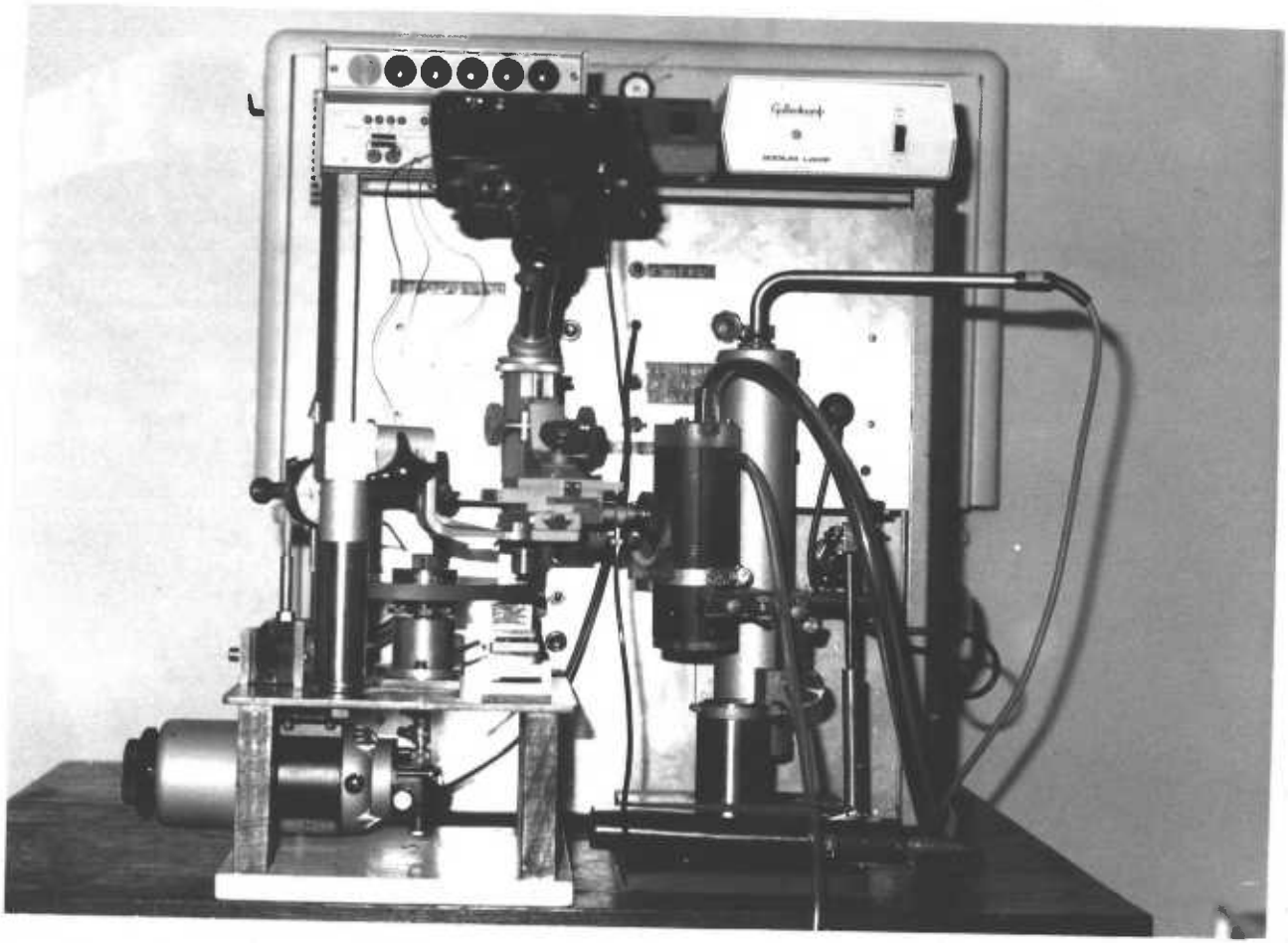

Fig.2.1 General View of Apparatus

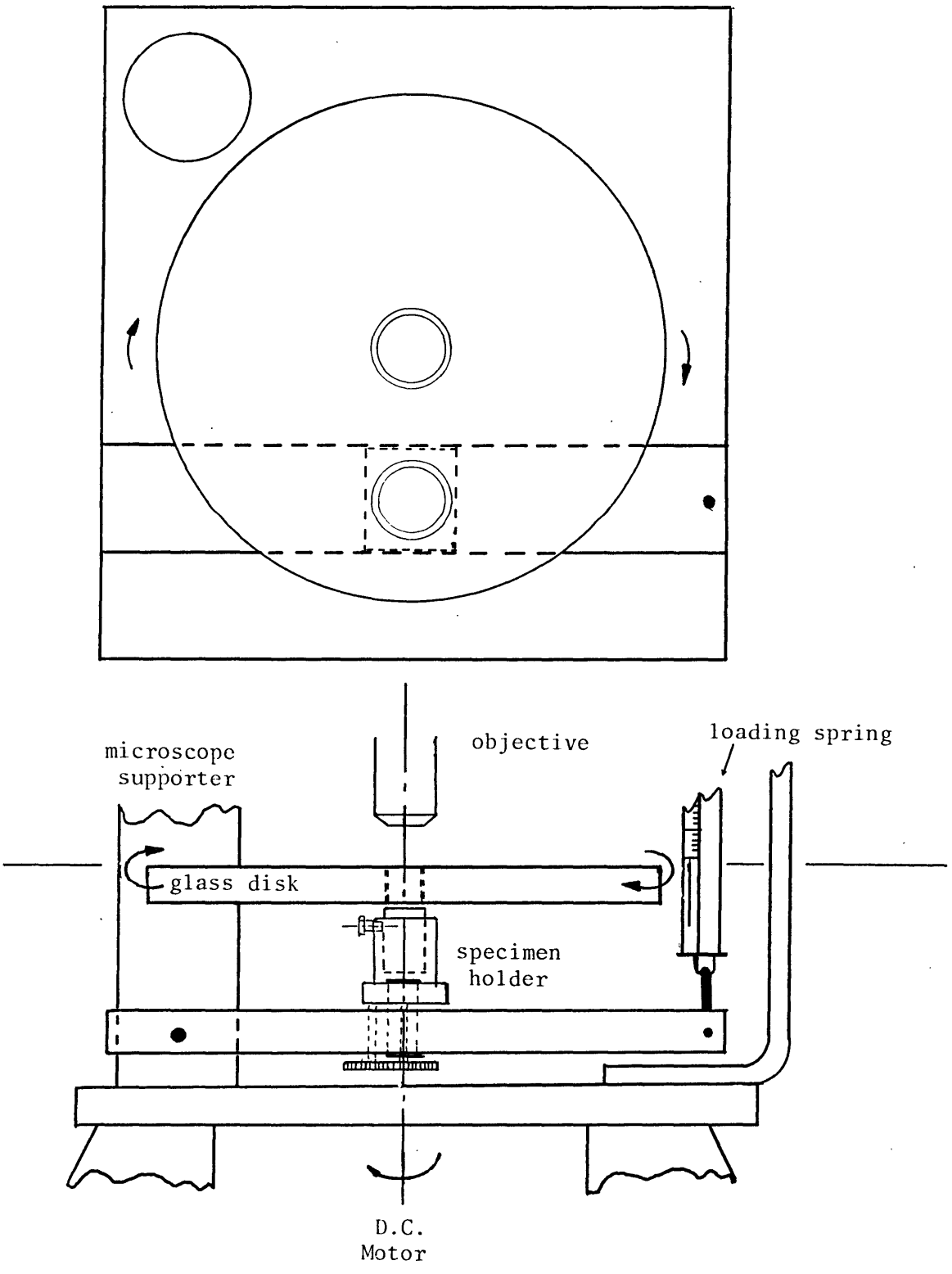

Fig. 2.2. Schematic drawing of Mechanical system.

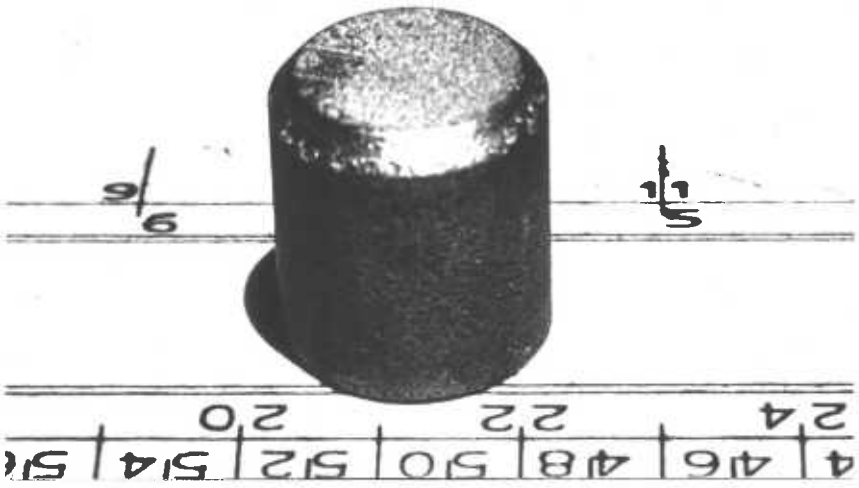

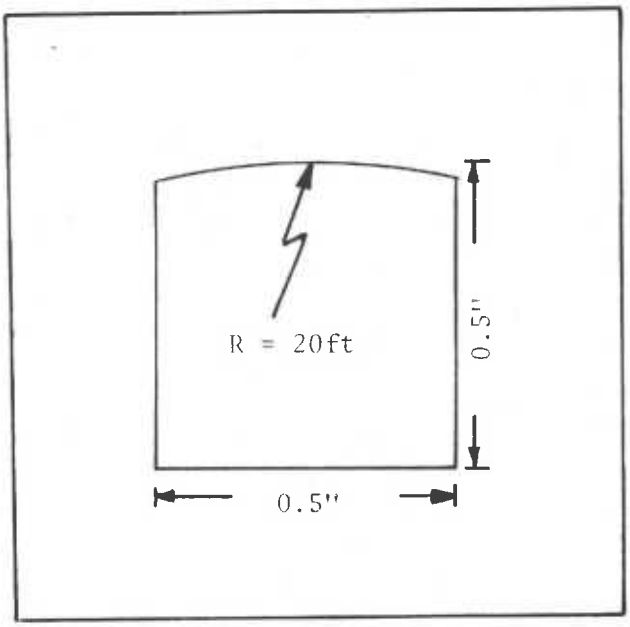

Fig. 2.3. Porous specimen employed in the experiment.

under starvation conditions the macroscopic hydrodynamic oil film cannot be created in either case; also the flow of oil is on a microscopic scale and is limited to the area very close to the contact zone. This means that from a microscopic point of view the flow of lubricant in both the real and the analogous case is likely to behave in a similar way. The density of the sample fell between 5.7 gm/cc and 6.3 gm/cc, with the corresponding porosity of 35% and 28% respectively. However, the effect of a different porosity was not detectable with the present experimental arrangement. This is because porosity is a bulk or macroscopic quantity whereas in optical interferometry oberservations are on a microscopic scale. In some tests about 1% of graphite particles were added to the samples during manufacture to assess their effect.

2.3. Specimen Holder

Since the clearance in the contact zone is extremely small, it is very important that the surfaces of the glass disk and the bearing should be aligned accurately. To achieve this a specimen holder was made, which had two special features: firstly, it was capable of tilting in three dimensions within a small solid angle with respect to the verticle axis. Secondly, once the desired angle of tilting had been set up the orientation of the specimen in space would remain unchanged regardless of the tangential frictional force acting on it. A schematic diagram of this device is shown in Fig. 2.4. It consists

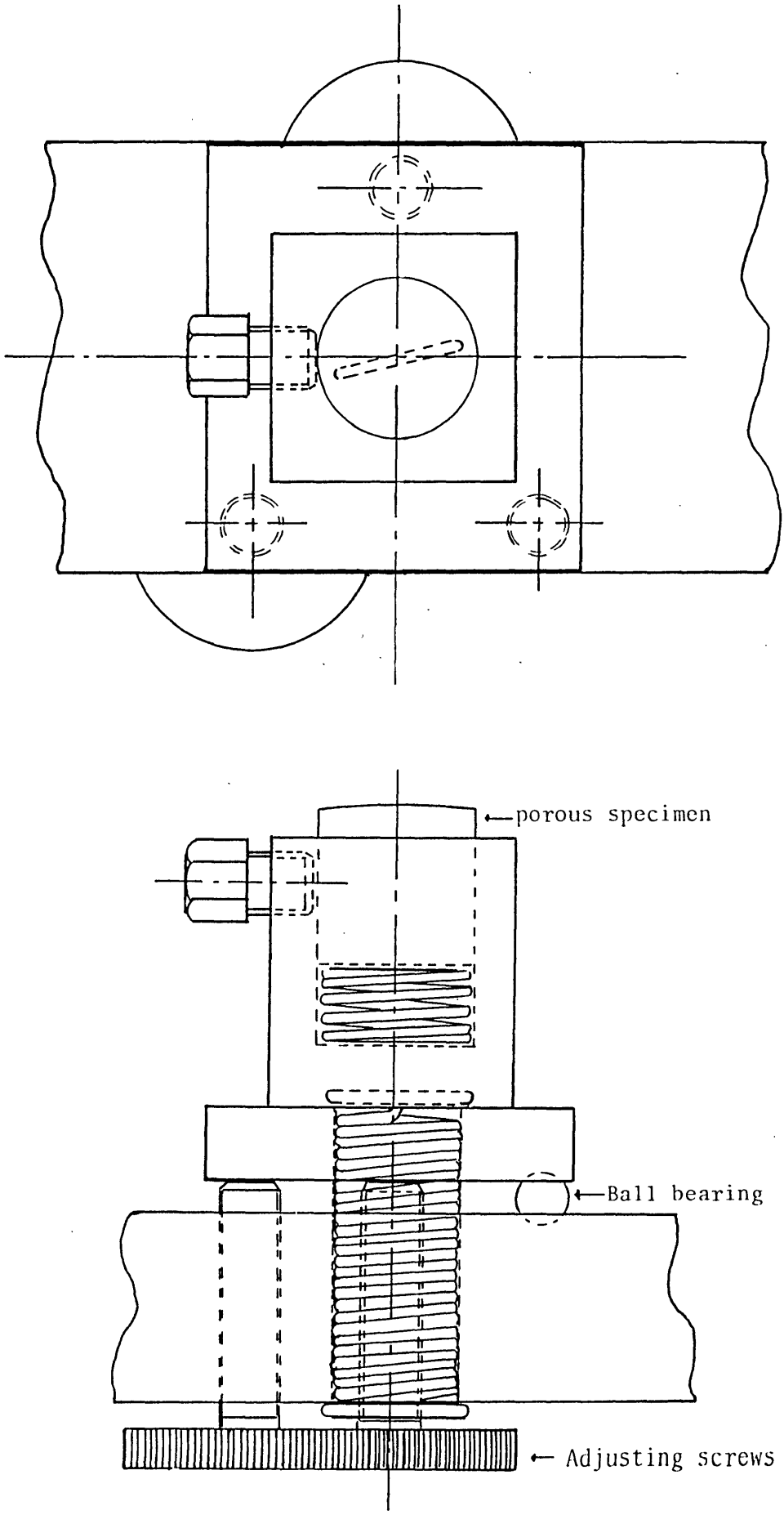

Fig. 2.4. Schematic view of specimen holder.

of a housing, in which the porous specimen was secured. The spring connecting the housing and the loading arm was always under tension. Therefore any tangential force, which might arise from friction, acting on the porous bearing would have a negligible effect on the position of the specimen holder. Two screws with fine threads served to achieve this accurate alignment. The system can be regarded as a three dimensional lever, with the spring as the fulcrum, the ball bearing and the screws as the force and weight, respectively. By adjusting the screws the porous sample could be made to tilt to any desired angle with respect to the glass surface.

2.4. Loading System

The loading arm was a lever beam and at the centre of which the specimen holder was situated. By adjusting the turn buckle of the spring balance at the free end of the beam, a continuous range of loads was achieved. The arm could be moved in and out relative to the centre of the glass disk, so that when one track on the glass became scratched, other tracks could be used simply by shifting the position of the arm.

2.5. Driving System

The glass disk was driven by a D.C. motor which could be operated in both the forward and reverse directions. The motor had a maximum angular velocity of 300 r.p.m. which was equivalent to a surface velocity of 500 ft/min.,

if the outer most track of the glass plate was used. This is similar to the surface velocity of a 1" diameter journal running at 2,000 r.p.m. The ability of the motor to work in both directions was very important in investigating the effect of particle shape on the formation of the hydrodynamic films.

2.6. Speed Measurement

The angular velocity of the glass disk was measured using a photo-detector in conjunction with an electronic counting system. The photo-detecting unit directed a collimated beam of light onto a small mirror which was attached to the edge of the glass plate, and the reflected signal was picked up by a photo-diode. The electronic clock was switched on and off by two successive passages of the mirror through the detector, thus recording the time required for one revolution of the glass disk.

2.7. Temperature Measurement

The temperature associated with sliding contacts is generally high due to the high coefficient of friction. The effect is especially important in porous bearings whose thermal conductivity is low. There is not a simple method to measure the surface temperature directly within the contact region. Therefore only the bulk temperature of the bearing was measured. This was done by drilling a small hole a few millimetres beneath the working surface, into which a copper/constantan thermo-couple was inserted.

The hole was so small that it would not have a significant effect on the fluid flow. The temperature was read directly from a pyrometer which monitored the potential difference of the thermo-couple.

CHAPTER THREE

OPTICAL INTERFEROMETRY

3.1. Introduction

During the past two decades, many physical techniques have been employed to measure the thickness of the fluid film between two lubricated surfaces. Some of these techniques, such as the electrical capacitance method, the resistance method and the X-ray method, suffer from defects. This is for several reasons, either because only an average value of the parameter is given, or because the size of the equipment is inconveniently large. Again, the sensitivity of the measurement may be too gross compared with the small dimensions of the object or distance to be measured. It was only with the introduction of optical interferometry that the knowledge of lubrication in many fields was successfully exploited, especially in elastohydrodynamic lubrication. One special advantage of the optical technique is its direct observation and monitoring of the contacting surfaces. As a measuring tool this technique is intrinsically more accurate than other methods. This is because the unit of measurement is based on the wavelength of light, which is comparable with the thickness of the lubricant film generally found in practice. The optical system employed in this project is shown schematically in Fig.3.1. and 3.2. Interference is established between the glass plate and

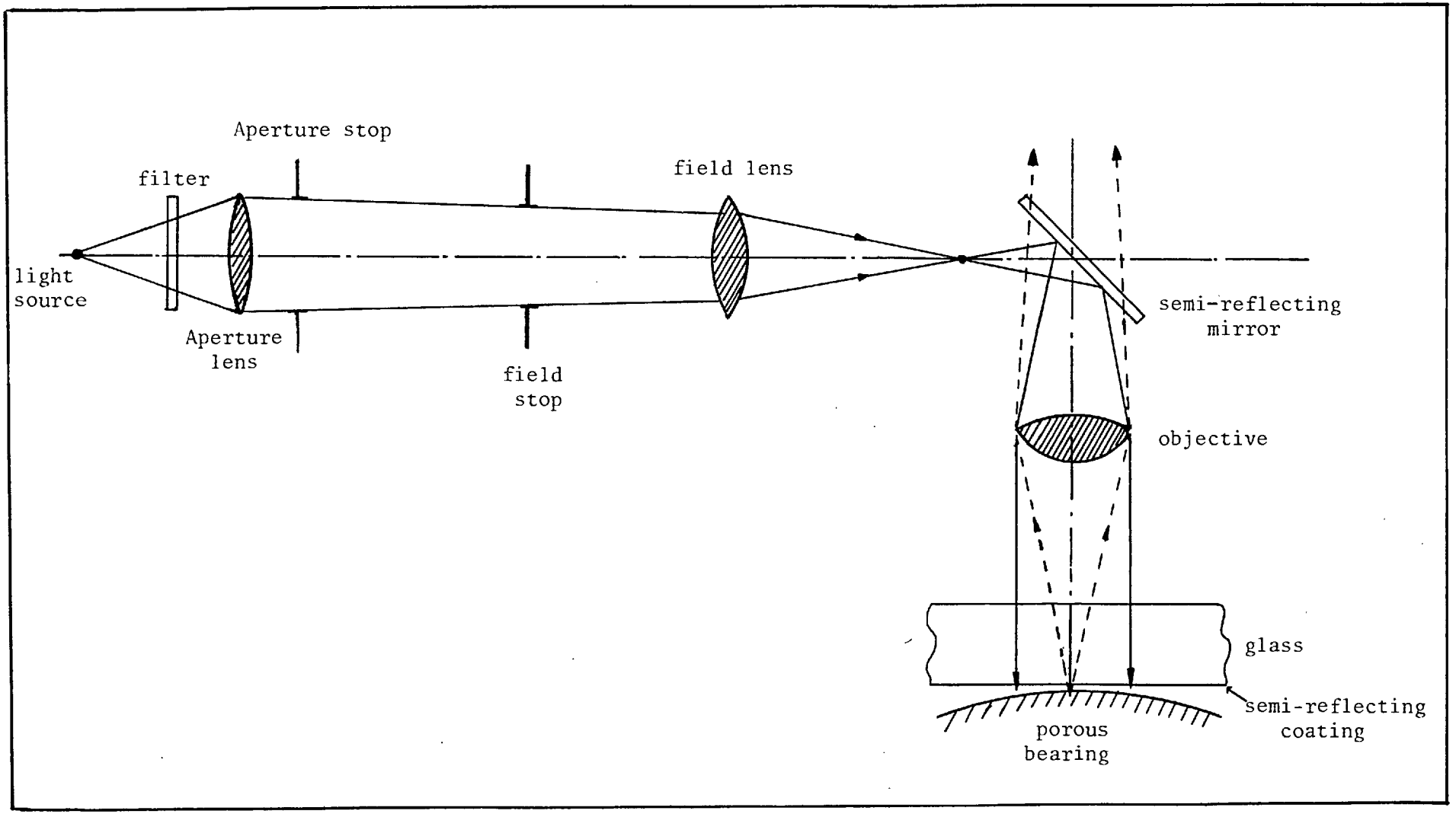

Fig. 3.1. Schematic view of optical system.

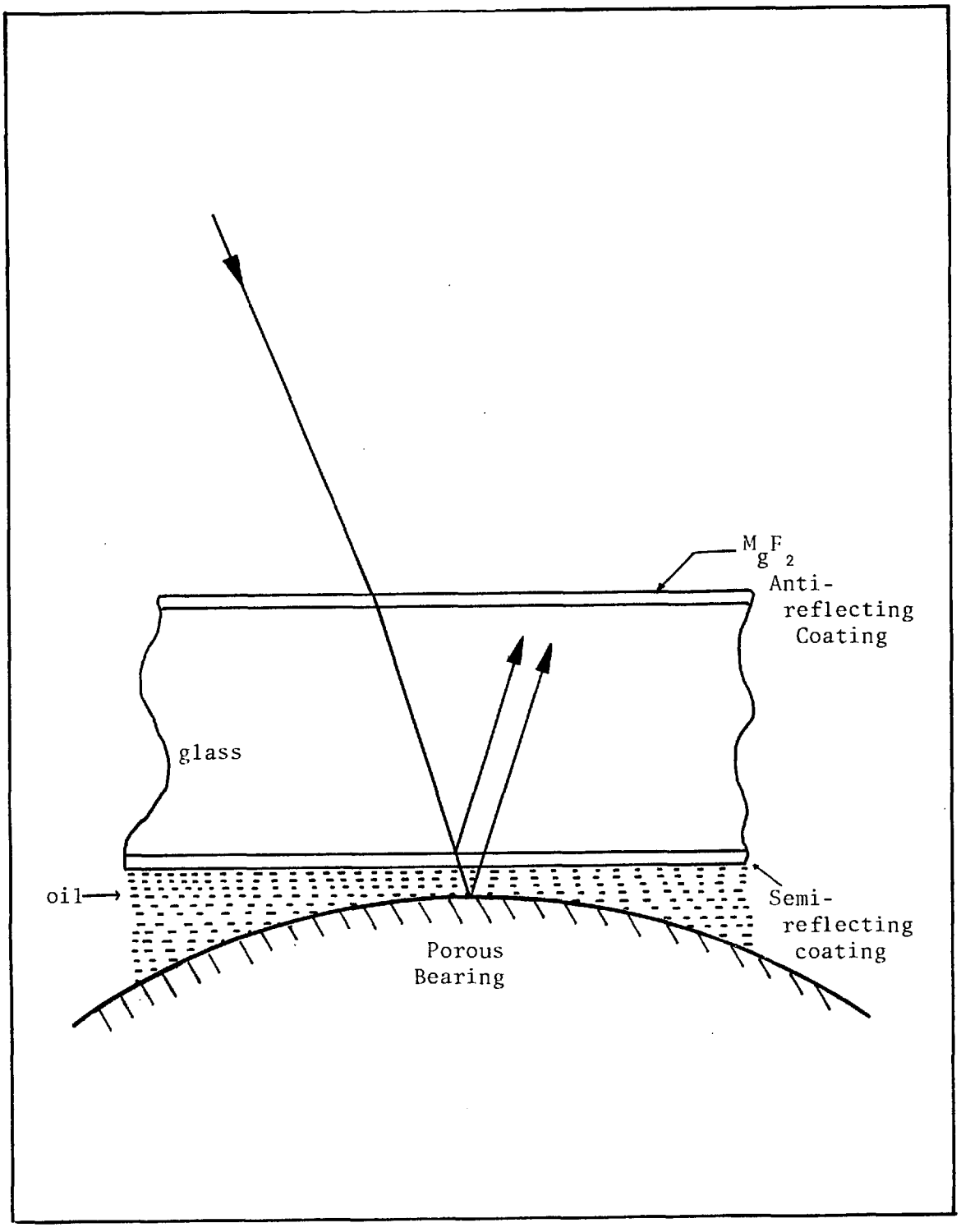

Fig. 3.2. Illustration of two beam interference.

the bearing surface. The interface is illuminated by a vertical illumination system which consists of a light source, a condenser and the objective of the microscope. In this chapter the basic principles underlying the theory of interferometry and the way it is applied to the study of porous bearings are presented. They are treated in the first part and second part of the chapter respectively.

3.2. Previous Interferometric Work on Lubrication Mechanisms

The earliest application of interferometry to lubrication problem can be dated back to 1919 when Hardy [45] used white light interference to measure the thickness of the lubricating film on glass. Later, Skinner [46] employed this technique to observe cavitation formed in the oil film between two lenses. In 1921, Stone [47] measured the film thickness in an air lubricated tilting pad bearing by using a monochromatic light source. The extension of this technique to elastohydrodynamic lubrication was first made by Kirk [48] and Archard and Kirk [49]. They measured the film thickness between two crossed perspex cylinders with white light interference.

In the earlier work there was one major problem in the application of this technique to real bearing materials, the poor resolution of the fringes. According to the theory of interference, the two interfering surfaces must have approximately the same reflectivity in order to give a well defined fringe system. The reflectivity of a glass-oil interface is

about 1.7×10^{-2}% whilst that of the bearing element, such as a steel ball can be as high as 50%. In this case the fringe visibility is extremely poor, thus making measurements very difficult.

To upgrade the relectivity of the transparent element Gohar and Cameron [50] used materials of higher refractive index, such as sapphire and diamond for the study of ball bearings, with considerable success. In 1969 an entirely new era of the technique began, following the development of improved vacuum deposition methods. By coating the glass with a thin but controlled thickness layer of a transparent or partially transparent material, the reflectivity of the surface can be increased and adjusted to any desired amount. Several authors [51,52, 53,54] have since been successfully applying this method to the study of the EHD point and elliptical contact, as well as to tilting pad thrust bearings, etc.

3.3. Interference

The simplest way to understand the theory of interference is to regard light as being made up of sine waves, which propagate through space or a transparent medium, and to remember that the so called 'intensity of light', which is familiar in our daily life, is merely the square of the amplitude of these sine waves. As required by the principle of continuity,reflections happens whenever these waves pass through an interface between two media. Thus, on travelling through a layer of a dielectric, such as a film of lubricant,the two reflected components of the

sine waves will travel a different path length according to the thickness of the layer, as shown in Fig.3.2. Under appropriate conditions, these two reflecting beams will superimpose together and hence give rise to interference. The interference formed in this way is classified as division of amplitude. The resulting intensity in the region of superposition will vary from a maximum to a minimum. For example, when the 'tops' of the two waves are added together, they strengthen each other and give a strong light intensity. However, at some other points, the two waves which are added may be such that the top of one wave meets a 'hollow' of the other, they then destroy each other and cause darkness. The alternate bands of brightness and darkness are called interference fringes. The region of superposition is known as the localization of fringes. At normal incidence, the fringes are localized on the front reflecting plane. For very thin films the two reflecting surfaces can be regarded as coincident from the view point of localization and of focus. Therefore, when the bearing is viewed through the glass plate from above with a microscope, both the bearing surface and its associated pattern of fringes can be brought coincident into the same focus. Thus, fringes can be seen to contour critically over the surface microstructure of the bearing. The condition for which interference occurs is dominated by the degree of coherence of the light, the idea of which is well documented and can be found in many texts, such as Born and Wolf [55] and Francon [56]. The basic principle in connection with this condition is briefly discussed in the following.

From atomic theory, the waves associated with the light produced by a physical source have their amplitude and phase undergoing irregular fluctuations at an extremely fast rate. These fluctuations,corresponding to each beam of light coming from the same source, are mutually correlated. The amount of correlation is known as the degree of coherence. For example, beams from a straightly monochromatic light source are said to be completely coherent,and they always give rise to interference when superimposed together. In the other extreme, beams from different sources will have their fluctuations completely uncorrelated, e.g. incoherent, and the superposition of these beams cannot give rise to interference at all. Any real physical source of light has a finite size and it emits a finite distribution of the spectrum. The concept of coherence can thus be classified into two types, namely, spatial coherence and temporal coherence. A light source of a small size is 'more coherent' than a large light source. This is because a real light source can be considered as composed of many, infinitesimally small, point sources, each of which is emitting waves in all directions into space. The fluctuations of phase and amplitude corresponding to the waves emitted by neighbouring point sources are to some extent inter-dependent. For two observing points which are close to each other but are far away from the light source, they will 'see' the waves coming from all the points of a small source to have more similar fluctuations than that from a larger source. We are thus lead to the concept of spatial coherence. In practice, however, smaller sources

are generally associated with a lower intensity of the beam. Hence, the best source size is a compromise between the degree of coherence and the amount of intensity required.

On the other hand, the rapidity of the irregular fluctuations of the amplitude and phase, in connection with a real light source, depends essentially on the effective width of the spectrum. The complex amplitude of the waves remains substantially constant only during a short time interval, Δt, which is equal to $\frac{\lambda^2}{\Delta\lambda}$ where λ is the wavelength and $\Delta\lambda$ is the width of the spectrum emitted by the light source. Within this time interval the disturbance behaves like a monochromatic wave of mean frequency. This leads to the concept of temporal coherence.

In general, the degree of coherence affects the sharpness of the fringes. For instance, sharp fringes are expected when the coherence is high. This happens when the light source is small (spatial coherence) and has a narrow spectral range (temporal coherence).

3.4. White Light Interference

The interference fringes given by a thin film from a white light source are characterized by the appearance of different colours. According to the concept of temporal coherence, a white light source has a wide distribution of spectrum, and hence its corresponding 'coherent time' is very short. Therefore it is only when the thickness of the film is small compared to the distance which the light

has travelled within its 'coherent time', can the interference fringes be observed. For a given thickness of film, the light of one wavelength (e.g. green) may be strengthened but the light of other wavelengths (e.g. violet) may be cut out. The fringes therefore appear coloured. Technically speaking, white light interference is very important because its coloured characteristic provides a convenient way of direct measurement of the film thickness. However, it is not suitable for the measurement of either very thin films or very thick films. For a very thin film (<1,000Å), the intensity distribution produces haze near the colour of zero order, and it is therefore difficult to resolve. On the other hand, if the film is too thick, so many colours are present at a given point that the resultant colour is not readily distinguishable, unless a spectrometer is employed.

3.5. Fringe Order and Visibility

With the interference of two beams the resultant intensity at normal incidence is expressed [55] as:

$$I = I_1+I_2+2\sqrt{I_1}\sqrt{I_2}\,|\gamma|\cos\left[\frac{2\pi}{\lambda}(2nh)-\delta\right] \quad \ldots\ldots\ldots \quad (3.1)$$

Where I_1 and I_2 are the intensity of the two interfering beams,

$2h$ is the path difference of the two beams,

δ is the phase change on reflection,

and γ is the complex degree of coherence.

The intensity is a maximum when $\frac{2\pi}{\lambda}(2nh)-\delta=2m\pi$ or when

$$h = \frac{\lambda}{2n}\left(m+\frac{\delta}{2\pi}\right) \quad \ldots\ldots\ldots\ldots\ldots\ldots\ldots\ldots\ldots\ldots (3.2)$$

Where m is an arbitrary integer and is called the order of interference.

Therefore, $I_{max} = I_1+I_2+2\sqrt{I_1}\sqrt{I_2}\,|\gamma|$ .....(3.3)

Also the minimum intensity occurs when

$$h = \frac{\lambda}{2n}\left[(m+\frac{1}{2}) + \frac{\delta}{2\pi}\right] \quad \text{.....(3.4)}$$

and $I_{min} = I_1+I_2-2\sqrt{I_1}\sqrt{I_2}\,|\gamma|$ .....(3.5)

The measure of the distinctness of the fringes is known as 'visibility' and is defined as

$$V = \frac{I_{max} - I_{min}}{I_{max} + I_{min}} = \frac{2\sqrt{I_1}\sqrt{I_2}\,|\gamma|}{I_1 + I_2} \quad \text{.....(3.6)}$$

It is seen from this expression that whether the fringe is clear or not depends upon two factors. The first one is the absolute value of the complex degree of coherence, $|\gamma|$. It is a complicated function of the source size, the width of the spectrum and the path difference, and it has a value between 0 and 1. To have good visibility of fringes, $|\gamma|$ should be close to unity. This is most easily done by using a small light source with a narrow spectral range, and arranging that the path difference of the interfering beams is small. The second one is the relative intensity of the beams. The larger the difference the smaller the value of V. Therefore, to obtain fringes of good visibility it is necessary for the two interfering beams to be of similar intensity.

3.6. THE REFLECTING SURFACE

3.6.1. The Glass Disk

The rotating element was a transparent disk made of homogeneous optical crown glass of $6\frac{1}{2}$" diameter and half an inch thick. The upper and lower faces were ground flat to within 500Å. The glass had a thermal conductivity of 0.0024 $^{cal}/_{cm.s.°c}$. and a specific heat of 0.2 cal./gm./deg.C. The refractive index was 1.52. To increase the intensity of the light beam reflecting from the glass-oil interface it was necessary to coat a thin layer of material onto the glass disk using the vacuum deposition technique. Either a metallic or a dielectric coating would be suitable. Both types of coating were employed in the experiments, as will be described later. The former was a partially transparent layer of chromium of 170Å thickness. It reflected 15% of the incident light and absorbed about 30% when immersed in oil.

The latter was a layer of TiO_2 whose optical thickness was about $\frac{1}{4}$ of the wavelength of light. With this layer the reflectivity of the glass-oil interface was greatly increased. The physical principle is that the beams reflected from the two sides of the quarter wavelength layer suffer from a path difference of half a wavelength. Bearing in mind that there is a phase change of $\frac{\lambda}{2}$ in the reflecting beam when light travels from a low density medium (glass) to a more dense medium (TiO_2), the two reflecting beams will therefore appear at the front surface in phase. Hence they will recombine

together constructively, giving a high reflectivity. A coating made of TiO_2 has only a slight absorption in the visible region of the spectrum. The refractive index of TiO_2 depends upon the rate of evaporation during deposition and can be varied between 2.2 to 2.7. This gives the reflectivity of the coating to be between 30% to 50% when it is a $\frac{1}{4}$ wavelength thick.

3.6.2. The Bearing

The surface of a porous bearing consists of pores and lands with random size and shape. Also it was rough and had a low reflectivity before running, such that no significant interference pattern could be obtained. On the other hand, a preliminary study of the run-in bearings showed that the surface of the lands in the loaded region had been polished and were flat and shiny. The reflectivity of which was as high as 50%, therefore it was possible to produce a sufficiently smooth porous surface suitable for interferometric study, by simply pre-running the porous sample against a steel plate. In normal conditions this running-in took less than half an hour. This treatment introduced a serious effect on the measurement of the film thickness. The polishing process produced quantities of very fine debris, consisting of work-hardened metal or metal oxide particles with a size range from 0.5μ to 2μ. In particular, some of this debris followed the circulation of oil and became trapped deep inside the porous matrix. Even ultrasonic cleaning of the sample could not remove the particles completely. Therefore

when tested with optical interferometry these particles might eventually come out into the oil film and act as grinding paste, causing irreversible damage to both the coating and the polished bearing surface. This effect restricted the time available for measurements to about five minutes.

3.6.3. Phase Change

When light is reflected from the interface between two media, it suffers a change in phase. For opaque metal such as the bronze surface the phase change at normal incident is very close to π. For thin films of a metallic or a dielectric material, however, the phase change is not easily predictable. Its value can be anything between $-\pi$ to π, depending upon the thickness of the layer. The effect of a phase change is the same as the introduction of a constant layer of lubricant separating the two surfaces. Therefore, it is necessary to calibrate the interference fringes before the measurement of film thickness can be made. This is given in chapter 4.4.

3.7. The Microscope and Illumination Systems

The surface of a porous bearing has a fine structure which is composed of pores and lands which vary in size from about 5μ to 100μ in diameter. Hence a medium power microscope (about X150) was suitable for observation. Note that the thickness of the glass plate limits the

closeness of approach of the objective to the object plane. To overcome this problem, a special objective with a long working distance, a Beck X10, was used. It was capable of working at a distance of about 0.75" away from the object. The eyepiece had a wide field of view and a magnification of X15. One disadvantage of using high magnification in the microscope system was that the field of observation was much smaller than the specimen surface area. To overcome this problem, the microscope was mounted onto a travelling support, so that a larger area of the bearing surface can be viewed.

The function of the vertical illumination system was to produce a well collimated beam of light and to provide a convenient means of controlling the source size, which in turn affected the quality of the fringes, as well as the intensity of the image. The illuminator employed in this project was a Beck Vertiphase, as shown schematically in Fig.3.1. The effective source size was controlled by adjusting the aperture stop, whilst the illumination area was controlled by adjusting the field stop. With this arrangement the rays of light emerging from the objective were conical with a maximum of 8^{o} deviation from the normal.

3.8. Light Sources

Three light sources were used in the experiments. First a sodium lamp giving a wavelength of 5890Å was used for general observation. It emitted a very narrow spectrum of light so that the visibility of the resulting fringes was excellent. Secondly a white light tungsten lamp was used for measurement of the film thickness. Thirdly a xenon high voltage discharge lamp (Ferranti type CC 10) was employed for high speed photomicrography. It had a continuous spectrum similar to daylight, but could be converted to a monochromatic light source by using a very narrow band pass filter (λ=5460Å, $\Delta\lambda$=100Å). The maximum output energy was about 150 joules and the pulse width was approximately 150 microseconds, which was short enough to freeze any high speed movement in these tests.

3.9. High Speed Micro-photography

Due to the complexity of the topology of the porous surface, it was very important to record events under different operating conditions. The exposure time was fixed by using a single discharge from the xenon lamp and the photographs were recorded with a 35mm. motor-driven camera working in conjunction with the microscope system. Since the energy of the pulse was constant, the exposure was controlled solely by adjusting the aperture stop of the illumination system. Kodak Chromat slide (ASA 80) was used for the colour photographs, but extremely high speed

black and white film was necessary when the narrow band-pass filter was employed. This was done by using HP-4 (ASA 400) and upgrading the speed to ASA 1250 by a special developer - Accuspeed by Peterson.

3.10 Multiple Beam Interference

So far the simplest case of interference which involves only two reflecting beams, one from the chromium or TiO_2 layer and the other from the bearing surface has been described. However, the situation is entirely different with multiple-beam interference. As will be seen later, it was a general feature in the operation of porous bearings that two-phase flow occured within the pores at the working surface. When this happened, one or two more interfaces were introduced into the path of light, making the total number of reflected beams up to three or more. Some of these beams might, or might not, participate in the interference, depending upon their relative intensity, their path difference, and the propagating angle of the beams. The fringe patterns produced in this way no longer represent the contour map of the surface, and a rather complicated analysis had to be made for interpreting the pattern quantitatively. The analysis involves the theory of wave propagation in a stratified medium [55]. Such analysis is not the major purpose in this project. As the reflectivity of other interfaces was different it was therefore necessary to use coatings of different types in order to achieve the requirements for good fringe visibility. A schematic diagram, showing

the conditions of multiple beam interference, is given in Fig.3.3.

Having described in general terms the apparatus and the operation of interferometry, the details of the test procedure will next be described.

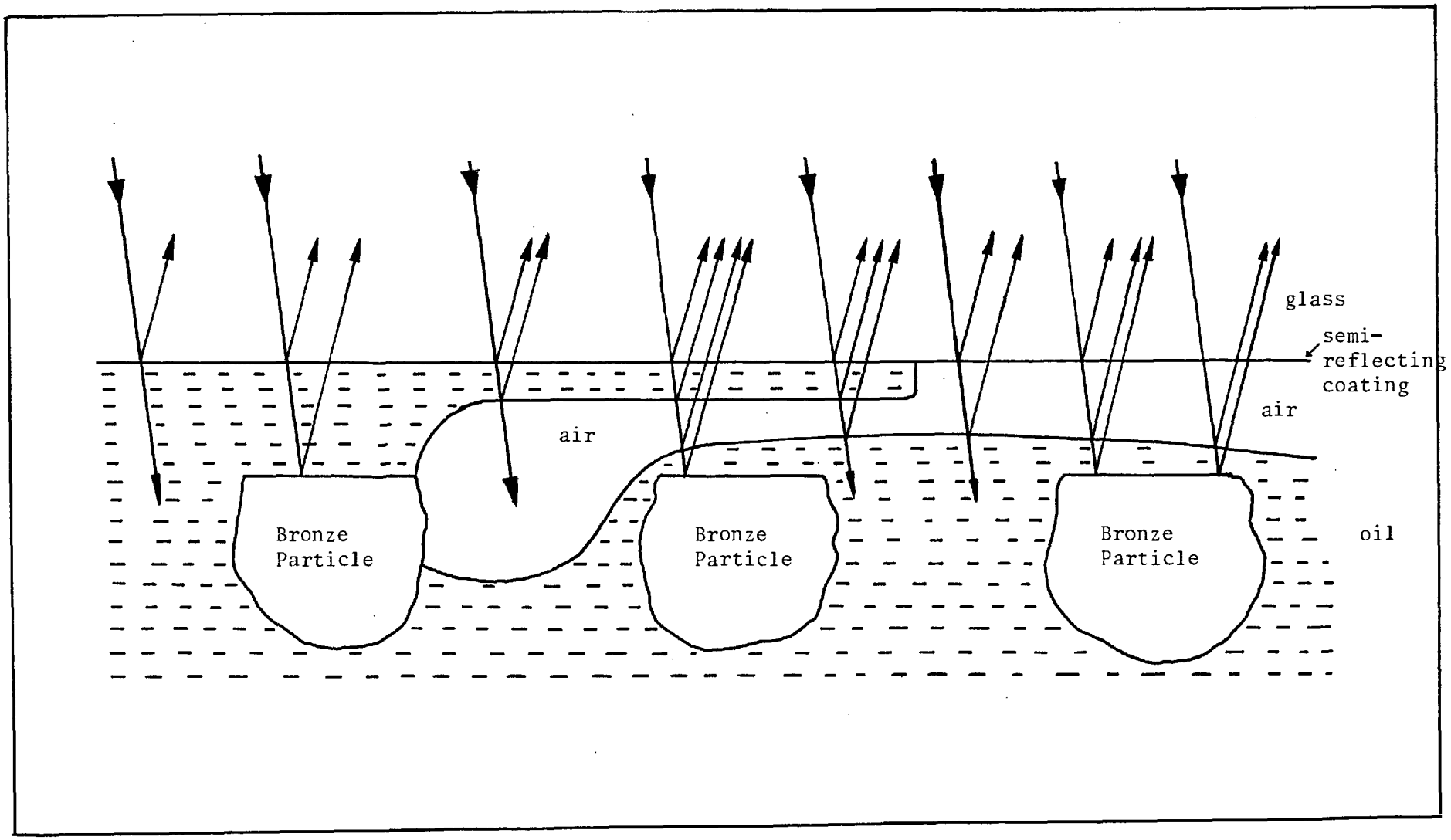

Fig. 3.3. Illustration of interference involved in the two phase flow in porous bearings.

CHAPTER FOUR

EXPERIMENTAL PRELIMINARIES

4.1. Description of the Lubricants Used

The main lubricant employed in the experiment was a Turbine oil, Shell Turbo T41, which is typical of the oil most frequently used in porous bearings, having good anti-oxidant characteristics and hence long life. It was found later that the viscosity of this oil was inconveniently low because a high sliding speed was required to build up a sufficiently thick hydrodynamic film for easy measurement. A thicker oil, Teresso 140, was therefore employed in experiments involving quantitative measurement of the film thickness. To measure the thickness of the hydrodynamic film it is necessary to know the refractive index of the oil, which in general depends upon the temperature and the pressure. However, the variation of both temperature and pressure encountered in the interferometric experiments was low. For example, the pressure was in the range of 100 psi to 1,000 psi whilst the temperature range was from $20^{o}C$ to $35^{o}C$. The change of refractive index over these ranges is negligible in comparison with the other sources of error, such as the broadening of the fringes and vibration. Hence the refractive index was regarded as constant in these experiments. Some of the properties of the two oils used are listed in Table 4.1.

Table 4.1. Properties of Lubricant

Lubricant	Specific Gravity	Surface Tension	Viscosity (cS) $20^{o}C$	$30^{0}C$	$40^{o}C$	$50^{0}C$	Refractive Index at $25^{o}C$
Turbo 41	0.878	33.0 dynes/cm	330	170	100	60	1.48
Teresso 140	0.83	33.8 dynes/cm	1600	750	400	220	1.49

4.2. Examination of 'run-in' Porous Surfaces

The first task of this project was to explore the feasibility of using optical interferometry as a suitable technique with which to study the lubrication of porous bearings. For this purpose typical porous journal bearings were tested under real-life conditions at various bearing loads and running times. After the test, the bearings were cut into pieces of appropriate size and the working surface was investigated using an interference microscope. It is to be noted that the interference microscope used here was different from that mentioned before. This one was a Linnik type which has a built-in reference mirror. The working distance of the microscope is only 0.025". The diameter of the journal bearings used had to be larger than 2", since below this value the curvature introduced distortion and limited the magnification which could be used. The conditions of the test are listed in Table 4.2.

Table 4.2. Conditions of the running-in Test

1.	Angular velocity of shaft	=	2,800 r.p.m.
2.	Bore diameter of bearing	=	2"
3.	Wall thickness	=	$\frac{1}{8}$"
4.	Bearing length	=	1"
5.	Bearing load	=	12.5 lb to 50 lb
6.	Shaft material	=	hardened and polished HCD steel (high carbon high chromium)
	Minimum hardness	=	57 Rockwell 'C'
7.	Shaft diameter	=	1.9937"
8.	Impregnation oil	=	Turbo T41, plus 3 drops smeared on at fitting and before running
9.	Running Clearance	=	0.001" to 0.002" (i.e. 0.0015"±0.0005")
10.	Wet Density of bearing	=	6.31 gm/cc
	Dry Density	=	6.06 gm/cc
11.	Oil content	=	27.2% v/v

Fig. 4.1 shows the scanning electron micrograph of a typical virgin surface of the porous journal bearings. The interferogram of such a surface is shown in Fig. 4.2. Straight line fringes parallel to the sliding direction have been deliberately introduced to increase the sensitivity. In this way, very small changes in the surface topology, which result in the departure of the fringes from the straight and parallel, can be readily detected. The difference in the height between two neighbouring fringes is 11 microinches. The scratches

which run parallel to the axis of the bearing were caused by the roughness of the tool used for the sizing or coining operation. The height between the peaks and the valleys of these scratches varied from 0.1μ to 0.5μ. Note the fringes within the pores produced by the surface of the oil held in the pores by surface tension. These fringes are determined by the geometry of the pores, and the average distance from the oil surface to the bearing surface is a function of the effective pore diameter. It will be seen that the smaller the pore size the closer the oil level is to the bearing surface, as would be expected from capillary theory. After running for a short time the porous surface became flat and shiny. The mechanism which produced this change was a gentle grinding away of the top layers of the metal, especially the peaks of the asperities, together with metal smearing which causes transportion of surface material along the running direction, partly filling up the porosity, and hence increasing the area available to support the load. Thus, the running-in process includes two mechanisms:

First, the wearing away of the peaks of the asperities; and secondly the plastic deformation of the metal surface by a smearing action, both of which contribute to an increase in area, and a smooth and flat surface which is more acceptable for hydrodynamic lubrication. The scanning electron micrograph, interferogram and Talysurf trace in Fig. 4.3 , Fig. 4.4 and Fig. 4.5 respectively show typical surfaces after running-in. It will be seen that the surface has been highly polished and this gives excellent

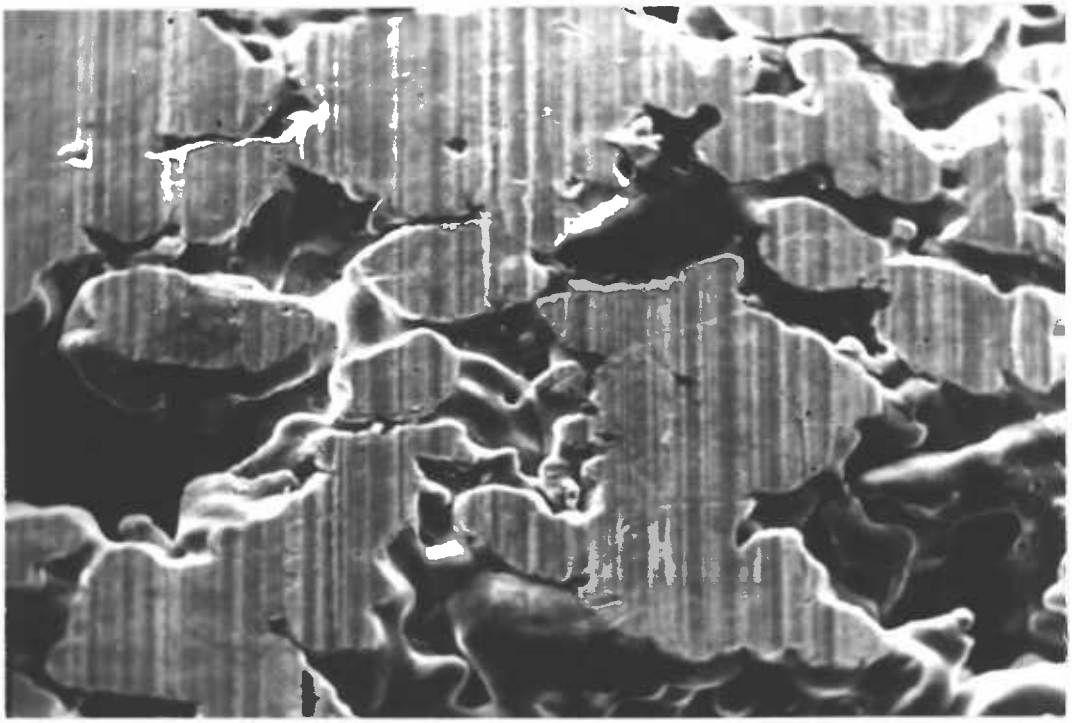

Fig. 4.1. Scanning Electron micrograph of virgin porous surface. Magnification x 200.

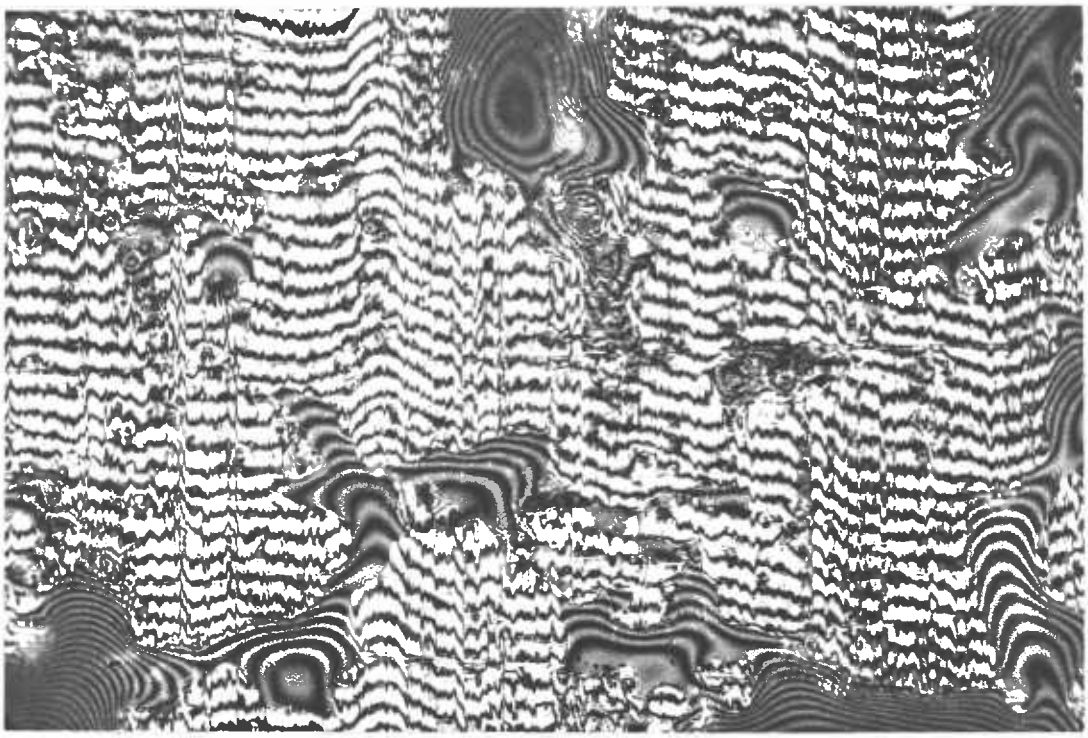

Fig. 4.2. Interference micrograph of virgin porous surface. Magnifcation x 600.

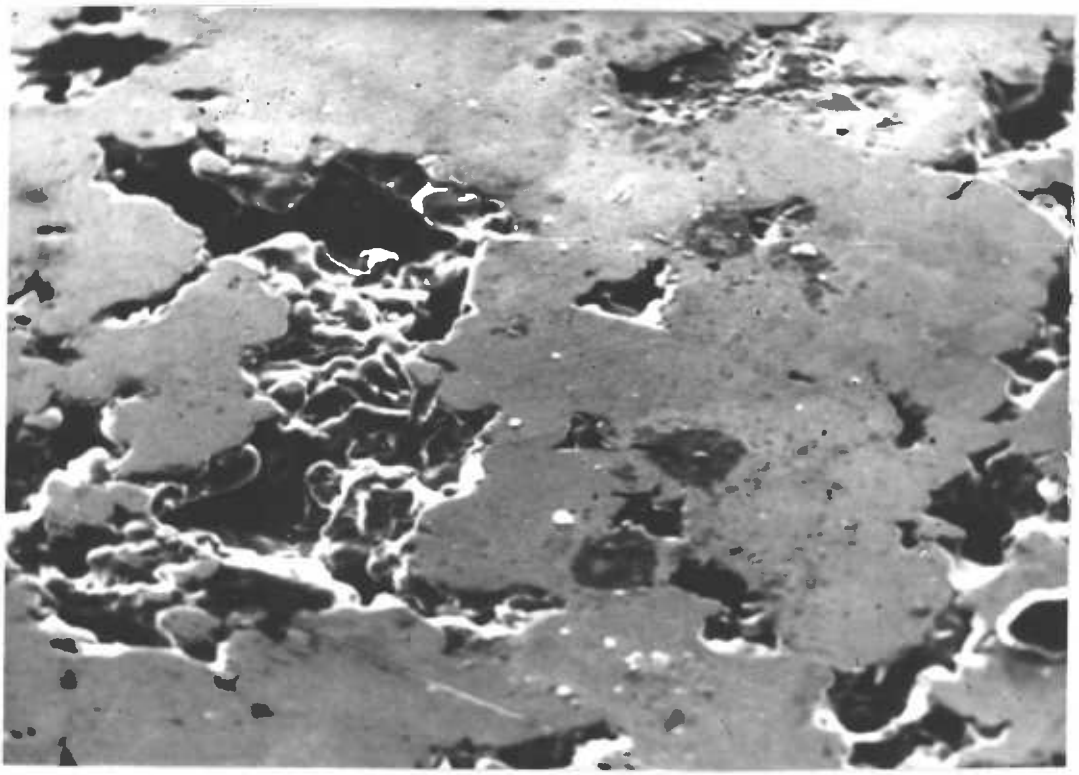

Fig. 4.3. Scanning electron micrograph of run-in porous surface, x 200.

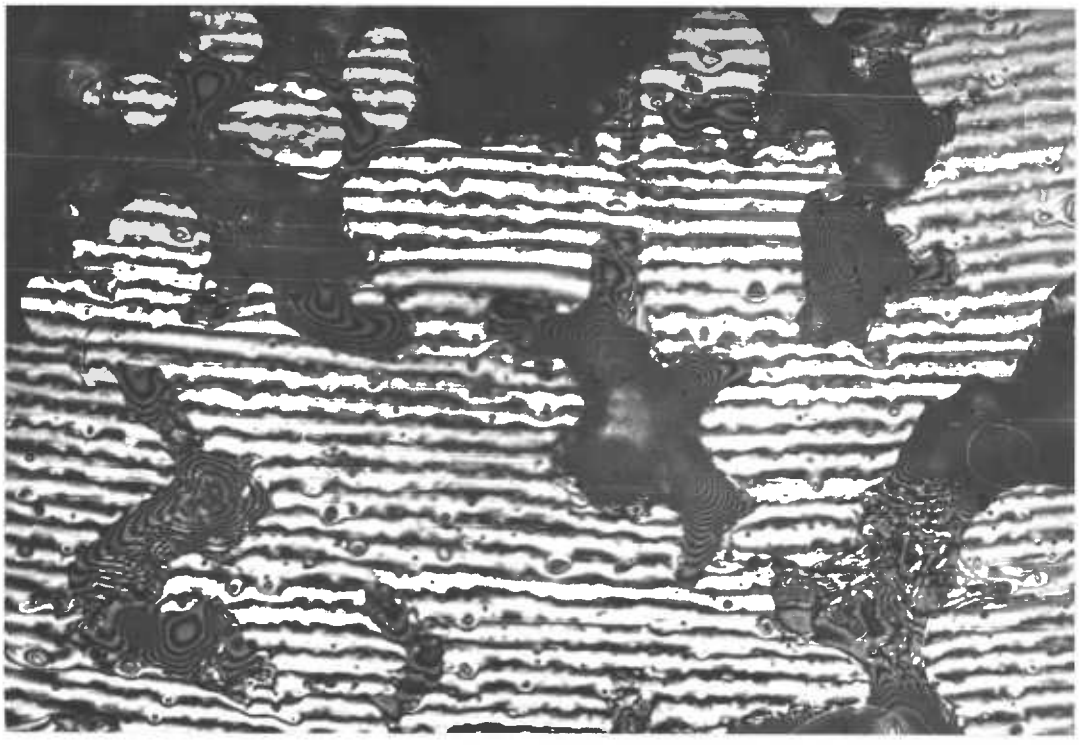

Fig. 4.4. Interference micrograph of run-in porous surface, x 600.

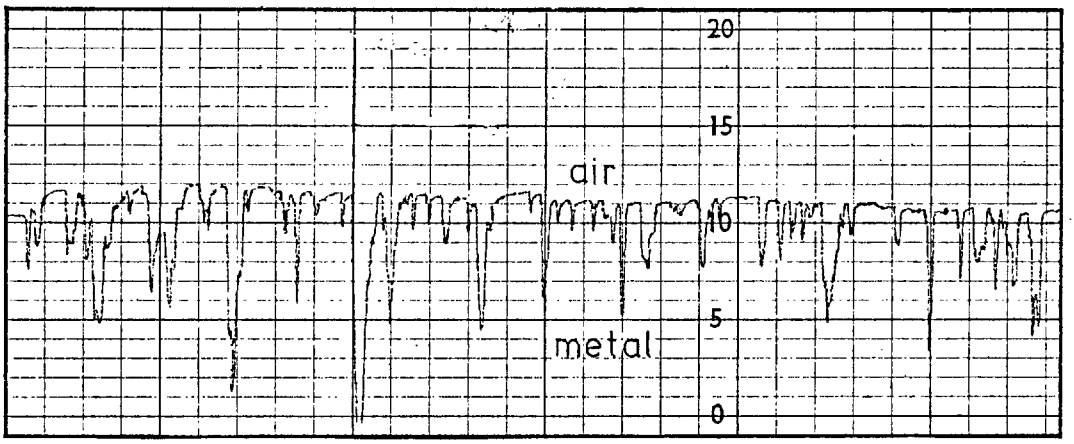

Fig. 4.5. Talysurf trace of porous surface.
Horiz. scale 20 : 1
Vert. scale 2000 : 1

interference fringes. The straight and parallel fringes in Fig. 4.4 indicate that the top surface of the lands is smooth and flat. Note that the fringes bend slightly at the edges of the land, indicating a small taper, distributed homogeneously around the land. This taper may be due to residual elasticity. When subjected to compression during manufacture, the pressure on the surface of the lands is counterbalanced by an internal stress within the body. These internal stresses are acting in reverse direction to the externally applied pressure. After the external pressure is relaxed the internal stresses also relax and tend to increase the height of the compressed land, thus producing the taper at the edge. The taper area has the form of a narrow band around the land with a width of about 1 to 3μ. The angle of the taper is usually less than 2^{o} with respect to the horizontal direction. Another important result of this preliminary study is the amount of surface wear in the loading region, which was high. In all the 44 bearings studied, whose running time ranged from several seconds to several hours, some wear was always found and confined to the loaded region. Within the running-in period the amount of wear was found to be proportional to the running time and the applied load. One important consequence of this wear process is to make the rubbing surface conformable with the curvature of the shaft. There is strong evidence that the loaded part of the bearing surface after run-in was substantially parallel to the shaft, instead of having a converging wedge of about 0.06^{o}, as would be the case if this conforming process had not occurred. It

is of interest to note that a journal bearing of 2" diameter with a designed clearance of 0.001" will have half of its projected surface area made parallel with the shaft when only 3μ of material has been removed or deformed at the load line. Judging from the result of the running-in tests this amount of wear is readily achieved. Further experiments concerning the running-in process are given in Chapter 7.

The results of this preliminary study can be summarised by the following points:

1. The running-in process of a porous bearing is accompanied by an initial high rate of wear and of metal smearing in the loaded region.

2. The wear mechanism causes the peaks of the asperities on the lands to be polished away.

3. The effect of metal smearing and wear is to increase the area of the lands which are supporting the load.

4. The combined effect of wear and metal smearing does not produce any significant taper at the leading edge of the lands.

5. After running-in, the working part of the bearing surface is substantially parallel to the surface of the shaft.

4.3. Preliminary Treatment of Samples

In view of the fact that the roughness of a new porous surface is not suitable for interferometric study, and that a high wear rate occurs in the early life of the bearing, all the samples to be tested with optical interferometry were first run against a steel disc to eliminate these undesirable asperities. The condition for running was such that the PV factor was made to be between 30,000 to 60,000 $lb \cdot ft/in^2 \cdot min$. The time of running was adjusted according to the size of the lands required, and was usually more than half an hour. After running, the samples were then cleaned first with toluene and secondly with acetone in an ultrasonic bath for 20 minutes. After drying in an oven the samples were placed in fresh oil and vacuum impregnated. This ensured that all the available porosity was charged with oil. Finally the excess oil on the surface of the sample was wiped away. In this state the samples were ready for interferometric study.

4.4. Film Thickness Calibration

A chromium coating of 20% reflectivity was employed for film thickness measurements. To do this the change of phase on reflection from the coating had to be determined. Since the phase angle associated with a metallic layer is substantially constant in the visible range of spectrum, its value can be found using two different wavelengths. The method is described briefly as follows:

A porous specimen was heavily ground flat and was brought into contact with the glass disk at an extremely small angle, as shown in Fig. 4.6. The gap was filled with a layer of oil (Teresso 140, n= 1.49). According to Eq. 3.1., bright fringes occur when

$$h = \frac{\lambda}{2n}(m + \frac{\delta}{2\pi})$$

hence

$$\Delta h = \frac{\Delta\lambda}{2n}(m + \frac{\delta}{2\pi})$$

or

$$\delta = 2\pi(2n\frac{\Delta h}{\Delta\lambda} - m) \qquad \text{.....(4.1)}$$

In the calibration experiment a green filter (λ= 5460Å) was first used in conjunction with the tungsten lamp. The fringes so obtained were straight and parallel to the contacting edge. The position of the mth order of fringe was noted and the tilting angle of the specimen was calculated. Next the filter was changed to a red one (λ = 6300Å), and the shift of the mth fringe from its previous position was recorded. To a first approximation this amount of shift, when multiplied by the tilting angle, gave the value of Δh. Substituting Δh and $\Delta\lambda$ into Eq. 4.1 , the phase angle δ was obtained. Hence the exact optical path length at each point of the gap was known.

The value of δ obtained in this experiment, however, was found to be dependent on the degree of smoothness of the porous surface, and also dependent on whether the coating had been worn or not. The results fell between -80^{o} to -40^{o}. The cause of the problem was probably due to the presence of microasperities which prevented true

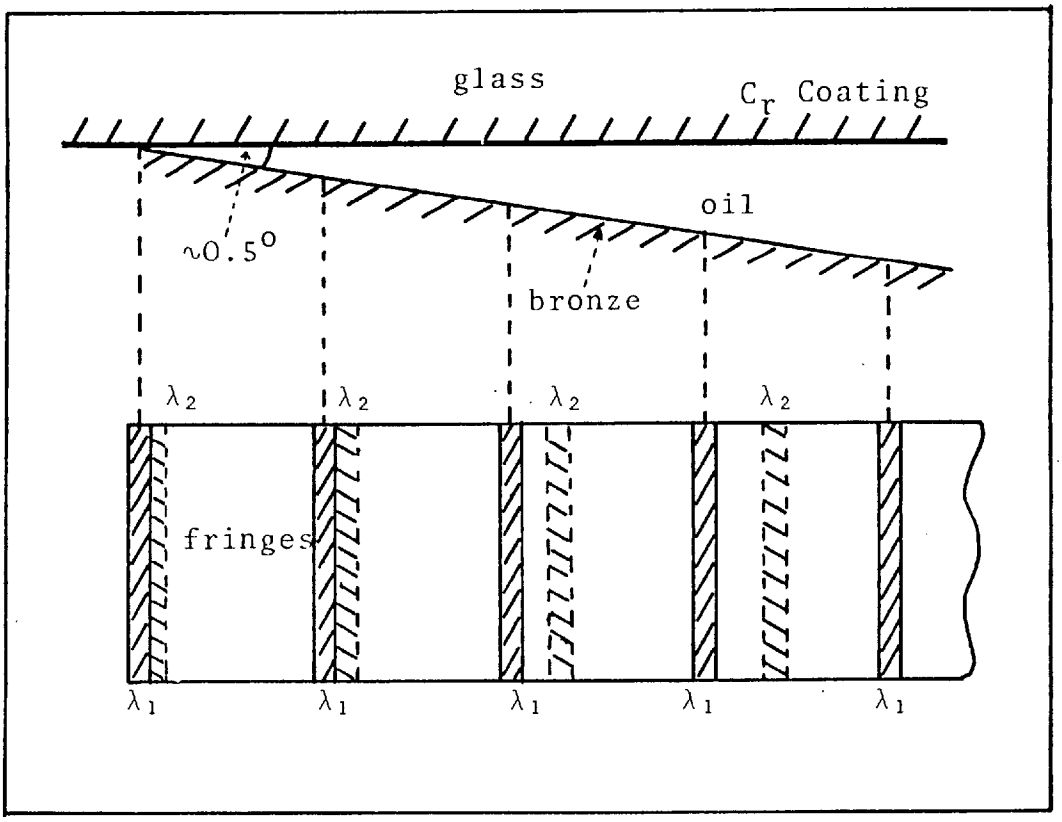

Fig.4.6. Illustration of film thickness calibration

contact being made. Therefore an average value of -60^{o} was adopted; this is comparable to the calibration carried out by Wymer[54] who found it to be -78^{o}. The error introduced by this slight uncertainty of phase angle is considered to be negligible.

Finally the filter was removed to obtain white light interference, from which the optical thickness of the oil film corresponding to different colours of the fringes was found. The results are listed in Table 4.3.

Table 4.3. Film Thickness Calibration

Fringe Colour	Film Thickness (h)
White	>0<2.5 µin
First Yellow	4.5
First Red	7.0
First Blue	9.2
Second Yellow	12.4
Second Blue	16.2
Second Green	17.8
Third Yellow	20·0

4.5. Wetting Mechanism

When a porous sample was first placed in contact with the dry glass disc, the gap did not immediately fill with oil from the pores. Instead, oil was gradually wicked out and spread out over the surface in a certain amount of time, as shown in the series of pictures in Fig. 4.7. To avoid confusion from the fringes, interference was not introduced

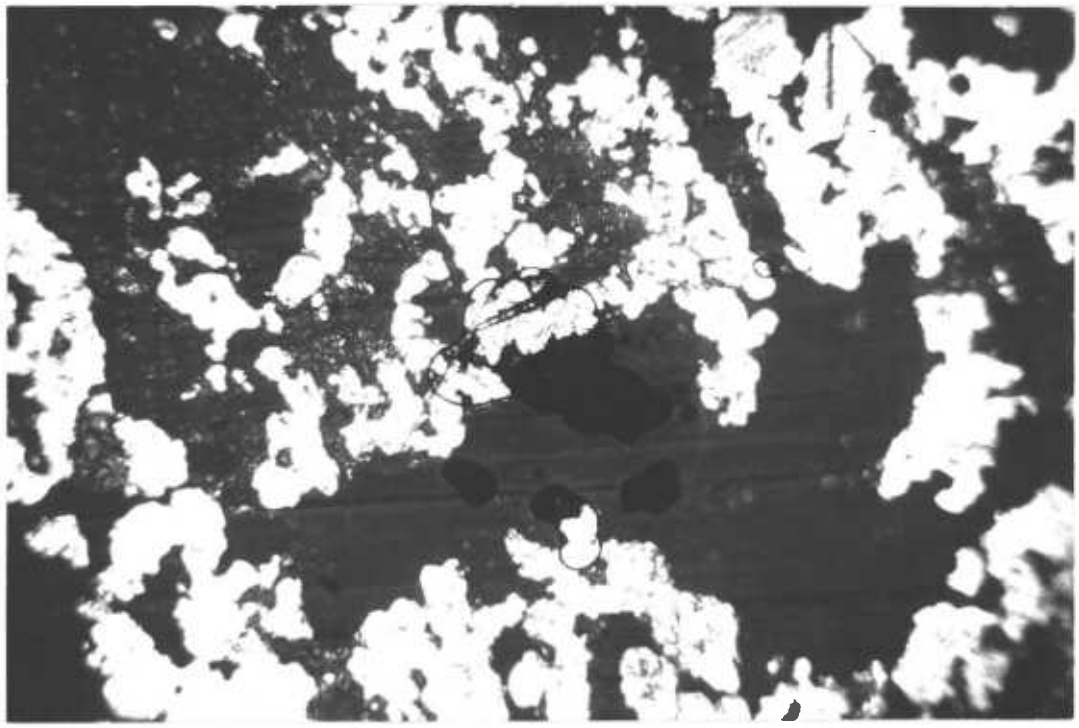

(a) t = 0

(b) t = 1 min.

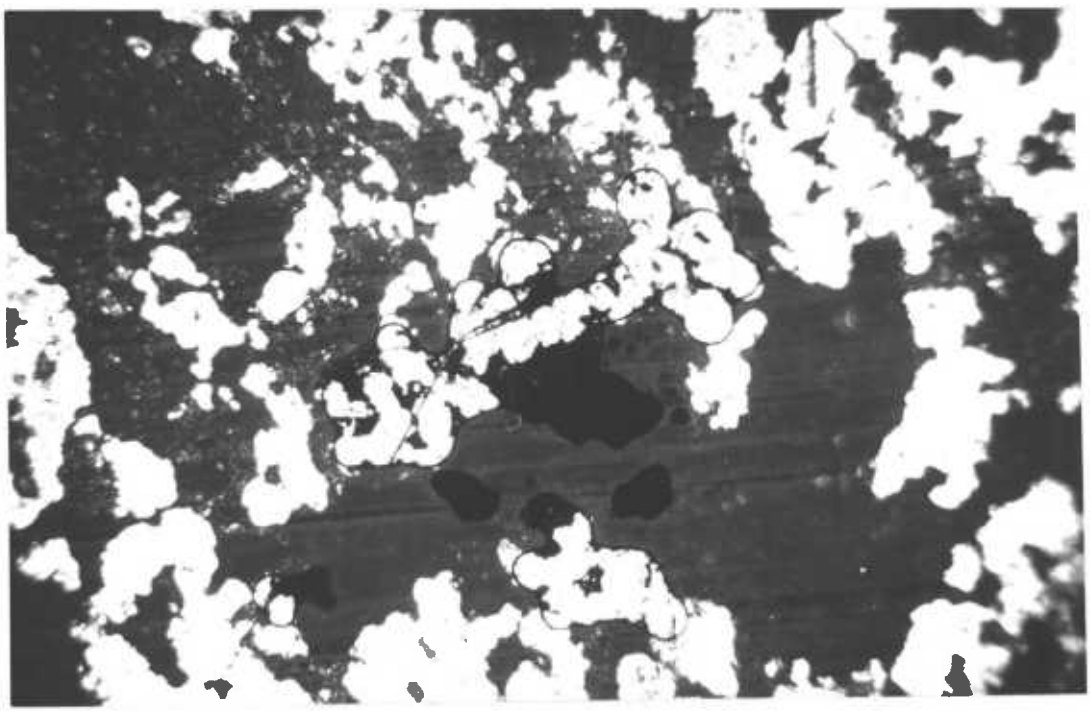

Fig. 4.7 Static contact micrographs, showing the effect of oil wicking, x 150, (continued on next page).

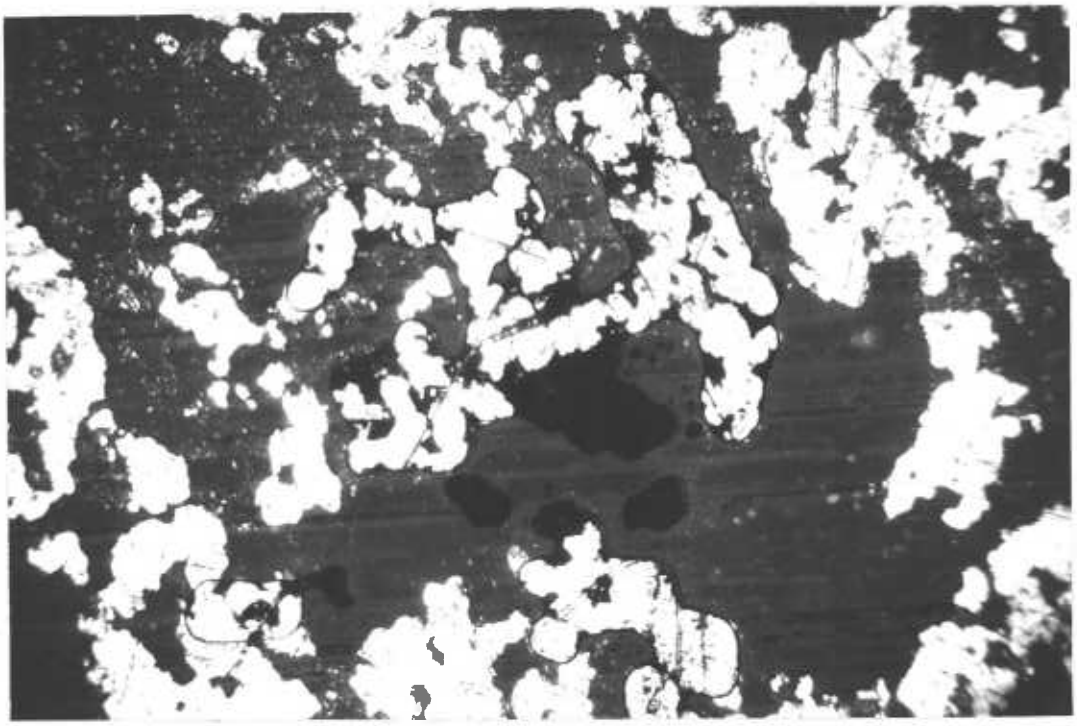

(c) t = 2 min

(d) t = 4 min

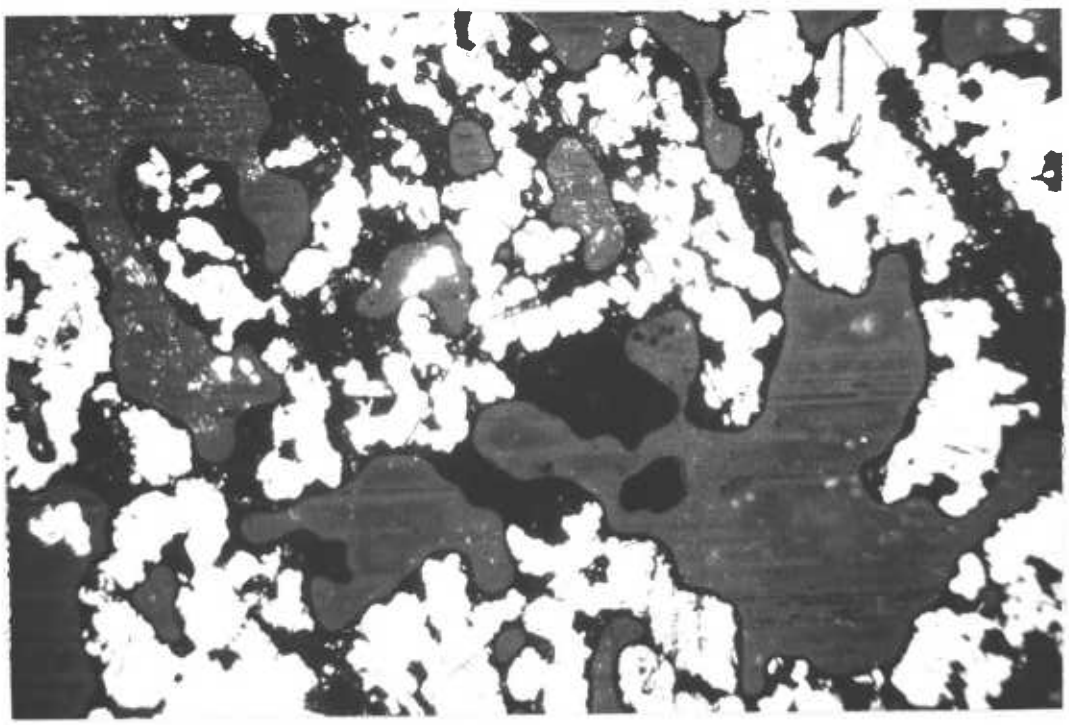

into these pictures. The entire wicking process was always characteristic - a few seconds after contact had been made some tiny patches of oil appeared over some of the lands in the region of closest contact. Then, based on these points, the patches of oil started to spread over the bearing surface along the shape of the lands. Finally, all the lands were surrrounded by a dam of oil. The oil also filled up the gap between the lands and the glass plate. The spreading rate depended on the quantity of oil available in the bearing. For a very starved bearing, as that shown in the pictures, it took several minutes to complete the wicking process, whereas only seconds or even fractions of seconds were required for bearings which were full of oil. Note also in the pictures that some air bubbles were trapped within the pores, but with a fully charged bearing this did not happen, and all the space between the bearing and the glass plate would be filled with oil.

The driving force for this process is obviously the interfacial forces (capillarity) between the media which exist in the contact area, namely, the glass, the oil, the air and the bronze. This can explain the wetting mechanism by which the oil tends to come out from the porous matrix to wet the glass surface. It has been noted that the wetting mechanism has a hystersis effect in that the flow of oil from the porous medium into the contact surface tends to follow a path which has already been established. If such a path could be cut off, or if it had never existed, the oil would remain stationary within the porous matrix.

This follows from the observation that the spreading of the oil did not happen simultaneously to all areas in the contact zone, but instead it began from certain areas which had already had some oil connection between the glass plate and the oil in the pores. Besides depending upon the amount of oil available, the spreading rate may also depend upon the surface tension at the shaft surface, which in practice is dominated by the pressure of the absorbed film. The higher the pressure the larger the wetting force, and hence the faster the spreading rate.

It is therefore concluded that the property of wettability, between the oil and the shaft, tends to draw oil into the working surface at a rate proportional to the amount of oil available in the bearing system. It follows that when oil is lost from the contact zone, this wicking mechanism takes place immediately and replenishes the contact zone with oil from the porous matrix. As will be seen later, this phenomenon plays an important role in the self-lubricating mechanism of porous metal bearings.

4.6. Experiments

The run-in specimens were loaded against the glass plate, with the axis of the cylindrical surface aligned perpendicular to the running direction. The working surface was observed through the microscope. To start with, a thin layer of oil was smeared onto the track on the glass surface in order to avoid the starting procedure damaging the coating. In this case the contact zone was fully filled with oil. At first the contact zone might not

be aligned correctly, as could be seen by the appearance of straight line fringes over the lands. The screws in the specimen holder were then adjusted so that the straight line fringes disappeared, and only a unique order of fringes appeared in the contact zone. In this condition the bearing was said to be well aligned and the clearance thus formed would be similar to that in a real porous journal bearing. The conditions of running were adjusted to be the same as was used during the running-in. The maximum values of load and velocity were 15lb. and 250 ft/min. respectively. According to the different phenomenon which was observed during running, the bearing surface could be conveniently divided into four regions as shown in Fig.4.8. The phenomena are briefly discussed below:

First, in Region A separation occurred in which the gap was filled only with air. The oil in this region remained within the pores, even though its surface was very close to the glass. Sometimes the oil level could be seen to be slightly higher than the average bearing surface.

Secondly, in Region B the space was completely filled with oil, and between Regions A and B oil could be seen to be being pumped from the porous matrix towards the gap.

Thirdly, the phenomena which happened in Region C were completely different from the other parts of the bearing. Here the two surfaces — the glass disc and the bearing — were more or less parallel. This is partly because of the effect of wear during the running-in process described above, and partly because of the

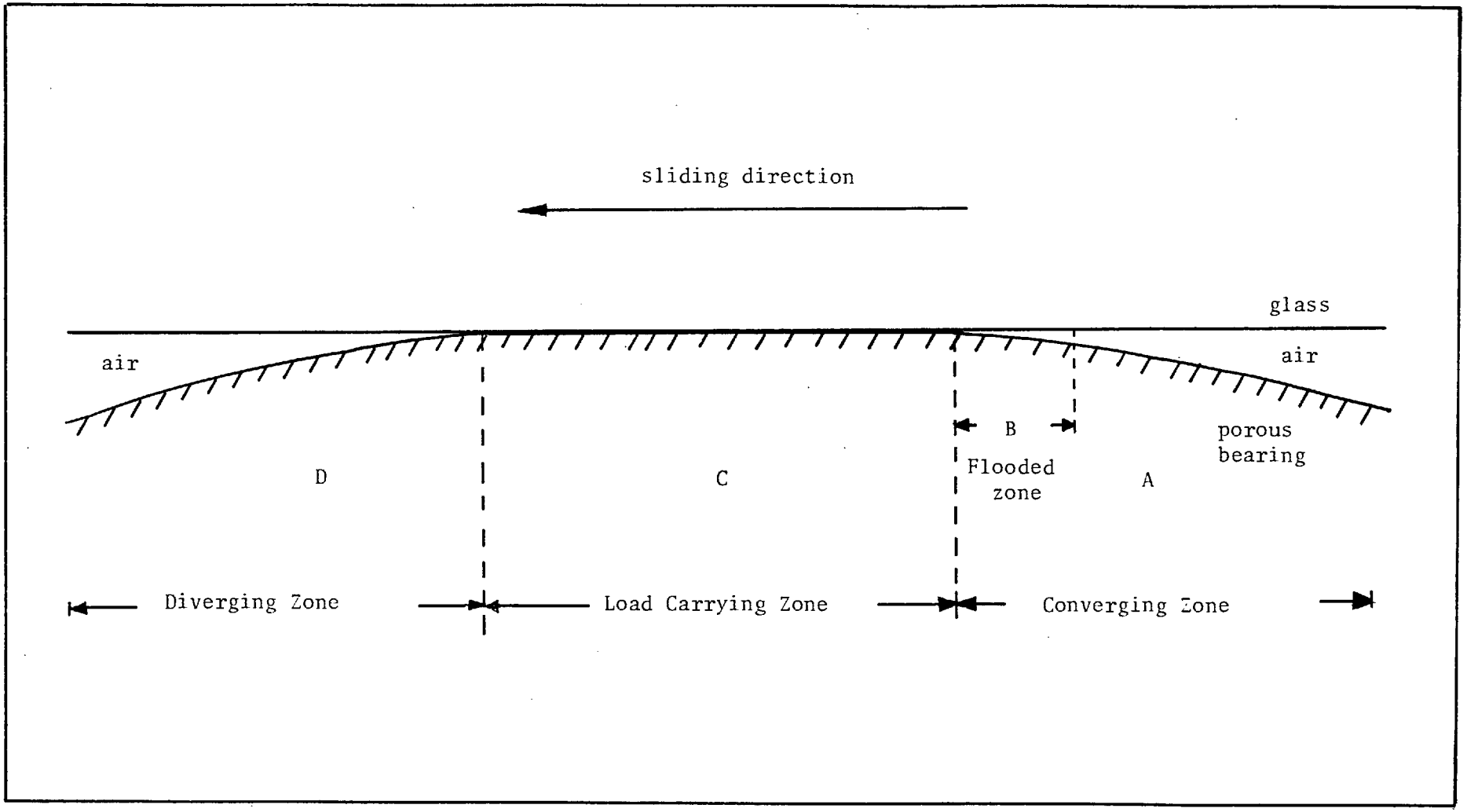

Fig. 4.8. Division of zones on the porous surface.

Hertizan deformation of the bronze material under the applied load. It is important to note that this region contributed to almost all of the load capacity of the bearing.

Fourthly, in Region D the same separation as in Zone A occurred, except that the oil in this region remained quite deep inside the pores, and that the amount of pumping was very much less than that in A. Details of these phenomena are discussed separately in the following chapters.

CHAPTER FIVE

LOAD CARRYING ZONE

5.1. Introduction

The area of this zone depended on how far the running-in process had taken place. For example, after one hour of running-in, this zone had a dimension of 0.15" long and 0.5" wide, this being the full diameter of the cylindrical specimen, and situated at the central part of the cylindrically domed surface. Due to the polishing effect of the running-in process, most of the area in this zone was flat and was substantially parallel to the glass plate. Only a very small region in the inlet and outlet of the zone exhibited signs of the original curvature of the surface.

This zone is considered to be carrying all of the applied load, because under normal conditions only this zone showed the existence of the hydrodynamic oil film that separates the bearing and the glass surfaces. Other zones of the bearing were merely separated from the glass plate by a gap of air. A typical high speed interferogram of this zone in operation is shown in Fig.5.1. Though this picture covers only a small part of the zone, the extension to other parts would be straightforward. In this picture there are four things to be noted. First, the cavitation which has developed immediately behind each land (or group of lands). Secondly, in front of the land (or group of lands), there is a dam of oil. Thirdly, the oil in the dam leaks downstream via the sides of the lands. Fourthly, over each land a hydrodynamic

lubricating film has formed. These penomena were almost the same whether the bearing were fully charged with oil or running under starvation conditions. The only difference being that the length of the oil dam tends to decrease as the amount of oil available in the system is reduced. Another high speed interferogram is shown in Fig. 5.2. The details of this zone are discussed separately in the following.

5.2. Cavitation

5.2.1. The Formation of the Cavity and its Properties

Before discussing cavitation in porous bearings, it is desirable to see some of the properties of cavitation in nature: The tensile strength of a liquid is quite low. A pure liquid can usually sustain tension of about one or two atmospheres. At higher tensions it begins to 'boil' and generates bubbles. There are two kinds of cavitation, namely, gas (air) filled cavitation and vapour filled cavitation [57]. The latter is formed by the vapourisation of the liquid when the pressure is reduced to below its vapour pressure. If the liquid contains some dissolved air, however, some of this air may come out of solution and form a gaseous cavity at a pressure which is much higher than the vapour pressure [58]. Some microscopic nucleii such as solid particles or ions in the liquid, may also cause cavitation at pressures above the vapour pressure [59]. The famous 'Bubble Chamber' in nuclear physics is one of the successful applications of

Fig. 5.1 Interferogram of load carrying zone, x 250.

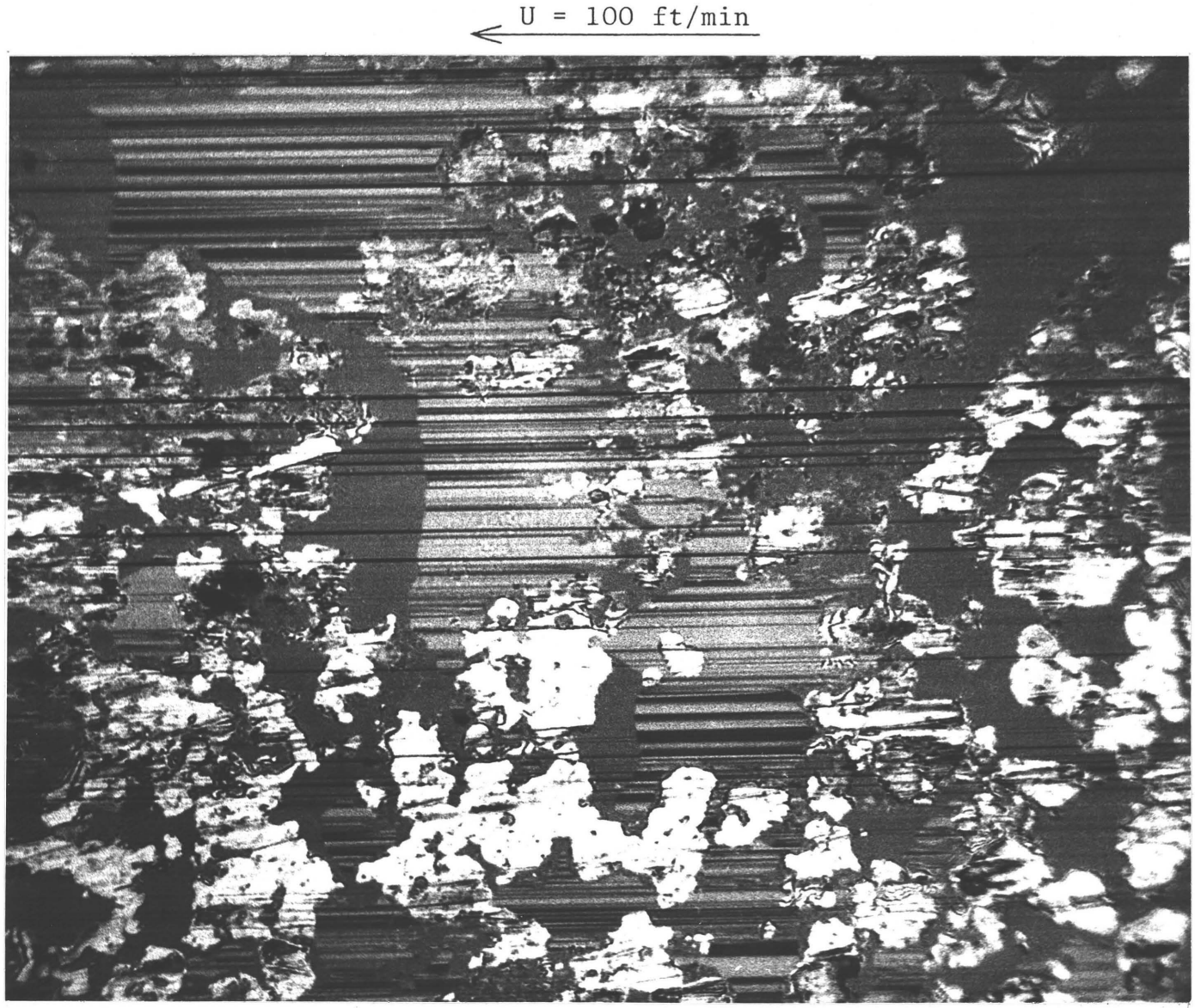

Fig. 5.1 Interferogram of load carrying zone, x 250.

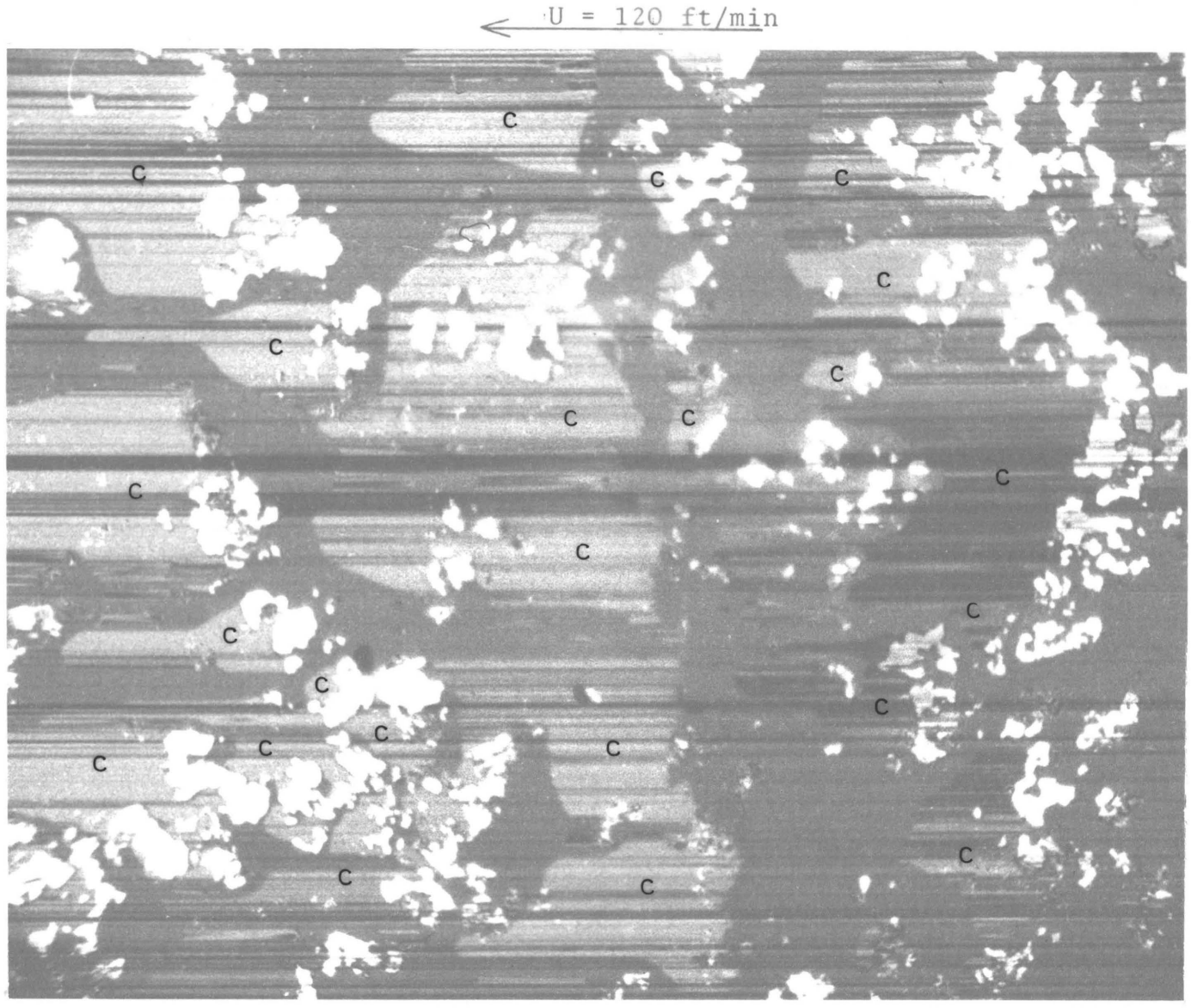

Fig. 5.2 Interferogram of load carrying zone from another porous specimen, x 250.

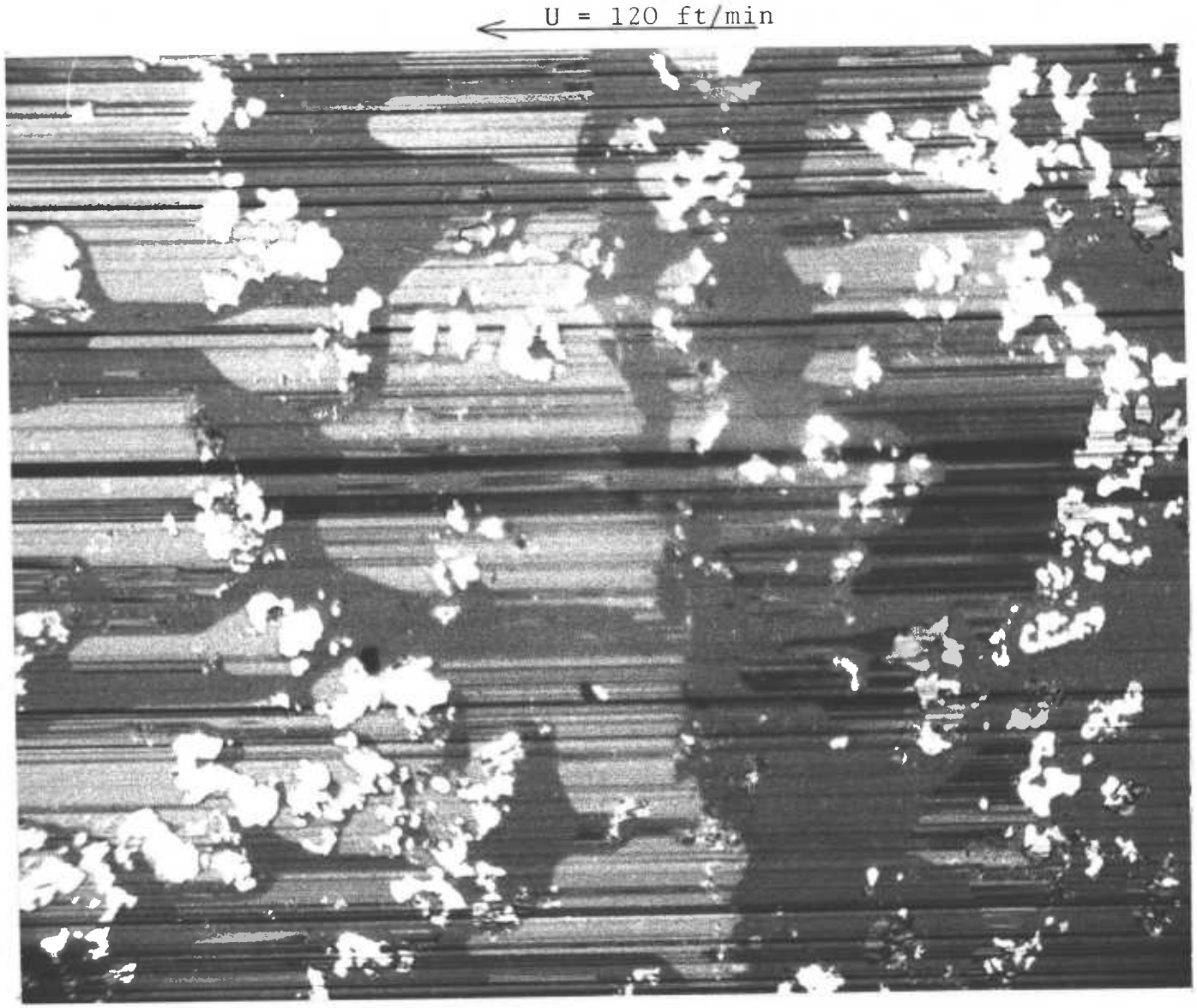

Fig. 5.2 Interferogram of load carrying zone from another porous specimen, x 250.

this effect.

With a spherical bubble there is a balance between the pressure, p_1, within the bubble, and a pressure p outside, so that $p_1 = p + \frac{2\sigma}{R}$ where σ is the surface tension and R is the radius of the bubble. This is the Laplace equation for a cavity in static equilibrium. It follows that the balance of the forces in a vapour bubble is unstable because a slight decrease in R leads to its collapse, and vice versa [60]. The driving force for this is the surface tension. Thus the formation and collapse of vapour bubbles is an explosive process. In particular, during the collapsing process extremely high pressures, of the order of 10^3 to 10^4 atmospheres are generated [61]. The shock waves and microjets [62,63] associated with these high pressures can cause damage to solid materials, and is known as cavitation erosion [64,65]. However, the intensity of the explosion can be greatly reduced if some gas is introduced into the cavity. The growth of a gas bubble involves the diffusion of the dissolved gas into the cavity and this is a much slower process. For a liquid which is just saturated with dissolved gas, the bubble will grow to a certain size, and then remain stable. The size to which the bubble will grow is quite critical, and if the nucleus is too small, say, less than 10^{-3} or 10^{-5} cm. in diameter, the force of surface tension tends to make the bubble collapse. Cavitation also exhibits properties of hysteresis [66], that it disappears at a higher pressure than that at which it first appears. The ability of a liquid to withstand high tension can be extended by high purity and pre-

pressurisation. Anti-foam additives can only break foam but cannot break bubbles [67].

In a flowing fluid, cavitation forms at points of highest velocity, where low pressures can occur. In a bearing system where the boundary layer is very thin, minute surface irregularities can cause spots of cavitation [68]. Zones of local separation also develop minute eddies in the boundary layer in which cavities can also be produced.

5.2.2. Cavitation In Porous Bearings

Cavitation is found to be a very general phenomenon in the operation of porous bearings. It occurs in most of the pores within the load carrying zone, regardless of the type of oil used. There are two important points to be noted. First, at atmospheric pressure oil can dissolve about 8% of air. Therefore, when the oil suffers a sudden drop of pressure, the air probably comes out of solution and thus causes cavitation, or perhaps more accurately, rupture of the oil film. Secondly, there is a discontinuity of tangential velocities between the oil in the film and the oil in the porous medium, the so-called slip flow. This would result in a ~~high~~ shear stress to the oil immediately behind the pores.

At extremely low speed, say .5 ft/min (2.5 mm/s), small bubbles begin to appear within the pores. The larger the pore, the more likely it is that cavitation will occur. At the beginning the cavitation appears in the middle of the pores, but as the speed is increased, the bubbles extend in width in both the upstream and downstream

directions, forming the shape of streamers. The upstream growth is limited by the rear edge of the land whilst the downstream growth ceases at a certain distance in front of the next land.

5.2.3. Cavitation at Low Speed

An interesting feature of bubbles at low speed is that they exhibit the same effect as is found is elasto-hydrodynamic lubrication. The EHD theory has been fully developed [69,70,71] and has been used to explain many lubrication problems such as gear teeth, cams and roller bearings. The theory is based on the fact that under high contact loads the contact surface suffers from appreciable local elastic deformations and the viscosity of oils increases with pressure. Thus, the film shape, as well as the pressure distribution, are completely changed. In brief, the lubrication of high pressure contacts can be regarded as a combination of two mechanisms, the elastic deformation of the contact surfaces and the establishment of hydrodynamic lubrication. The theory applies very well to cases where steel, or other metals, is used as the bearing element and oil is the lubricant. However, it was found here that the theory applied equally well to the case where an 'air bubble' is the bearing material and oil is the lubricant.

A bubble can be regarded as a spherical 'ball bearing' made of gas and loaded against the glass plate by the buoyancy force. The amount of load is of course dependent on the size of the bubble. The upper part of

the 'gas ball bearing' thus suffered from 'Hertizan' deformation. When the disc moves, the 'gas bearing'is lubricated elasto-hydrodynamically by the layer of lubricant which is generated between the glass plate and the bubble. So the bubble deformed just like that of a solid but elastic ball and the characteristic spike of EHD lubrication developed at the exit, as is shown in Fig.5.3. The thickness of the lubricant film increased with speed. However, as the speed was increased further, the bubble grew to a much larger size, and eventually at high speeds it no longer behaved like a 'ball bearing' and the EHD effect ceased.

Further, according to the EHD theory, a concave surface should develop on the bearing surface when the disc is stopped, and within it some oil should be trapped [72]. This oil can only leak out very slowly, via scratches on the surface. The bubbles formed in porous bearings exhibit this same property, as is shown in Fig.5.4. About 10 minutes after stopping, the oil had leaked away completely, leaving the top surface of the bubble in direct contact with the glass surface. The velocity at which the air bubbles exhibited this EHD effect was extremely low. Therefore, these phenomena are mainly of academic interest and probably contribute nothing to the general operation of porous bearings, which usually run at higher speeds than this.

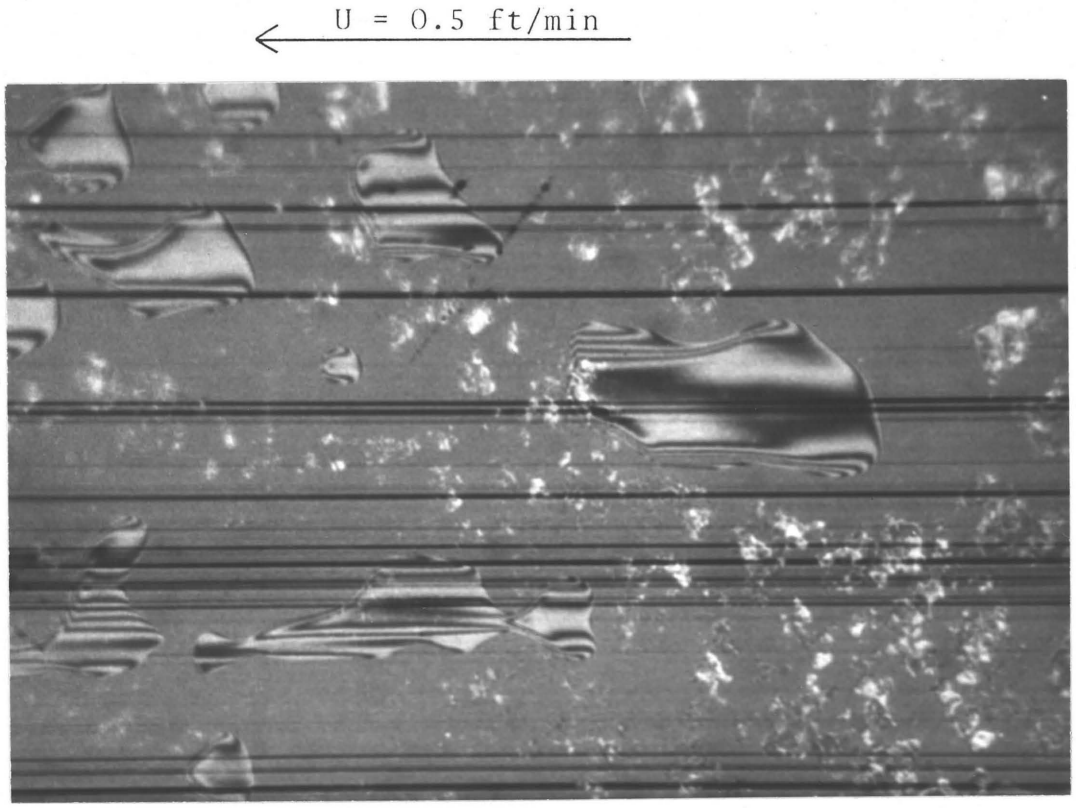

x 180

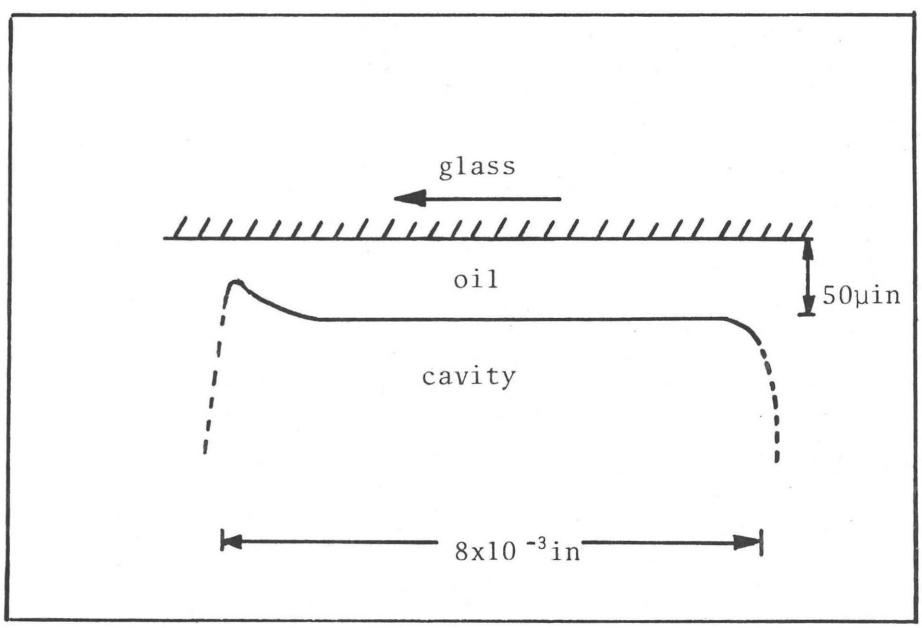

Fig. 5.3. Cavitation (top picture) and its profile at low speed, showing EHD effects.

(a)
t = 0

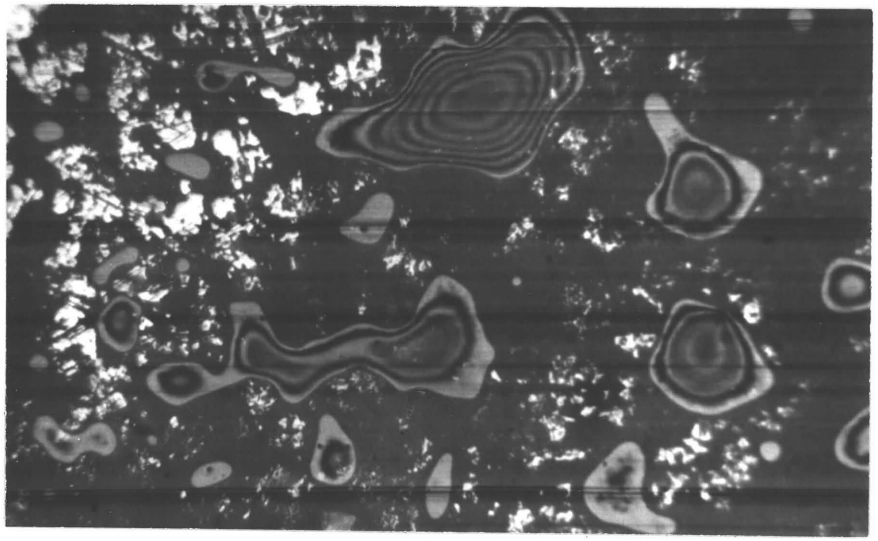

(b)
t = 10 min

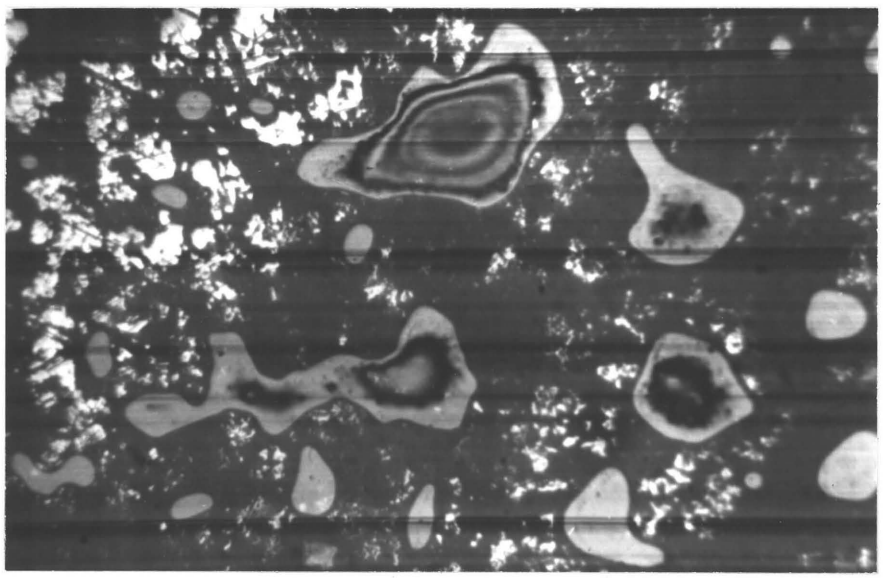

(c)
t = 30 min

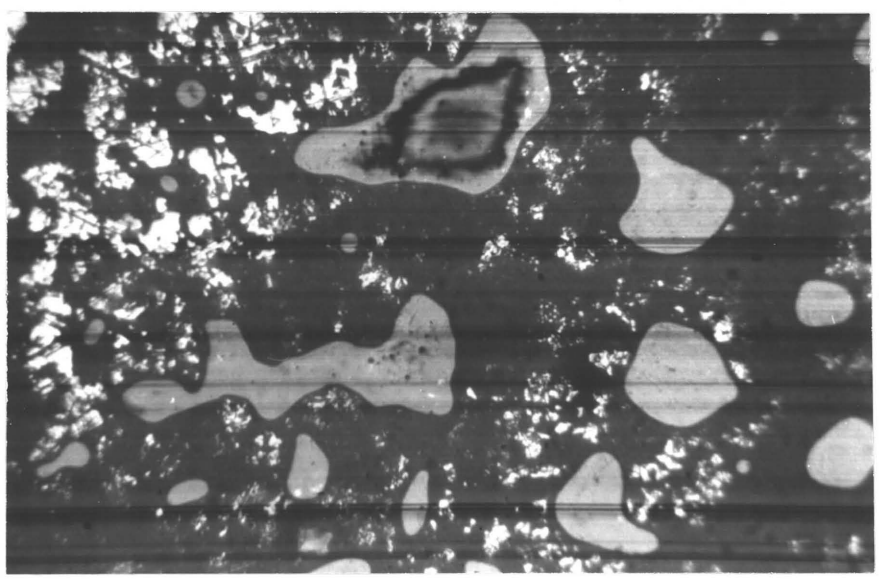

Fig. 5.4. Fluid entrapment within bubbles. The oil leaked out into the surrounding region gradually, x 180.

5.2.4. Cavitation at High Speed

At high speed (e.g. U > 40 ft/min = 200 mm/s) the cavitation became stable and was virtually unaffected by further increases of speed. The cavitation behaviour in this case was entirely different from that at low speed. At high speed the cavitation began immediately behind the land and occupied about 4/5 of the pore length. Unlike the cavities in the low speed regime, where only gas filled cavitation (air) occurred, at the higher speeds both types of cavitation (i.e. gaseous and vapour) existed side by side. This is because at the higher speeds the pressure became so low at some points that true vapour cavitation occurred. This fact was verified by stopping the motion of the disc suddenly. The vapour filled cavities were observed to vanish completely within a fraction of a second, whilst the gas filled cavities, or those with both gas and vapour, collapsed only partially to a smaller size and then remained stable.

Nevertheless, there are indications that the collapse of vapour cavitation in porous bearings will not give rise to erosion for the following reasons:- First, the amount of vapour cavitation is small compared with the amount of gas cavitation, or mixed cavitation. Secondly, the cavitation is happening at the upper part of the fluid, where the ambient pressure is not high.

In Fig. 5.1 it will be seen that there are fringes over the bubble regions. These are caused by the hydrodynamic film which is formed on the surface of the upstream land. Since the velocity profile of the film of fluid over the land is approximately triangular, and since

it is rectangular over the pore, the thickness of the oil film on the top of the cavity must be about half the thickness of the oil film on the land immediately upstream of it.

5.3. Dam of Oil

Oil dams are associated with most of the lands in zone C. Within the pores (between the lands) the cavitation and the oil dam exist side by side, with the cavitation at the exit and the dam at the entrance end of each land. The ratio of their lengths appeared to depend upon many factors, such as the quantity of oil available, the pore size, the land shape, etc. In an equilibrium running condition, the length of the dam did not appear to vary in the short term, but in the long term it decreased gradually as the bearing gradually lost oil. For example, in the flooded condition the dam occupied about 60% of the pore length, and this reduced to about 20% with continuous running. Under oil starvation conditions, the dam length became even shorter but it seemed that (unless the system was completely starved of oil), a dam of finite length was always formed.

5.3.1. Formation of Dam

There are two forces acting on the oil at the bearing surface which can directly affect the length of the dam. The first one is the viscous shear force caused by the motion of the shaft. This force tends to drive the oil downstream. The second one is the interfacial force, which causes the oil to wet the shaft surface. The static case of this force has been demonstrated in Chapter 4.5. A careful study of the dam system has led to the conclusion that it is the balance of these two forces which gives rise to the formation of the dam. The principles involved are discussed as follows:-

For simplicity consider first an arbitrary dam somewhere in the contact zone. There are two ways in which the oil can get into the dam. One way is from the hydrodynamic film which is formed on the upstream land, and is transferred by the motion of the glass disc through the cavitation zone to be injected into the dam. The second way is via the wetting mechanism bringing oil from inside the pores onto the surface. On the other hand, there are three ways in which the oil can leave the dam. The first is via the hydrodynamic film on the land downstream of the dam. The second way is by side leakage around the two sides of the land. The third way is downwards into the porosity. Each of these ways has its own flux rate, which is dependent upon several factors, such as the shape of the lands, the wettability of the metal, the film thickness, etc. Changes to any of these flux rates directly affect the dam length from completely filling the pore to almost zero length. For example, when the oil

supply rate is larger than the drain rate, the dam length is increased and some of the oil is probably flowing down into the pores; and vice versa. Under stable running conditions the dam length was found to be almost constant, indicating that an equlibrium condition had been established, with the supply rate equal to the drain rate. In the load carrying zone the hydrodynamic oil film thickness over each land is approximately the same and independent of the dam length. This means that the amount of oil which is attached to the glass disc leaving and entering the dam is the same. Add to this the fact that the oil in the dam is constantly leaking downstream via the sides of the land, we are immediately led to the conclusion that some of the oil in the dam must be coming from inside the porous matrix.

The principle mentioned above had been proved by several observations. One of these is discussed here, and the others are presented in the following sections. The hydrodynamic film thickness over two adjacent lands, arranged along the running direction, was carefully studied. Under stable running conditions the film thickness over the two lands was found to be the same and the length of the two dams was noted. The relative thickness of the film over the two lands was then deliberately changed, by tilting the specimen slightly (or it could be done by introducing a small amount of up and down wobble to the rotating disc). It was found that when the thickness of the film over the upstream land was thicker, the dam in front of the downstream land increased in length, and vice versa.

5.3.2. Effect of Starvation

Since the supply rate of oil due to the wetting mechanism increases with the degree of saturation, it follows that under oil starvation conditions the length of the dam must be shortened correspondingly. This fact was proved by pressing a piece of absorbent tissue against the glass plate so that some of the oil attached to the plate was continuously wiped away. This action progressively produced starvation conditions and is equivalent to the aging of the bearing in a practical case. The first result was that the dam length gradually decreased, but then it soon became substantially constant and this lasted for quite a long time (e.g. 5 to 10 minutes). An important aspect of the oil wicking mechanism was then discovered. After this starved condition had been created, the tissue was removed and the length of the dam was seen to increase, until finally it reached a new equilibrium state in which the length was longer than that before the removal of the tissue, but of course shorter than it was before the test was begun (Fig.5.5).

5.3.3. Effect of Flooding with Oil

By suddenly adding a drop of oil into the inlet, the surface reacted instantaneously in several ways: First, the thickness of the hydrodynamic film over the lands increased by a factor of 2 or 3. Secondly, the frictional torque decreased. Thirdly, the length of the dam increased. But these were only transient effects, and a stable condition, similar to that which existed before the addition

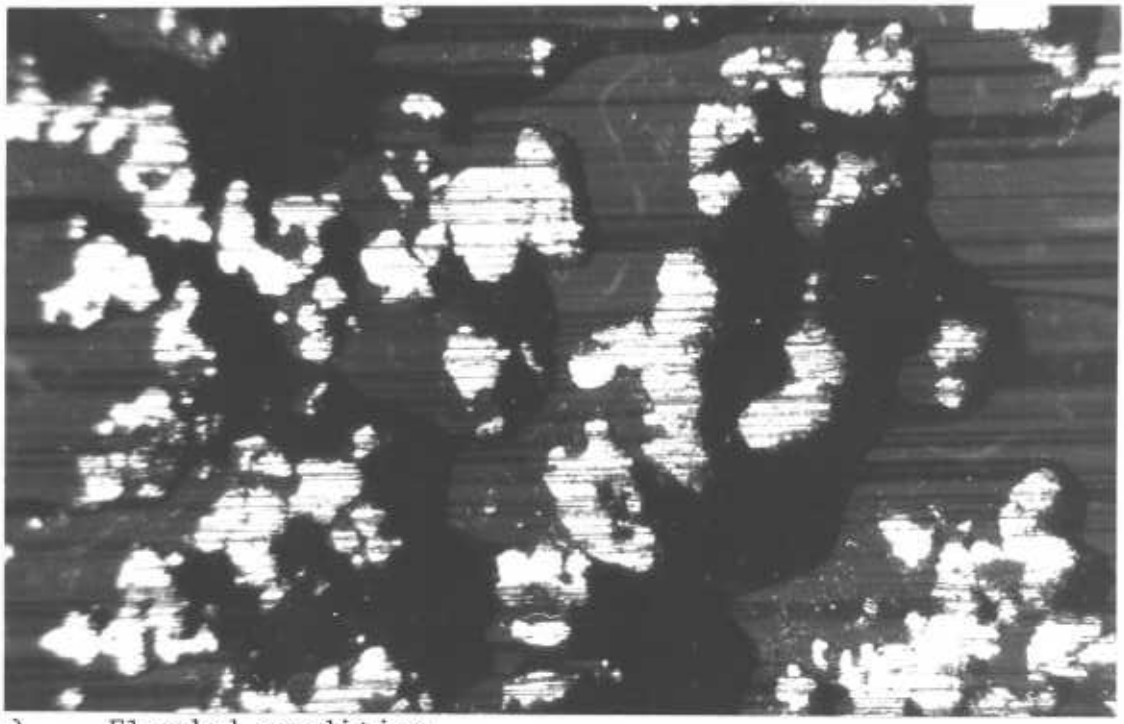

(a) Flooded condition

(b) Starved condition

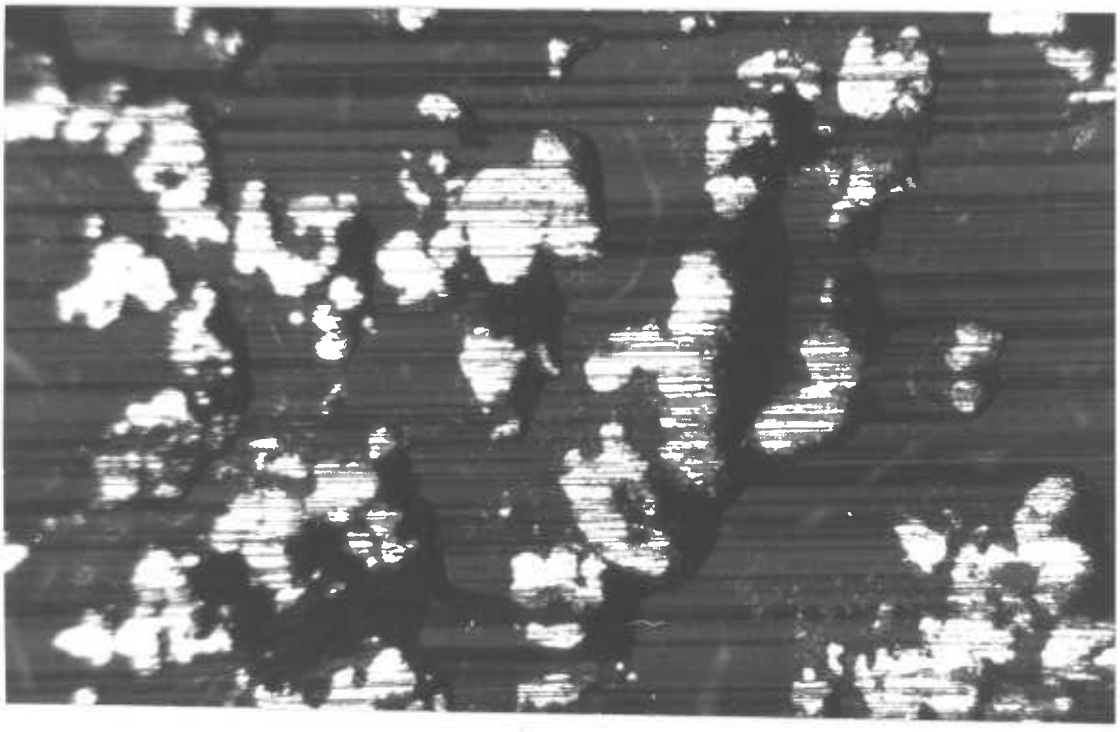

Fig.5.5. Effect of starvation on the oil dam, x 280.

of the oil, was gradually attained, with the length of the dam being slightly longer than it was before. The time during which these disturbances happened and settled down was of the order of several minutes.

5.3.4. Self-Lubrication Mechanism

We may now draw a clear picture of how the porous bearing manages to lubricate itself. The bearing system has the ability of self adjustment on its function, so that only a suitable amount of oil is maintained in the working surface. The system will reject any extra oil by simply pushing it away into the porous matrix,and when the amount of oil in the surface is insufficient it will adjust itself so that the oil held within the porous medium will come out and wet the surface for lubrication.

5.4. Other Factors Affecting the Dam

5.4.1. Effect of Land Shape

Fig. 5.6a shows how the oil in the dam leaks downstream. The oil which leaks away around the sides is eventually injected into the dam in front of the next land. This process of a cascade of oil from land to land continues until the end of the contacting surfaces. A land with a convex edge facing the dam has less ability to hold the oil in the dam than a land with a concave edge with which the dam is both longer and more stable. It is not unreasonable to speculate that the longer the dam, the higher

may be the hydrodynamic effect and hence the better the performance of the bearing. Although there is no evidence yet to support this theory, it would follow that it would be better not to have convex shaped lands. In practice it has been found that a porous bearing which is made from strictly spherical powder has much worse performance than that with powder of random shape [44]. This observation is consistent with this theory, although there could be other explanations.

Further, since the longitudinal dimension of a land does not affect the length of the dam, it follows that it would be better to have lands elongated perpendicular to the sliding direction than to have them parallel to it. The compacting action during the pressing of the powder tends to create lands which are elongated parallel to the direction of rotation of the shaft; whilst the action of the sizing tool is to smear the surface lands so that they tend to be elongated perpendicular to the direction of rotation. During the running, the shaft tends to smear the lands so that they are elongated parallel to the direction of rotation.

5.4.2. Effect of Land Size

For a given porosity the bearing can have either a large number of small lands and pores, or a small number of large lands and pores. For the wetting mechanism to be most effective, a large number of small lands and pores is to be preferred. This is because each individual land can be associated with its own dam of oil, and more lands

means more places for a dam to develop. The consequence of this effect has been observed in industry [44], that, for some applications, a bearing tends to perform better with a larger amount of small lands and pores than the opposite. But it should be noted that small pores will be closed more easily by metal smearing and hence there is a limit to the minimum size of lands and pores for optimum overall performance.

5.4.3. Effect of Land Distribution

The concept that a land with a concave leading edge should reduce the amount of oil lost from the dam by leakage around the sides can be extended to a macroscopic view. When several lands are distributed so as to present a concave configuration they preserve much more oil in their joint dam than when they are acting separately. This effect is shown in Fig.5.6b. Therefore it is not only the microscopic scale but also the macroscopic scale of the land distribution that can affect the build up of oil dams.

The importance of a dam of oil in front of every land is not easily seen when there is a flood of oil, because there is no problem getting enough oil to lubricate the lands. However, during the bearing's life the amount of oil available is reduced and the only way oil is supplied to the working surface is the wetting mechanism —— capillarity. Hence, when the rate of oil supply is reduced and the rate of oil loss from the dam around the sides of the land is still large, there could be insufficient oil

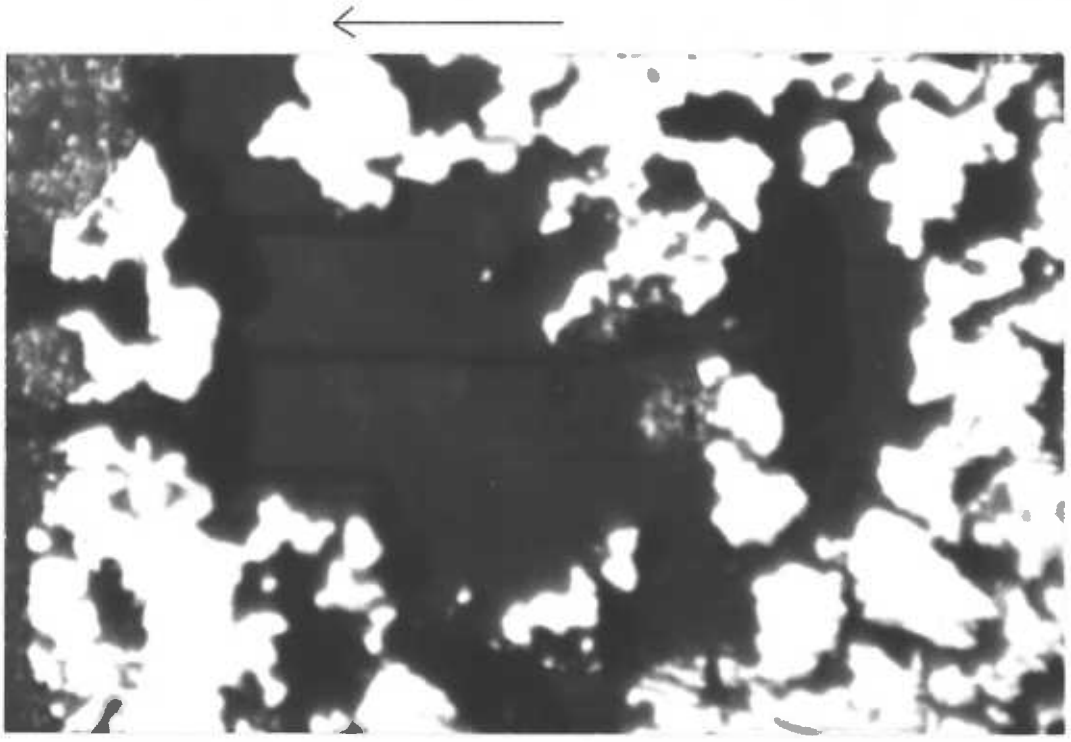

(a) x 600

(b) x 280

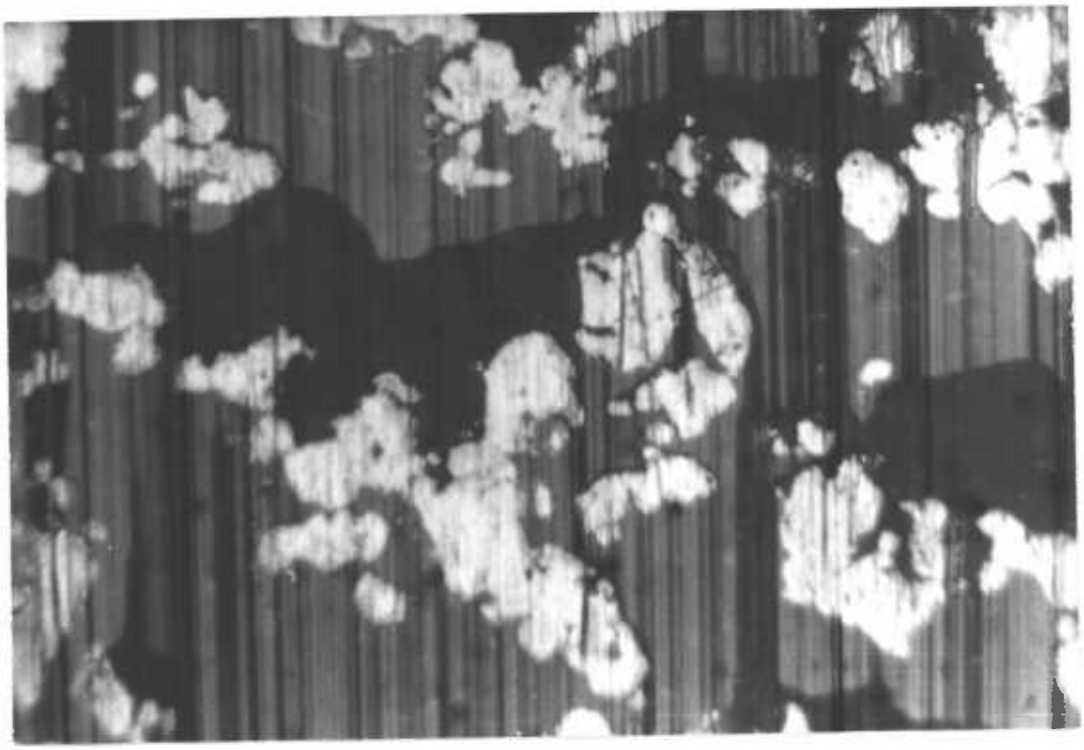

Fig.5.6. Effect of (a) side leakage and (b) land distribution on the oil dam.

in the dam for the building-up of the hydrodynamic film.

If the direction of the shaft is reversed, the oil dam again forms in front of the land (the space which was previously a cavity) and the cavitation forms behind the land. Hence the porosity and the lands to not care which way the shaft is moving. Fig. 5.7 shows the effect.

5.4.4. Limitation of Wetting Mechanism

The wetting mechanism is not only affected by the quantity of oil available but also the property of hysteresis, which has already been discussed in Chapter 4.5. The action of this principle has been observed in the experiments. A land having a convex leading edge with a small radius of curvature (or a land which was slightly lower than the surrounding lands) did not have any signs of a dam associated with it. The oil around these lands stayed within the pores. This special characterisation can affect the bearing such that only those areas in the zone of closest approach to the shaft receive enough oil to participate in the load carrying action.

5.5. Film Thickness Measurement

The variation of the hydrodynamic film thickness over the lands was measured using white light interferometry. The measurement was made by monitoring the colour of the fringes and at the same time recording the sliding velocity of the disc. Fig.5.8 shows the building up of

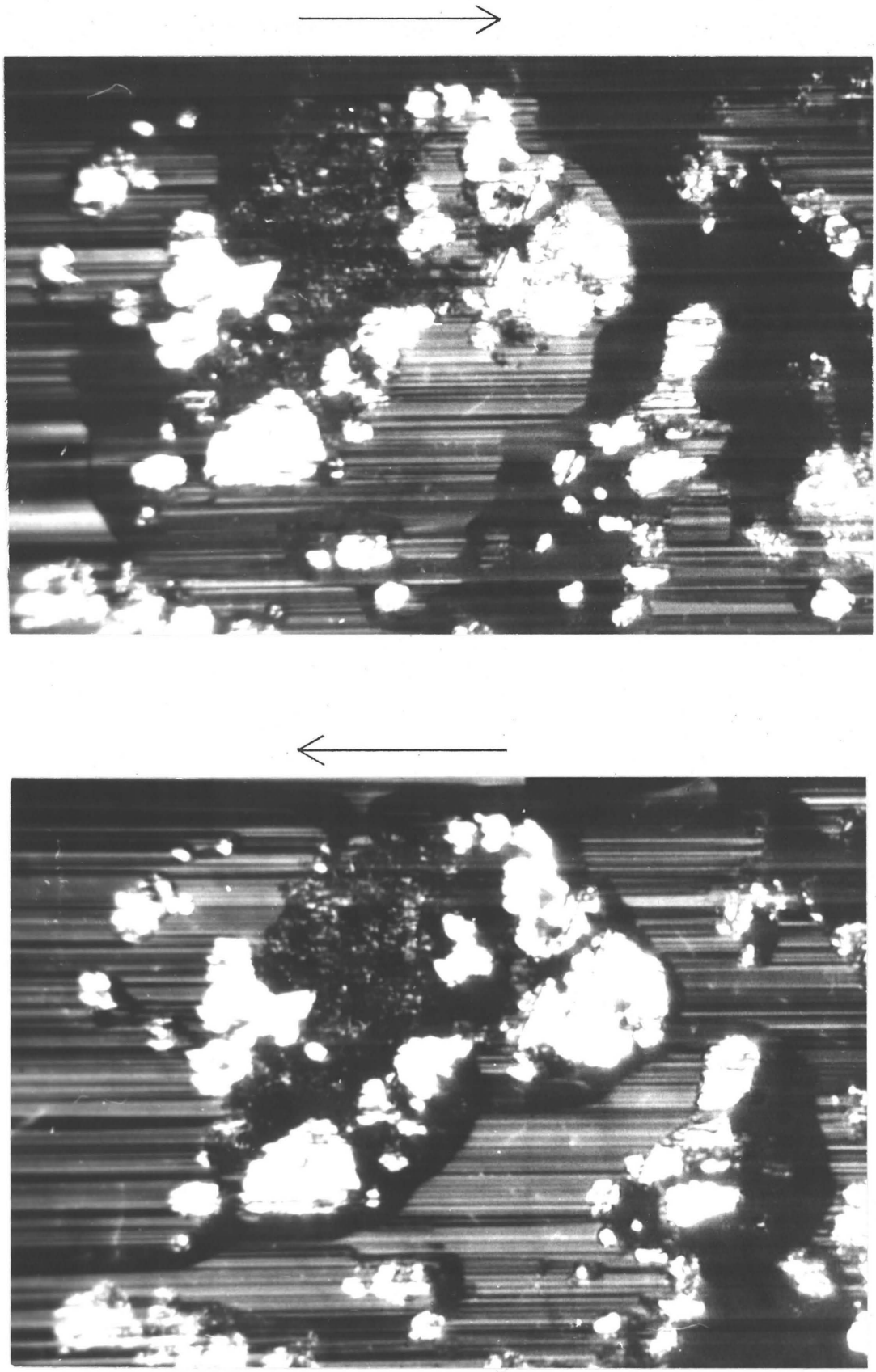

Fig. 5.7. Effects of reverse running, x 300.

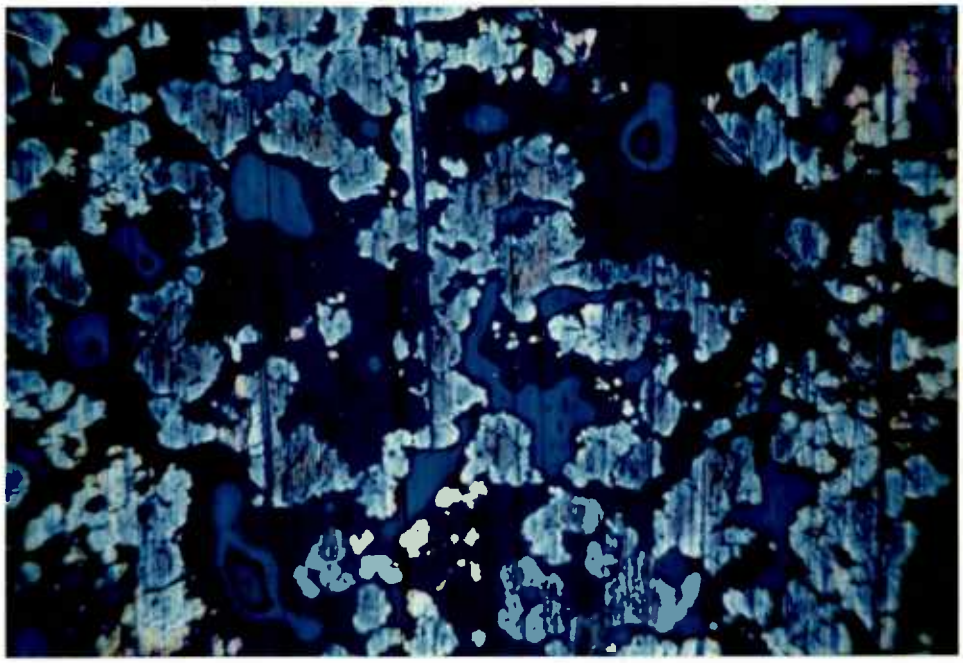

(a) U = 0 h ≃ 0

(b) U = 10 ft/min, h ≃ 2μin

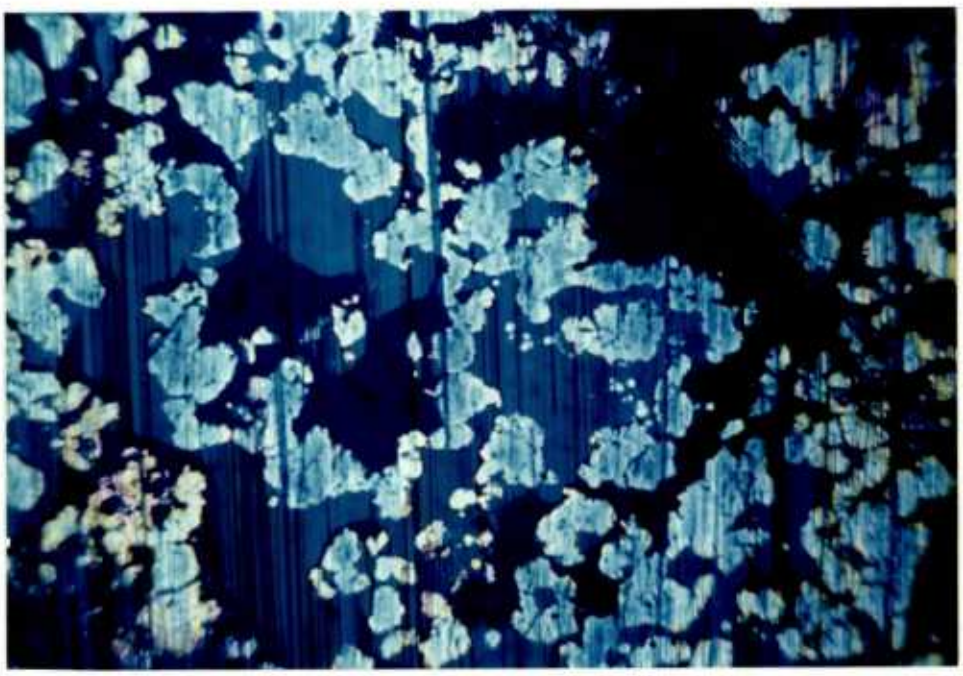

Fig. 5.8. Interferogram of load carrying zone, showing progressive increase of hydrodynamic film thickness as speed increased, x 180, (continued on next page).

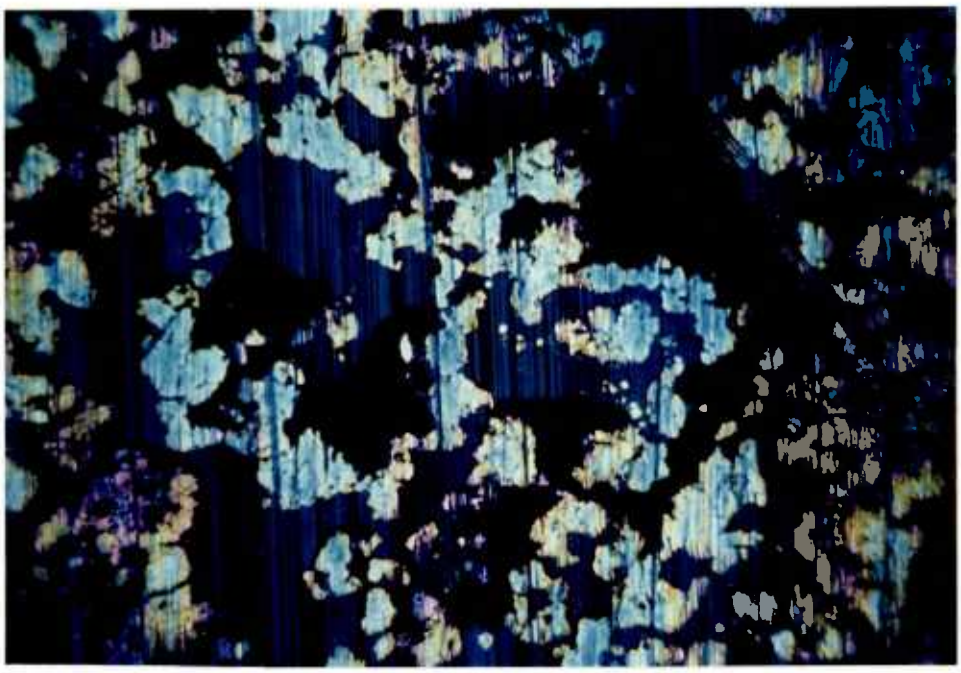

(c) U = 25 ft/min, h ≃ 4.5μin

(d) U = 70 ft/min, h ≃ 8μin

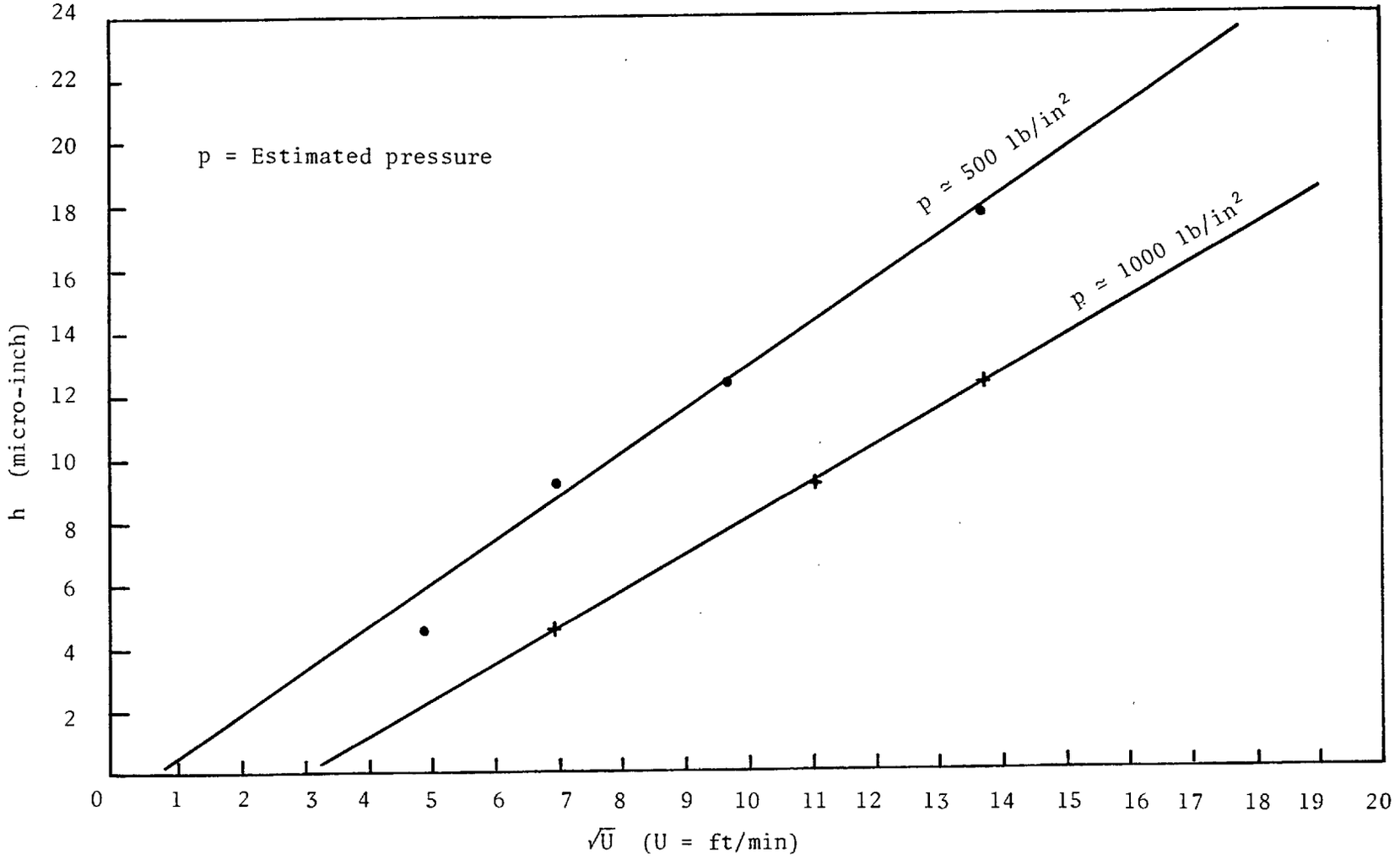

Fig. 5.9 a. Film thickness versus square root of speed.

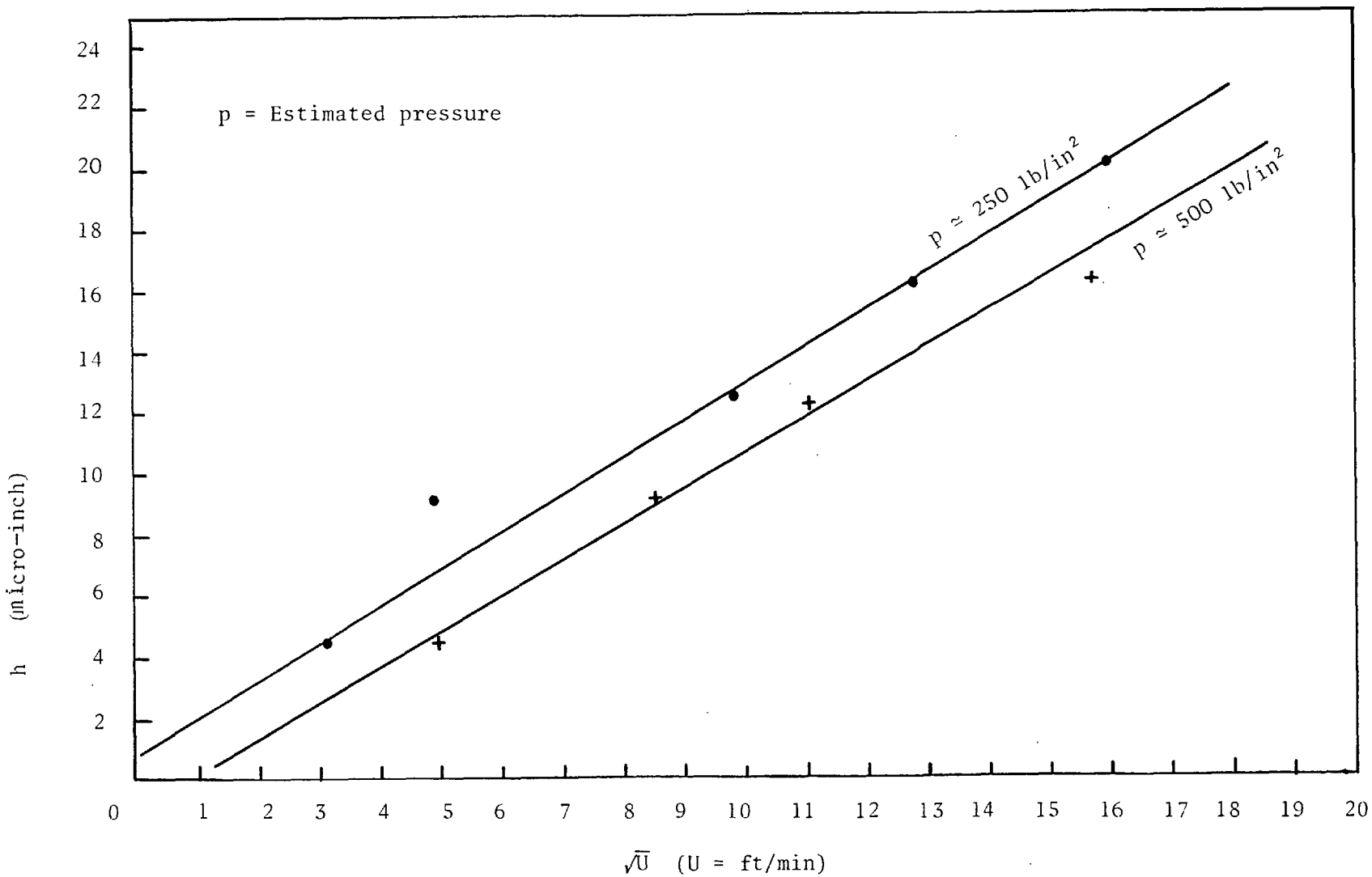

Fig. 5.9 b Film thickness versus square root of speed measured from another porous specimen.

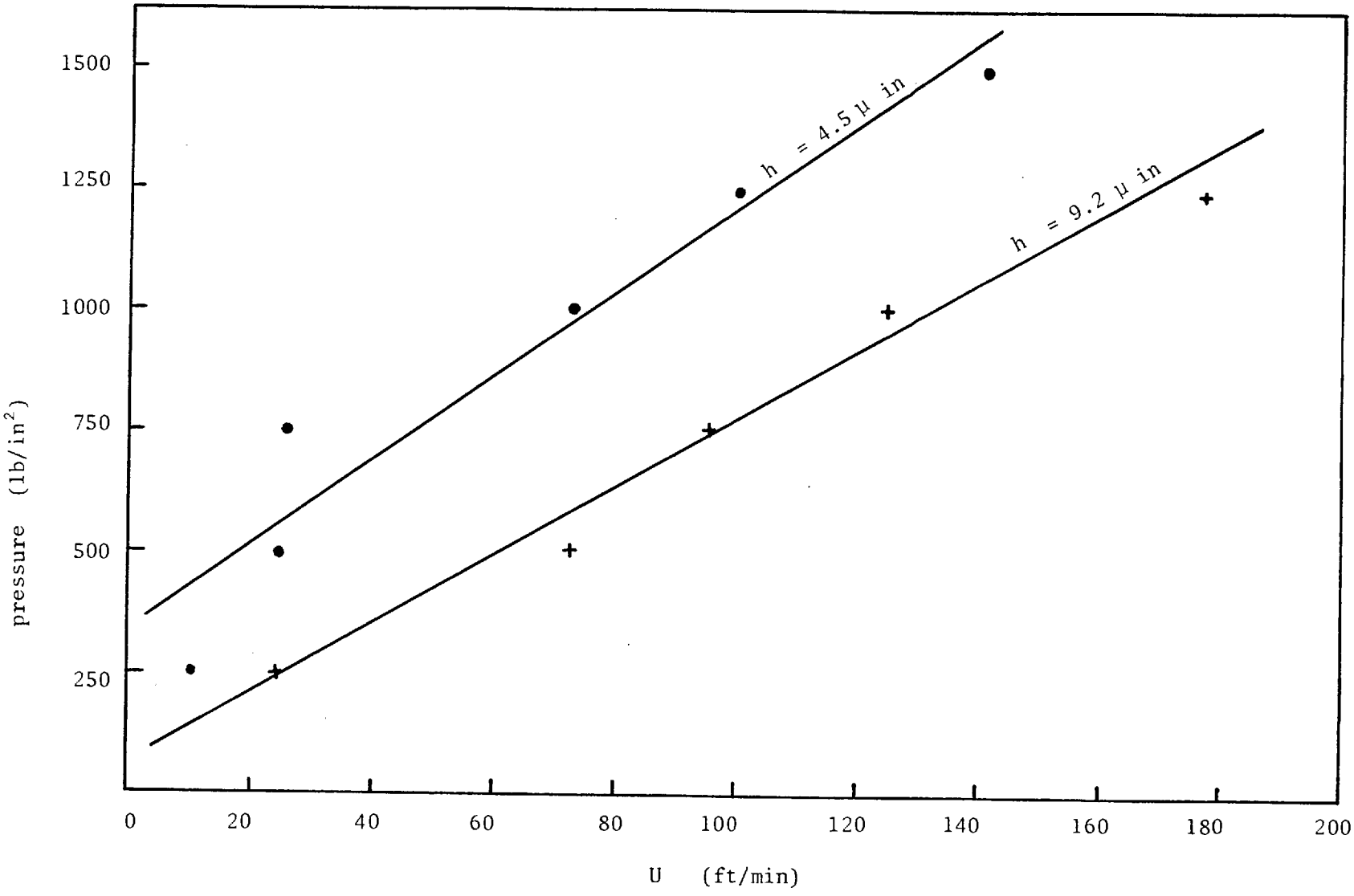

Fig. 5.10. Load Capacity versus Speed.

hydrodynamic film over the lands as the velocity increased. The lands are so small that it was not possible to measure their angle of tilt. All that could be achieved was an average value for the film thickness. The oil employed in these measurements was Teresso 140, which has a viscosity of 1600 cS. at room temperature. The results are given in Fig.5.9 , in which the film thickness is plotted against the square root of velocity. Fig.5.10 shows the relationship between the load and the velocity for which the film thickness was constant. Due to the small field of view of the microscope (compared with the actual contact surface), and also because the size and shape of lands are random, it was not possible to measure the exact load acting on the lands. Therefore, only an estimate is given here. Note that the measurements were made at the start of a run. It is concluded that for a given load the film thickness varies as the square root of the velocity. Also that for a constant film thickness, the ratio of velocity and load capacity remains constant.

5.6. Lubrication Mechanism

In the last few sections, the evidence for a new mechanism of lubrication for porous bearings has emerged. First, a macroscopic oil film, similar to that of solid journal bearings, has not been found. Second, the load carrying action of a porous bearing is concentrated in the small area of the surface which is at the closest approach to the glass plate. Third, the load carrying zone has virtually the same radius of curvature as the

sliding element. Fourth, the existence of cavitation in the pores eliminates the postulate that a continuous oil film exists in the load carrying zone. Fifth, the dam of oil which builds up in front of each land indicates that the units which participate in the load carrying action are fixed by the dimensions of lands. All these factors indicate that it is only the lands that are actually carrying the loads. Hence, it is possible that each land acts as a microscopic thrust bearing. This postulate is further confirmed by the square root relationship between the velocity and the film thickness, which is a known characteristic of tilting pad thrust bearings. Therefore it can be concluded that, even though the macroscopic hydrodynamic film can not exist, the bearing can still operate in the hydrodynamic regime by converting the lands into tilting pad thrust bearings.

5.7. Tilting Pad Thrust Bearings

The theoretical treatment of the lubrication of a tilting pad thrust bearing has been fully developed. Its derivation has been given by Cameron[67]. A brief discussion of the theory and its modification for porous bearings are presented here.

Consider a thrust pad of length B in the direction of sliding, of breadth L transverse and hence area "BL". The pad has a tilting factor 'Kp' defined as

$Kp = \frac{h_1 - h_0}{h_0}$ where h_1 and h_0 are the inlet and outlet separations respectively. The geometry of the contact is

shown in Fig. 5.11a. The load capacity of this pad is given by

$$W = 6U\eta\frac{LB^2}{h_0^2}KpS \qquad \ldots\ldots\ldots (5.1)$$

where S is the side leakage factor which Ettles[73] gives as

$$S = 0.37\frac{L}{B} \qquad \ldots\ldots\ldots (5.2)$$

$$\text{Therefore} \quad W = 6U\eta Kp\frac{0.37}{h_0^2}L^2B \qquad \ldots\ldots\ldots (5.3)$$

To apply this equation to the micro-lubrication of porous bearings several very broad assumptions are made:

1. All the lands are taken to be rectangular in shape and are distributed evenly over the porous surface, as Fig.5.11b shows.
2. The loads are equally shared.
3. The lands all have the same tilt ratio Kp.

From Fig. 5.11b the following relationship can be achieved

$$M = \frac{b}{B + \beta B} \qquad \text{or} \qquad B = \frac{b}{M(1 + \beta)} \qquad \ldots\ldots (5.4)$$

$$N = \frac{\ell}{L + \alpha L} \qquad \text{or} \qquad L = \frac{\ell}{N(1 + \alpha)} \qquad \ldots\ldots (5.5)$$

where M and N are the number of pads along and transverse to the direction of sliding respectively; and ℓ x b are the dimensions of the load carrying zone. Therefore the total load capacity can be written as

$$W = MNW$$

$$= 2.22\ U\eta \cdot \frac{Kp\ell^2 b}{h_0^2} \cdot \frac{1}{N(1 + \alpha)^2(1 + \beta)}$$

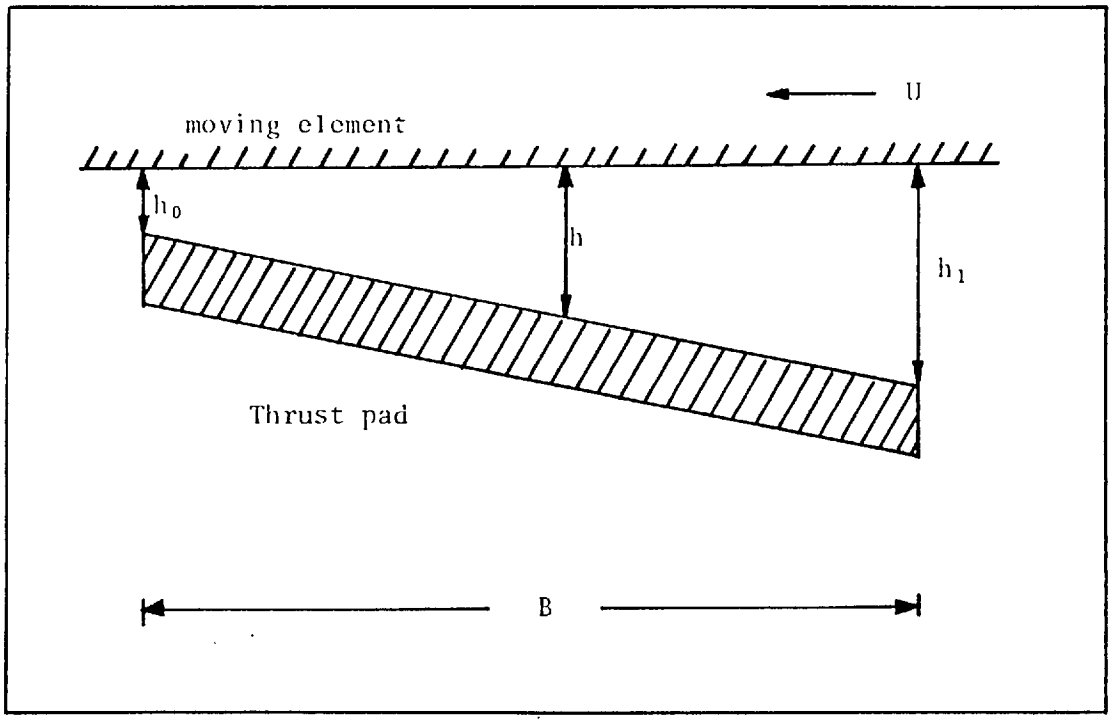

Fig. 5.11a Thrust Pad Geometry

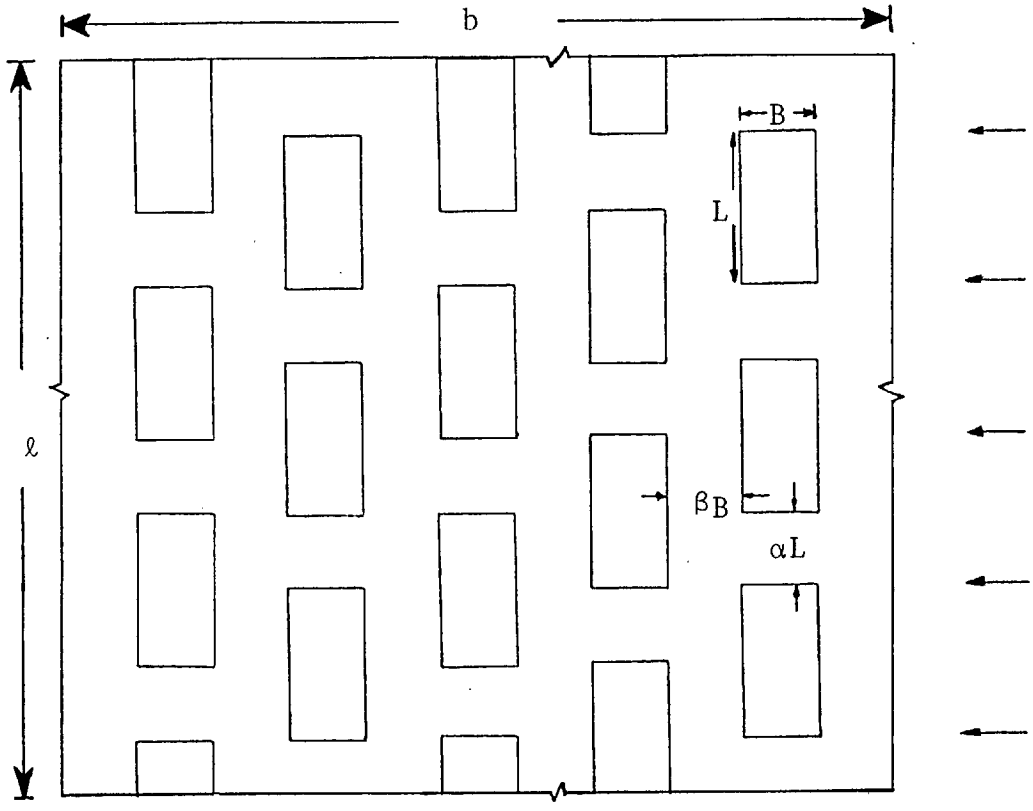

Fig. 5.11b. Ideal Porous Surface

$$= 2.22\ U\eta\frac{\ell^2 b}{h_0^2}\ Kp\ C \qquad \ldots\ldots\ldots\ (5.6)$$

where $C = \dfrac{1}{N(1+\alpha)^2(1+\beta)}$ $\qquad \ldots\ldots\ldots\ (5.7)$

Note that the measurement in Chapter 5.5 agrees qualitatively with this relationship. In these experiments it is not possible to find the exact value of n, α, and β because lands have large varieties of shapes and sizes and are distributed randomly over the bearing surface. But for a given run-in porous surface these quantities are constant, and so is the value of C.

Although Eq. 5.6 has not been verified quantitatively in the experiments, it is worthwhile discussing some of its implications.

1. Since W is proportional to L^2B, it follows that bearings with lands elongated perpendicular to the running direction would have higher load capacity than those parallel to the direction of motion.

2. The relationship between film thickness, load and speed in a porous bearing is similar to that of a tilting pad thrust bearing having the same size. The only difference is that a reducing factor C should be used.

3. C is a dimensionless factor whose value depends on those inter-relating parameters such as porosity, land size and the degree of running-in. It has a maximum value of 1 and a minimum value of 0. According to Eq.5.5, C can be written as

$$C = \frac{L}{\ell} \times \frac{1}{(1+\alpha)(1+\beta)} \qquad \ldots\ldots\ldots\ (5.8)$$

To get an idea of an actual value of this constant, consider a porous journal bearing of width 2.5cm and an average land size of L = B = 100μ, so that $\frac{L}{\ell} = \frac{1}{250}$. Assuming $\alpha = \beta = 1$, then C is equal to 0.001. Other calculations show that in the usual range of porous surface C falls between 10^{-4} and 10^{-2}. Note also that its value increases with the running of the bearing. As C approaches unity, e.g. when most of the surface pores are closed, the load capacity becomes that of a solid-metal thrust bearing. Hence the fewer the pores the greater the load capacity. However as porous bearings rely on their pores to supply oil, closing the pores means cutting off this supply to the working surface. This would obviously lead to seizure. It is of interest to note that the property of C is somewhat analogous to that of the permeability factor Ψ mentioned in Chapter One.

4. The inclination factor Kp apparently holds the key of the load carrying action of porous bearings. Cameron[67] shows that the load capacity of a tilting pad thrust bearing is optimum when Kp is about unity, but decreases for either larger or smaller Kp. However, it has been mentioned that the run-in surface of a porous bearing has the same radius of curvature as the sliding element, which means that the two surfaces are nearly parallel to each other. In this case the inclination factor Kp and hence the load capacity W_T would be equal to zero. Therefore, there must be some means by which the land can incline with respect to the sliding element. A very approximate analysis of the experimental data in

Section 5.5 indicated that Kp was around 0.05. The film thickness at the inlet of the land corresponding to this value of Kp would be only 1.05 times that of the outlet. This is too small to be detected directly in the interference experiment. The causes of this inclination are discussed in the following sections.

5.8. Plastic Flow

One possibility for an inclination of the lands is the plastic flow of the metal. It has long been postulated[44] that the effect of metal smear may create a taper at the leading edge of each land. This postulate arises from two facts. First, it is known that during manufacture a certain amount of plastic flow occurs in the surface layers of the powder. Secondly, some pores are closed during running-in which indicates that plastic flow of the metal must have occurred. One property of plastic flow is that the top layer of material suffers from tangential transportation from the inlet to the outlet, thus leaving a taper in the inlet area. However, vigorous investigation of the surface topology of the run-in surface using an interference microscope has shown that normal effect of metal smearing does not create any significant taper at the leading edge of the lands. Hence other reasons for the formation of a hydrodynamic film must be sought.

5.9. Thermal Taper

Consideration of the dam-land-cavitation system suggests the possibility of a temperature gradient along

the longitudinal direction of the lands. The effect of thermal heating, due to the sliding friction and the shearing of the oil film, is a homogenous increase in the temperature of the lands. The presence of the oil dam at the inlet edge of the land could lead to a cooling effect and hence a temperature gradient across the land. This follows because the efficient of cooling is proportional to the flow rate of the fluids and their densities. Since the flow rate of the oil in the dam is higher than the flow rate of air in the cavity, and since the density of oil is much greater than the density of air, therefore a temperature gradient should develop across each land in the sliding direction, with the temperature at the rear part higher than that at the front.

The coefficient of linear expansion of bronze is $0.000018/^{o}C$. Assuming the land to be a cube of 4 thousandth of an inch (100μ) at each side, and that the temperature diffference between the front and exit sides of the cube to be $50^{o}C$, a differential expansion of 8μin is achieved. This corresponds to an angle of 0.1^{o} between the land and the shaft surface. In principle it should be possible to detect such a differential expansion using an interferometric method. But this was proved to be impossible with the present arrangement, probably because continuous running of the bearing for several minutes may be needed to generate a detectable amount of taper, and with this period of running, without thick oil flow, the chromium coating on the glass disc

is worn away completely giving no optical interference effect.

5.10. Effect of E.P. Additive

Some further light on the problem of proving the thermal taper is available from an earlier experiment into the running-in process as mentioned in Chapter 4.2. It was noticed that with samples which have been run for more than 16 minutes at a high load, the colour at the rear part of each land in the contacting zone appeared redder than the front part, as shown in Fig.5.12 and 5.13. These pictures were taken with ordinary photo-micrography. Later, experiments performed with the cylindrically domed specimens running against a steel disc, showed exactly the same appearance. A study of these lands using an interference microscope indicated that the rear part (with the red colour) was always higher than the front part (bronze colour). The amount of difference in the height ranged from 2 μin (0.05 μ) to 8 μin (0.2 μ). A microhardness test revealed that the hardness of the part with the red colour was always softer than that of the bronze colour. Since ordinary metallurgical techniques cannot detect the composition of such a small amount of material, a more advanced metallurgical instrument was used to tackle this problem.

5.10.1. Electron Probe Micro-Analyser

EPMA is a device which is capable of measuring the concentration and spatial distribution of elements in

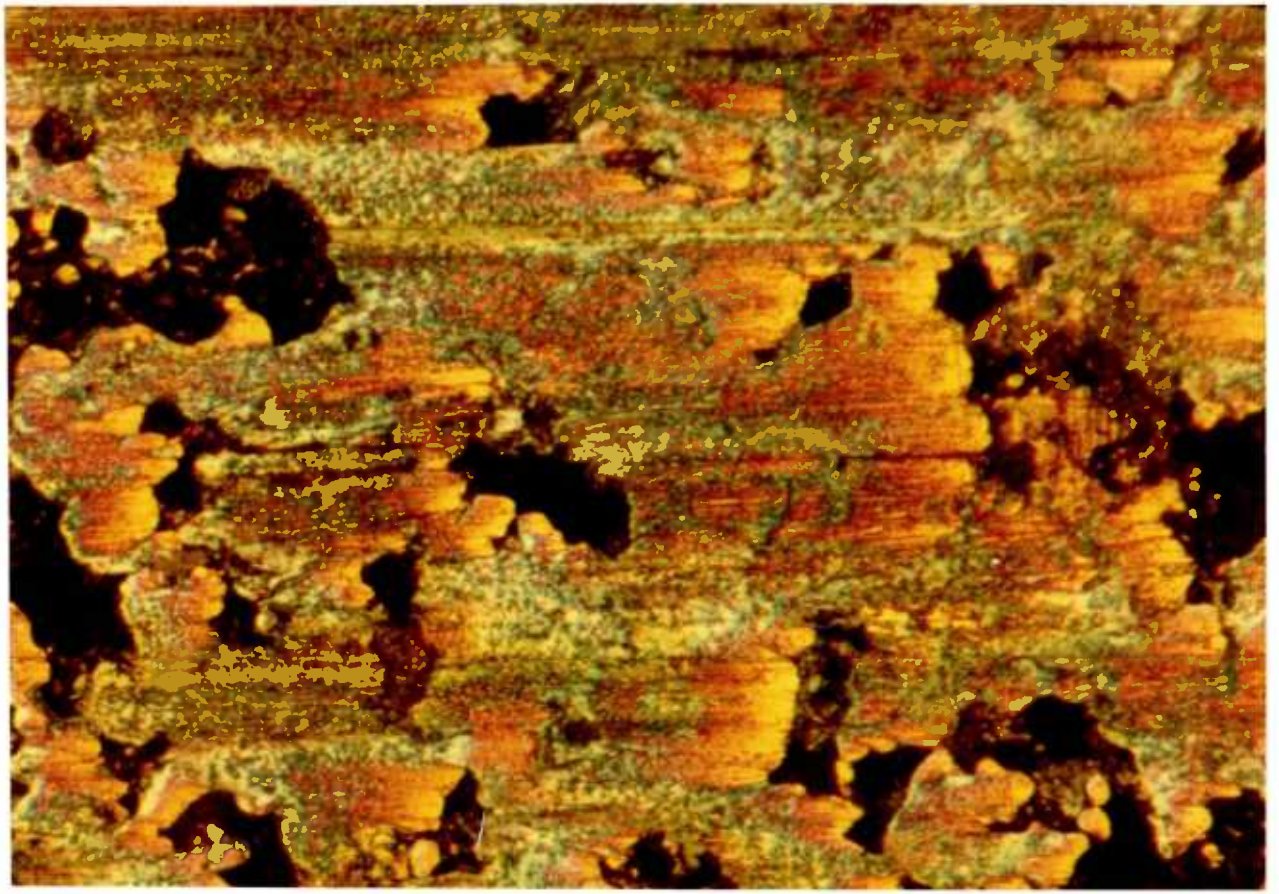

Fig. 5.12. Photomicrograph of a well run-in porous surface, x 250.

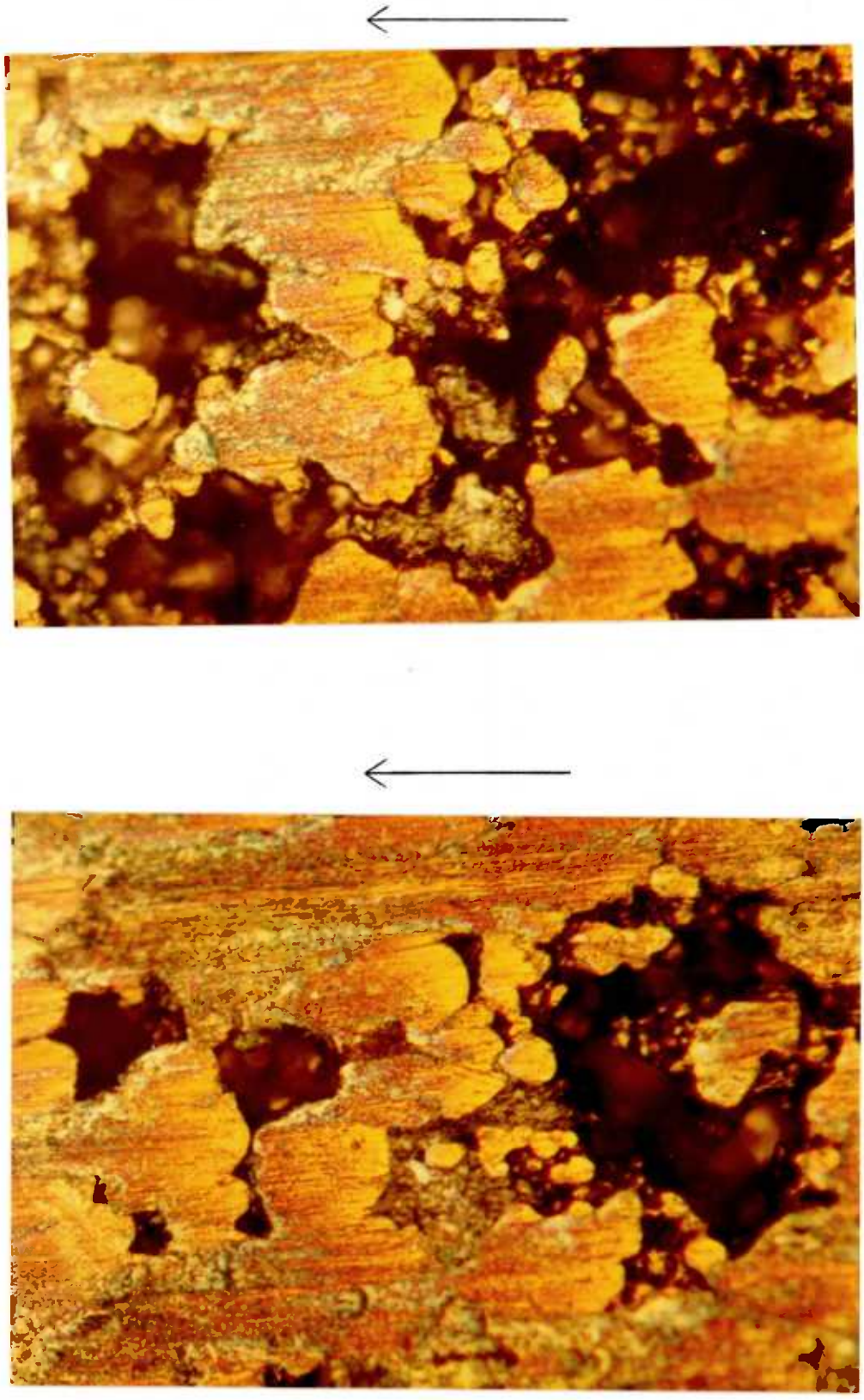

Fig. 5.13. Other photomicrographs of well run-in porous surface, x 200.

very small amounts. The principle of the instrument is to bombard the surface with an electron beam of high energy, so that the characteristic x-rays corresponding to the elements at the surface are emitted. The spectrum of these x-rays is then analysed by a crystal spectrometer. In this way the instrument can detect the elements, as well as their concentration.

The instrument employed was the Japanese Electron Optics Laboratory (JEOL) JXA-3A. A schematic diagram is shown in Fig.5.14. Electrons emitted by a tungsten filament are focused into a spot of about 1μ diameter on the specimen. The beam penetrates to about 2μ into the specimen surface. A co-axial electronised and optical system provides the facility for monitoring and detecting simultaneously. The spectrometer is made of a mica crystal which selectively reflects the characteristic wavelengths according to Bragg's law. The detected signal is amplified by a scintillation counter, which also quantifies the concentration of the element.

5.10.2. EPMA Results

Fig.5.15 shows the traces obtained from the land of a bearing which had been run for 15 minutes. There are three traces on the graph, each representing the variation of a particular element. Trace 1 indicates the change in the concentration of sulphur along the land. Trace 2 indicates the changes in the concentration of tin. Note that the EPMA only indicates the presence of the element, not the compound. To avoid errors from geometrical

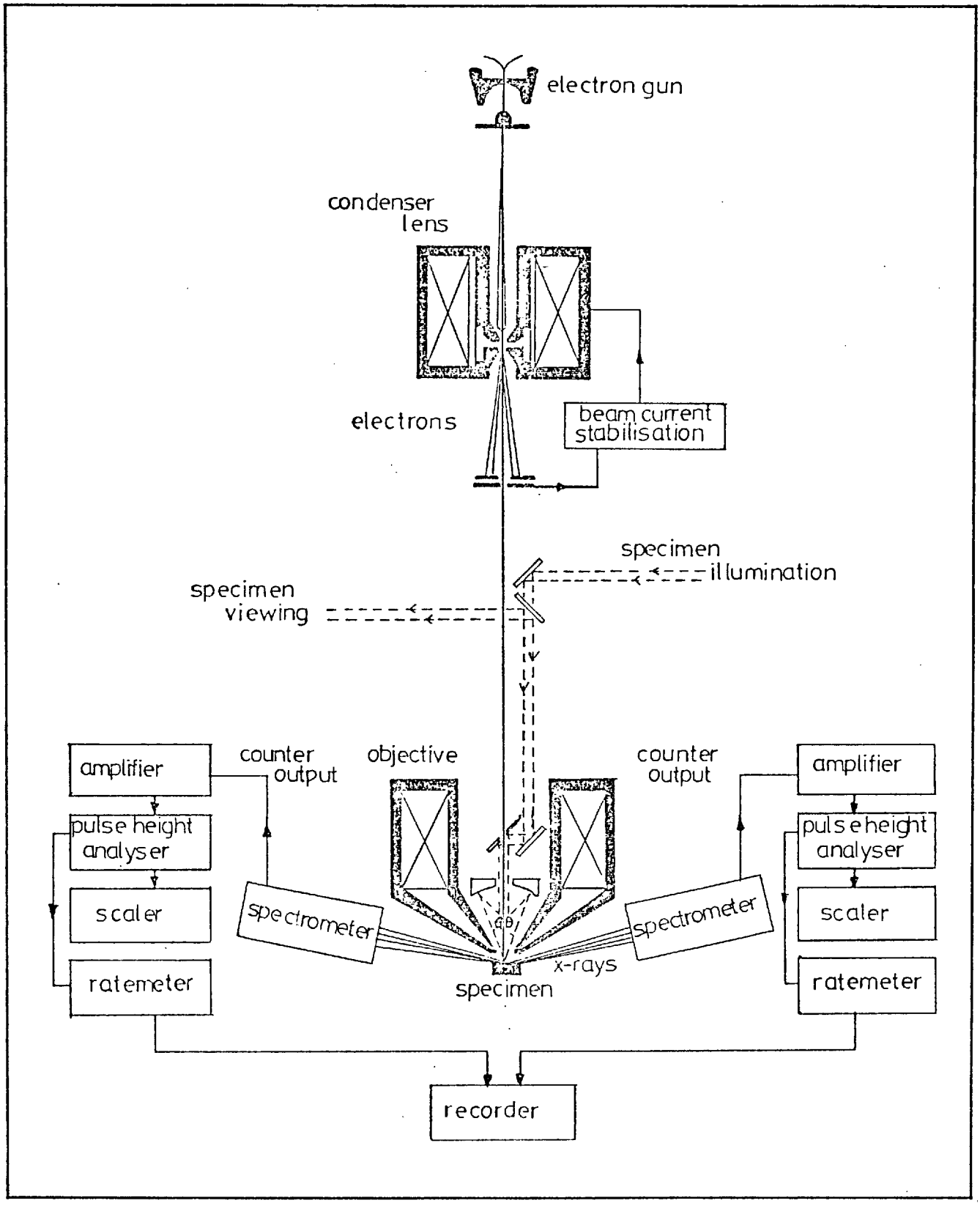

Fig. 5.14. Schematic drawing of Electron Probe Micro-analyser.

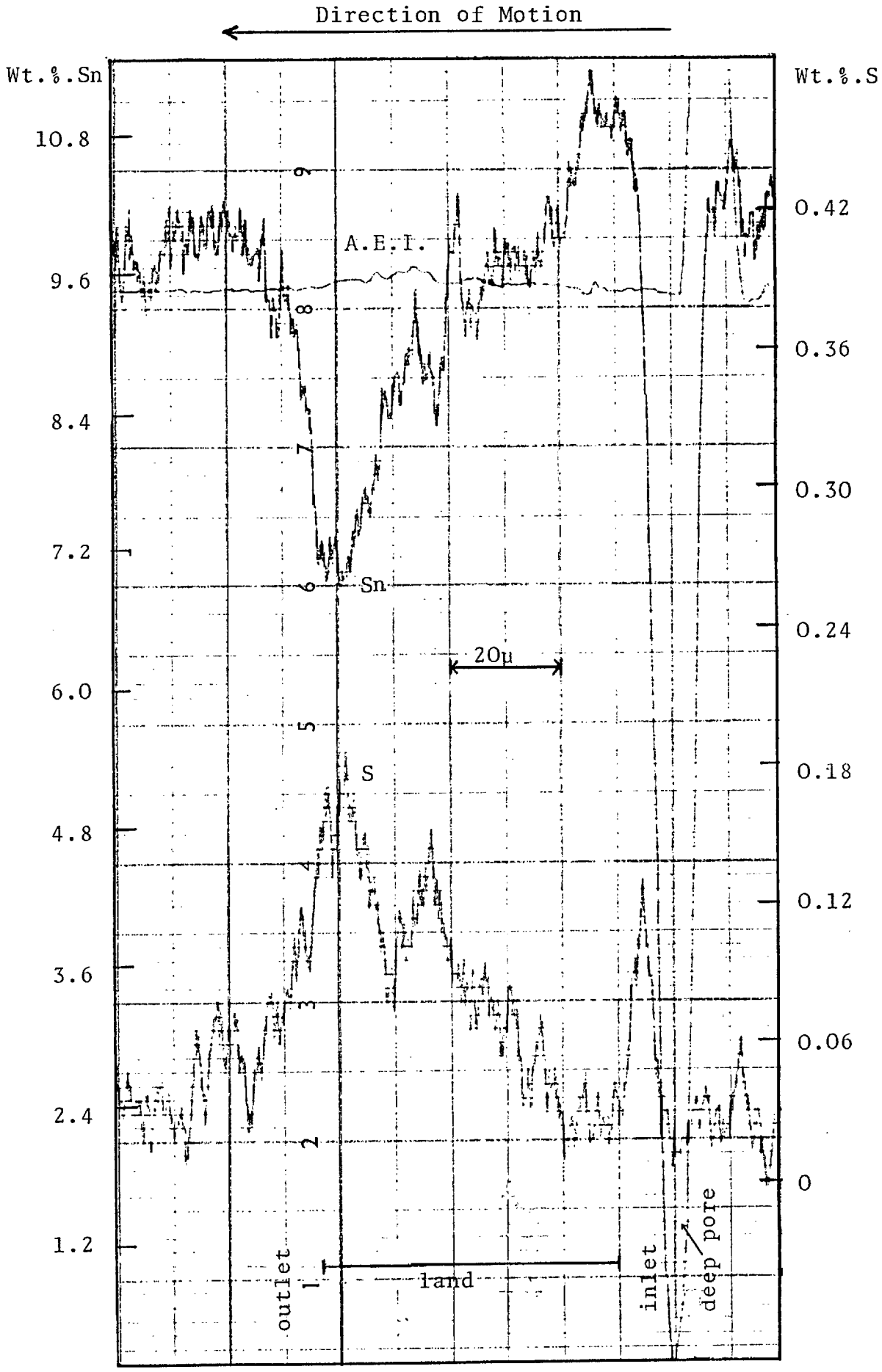

Fig. 5.15. EPMA trace along a land on a run-in porous surface.

variations, the absorbed electron current (AEC) is also recorded and is indicated by Trace 3. This current depends strongly upon the topology of the surface, and provides a clue to whether the variations recorded are due to the surface features or to a change in concentration of the elements. The specimen was scanned under the electron probe in the direction of the shaft's movement. The examination was concentrated on the colour patches as shown in Fig. 5.12 and Fig. 5.13. It was found that some parts of the lands contained appreciable amounts of sulphur. Other elements such as Si, P, Pb, Zn, Ni, etc. were also checked but none of these was found in detectable quantities. Fig. 5.16 shows the concentration of sulphur along another land. It is seen that the concentration of sulphur increases almost linearly from the front to the rear of the land. It is likely that this sulphur was present as a layer of copper sulphide on the bronze surface. This is supported by the decrease in tin concentration as the sulphur concentration increases. Repeated traces on other lands similar to those shown in the pictures showed the same characteristics. It can therefore be concluded that the colourful pattern in Fig.5.12 and 5.13 is due to a thin layer of sulphide deposited onto the rear part of each bronze land. The sulphur was later confirmed to be coming from the oil, Turbo T41. Another interesting observation is that the deposition of sulphur on lands is independent of their size. The same sulphur wedge was found on lands as small as 20μ and as large as 200μ in length.

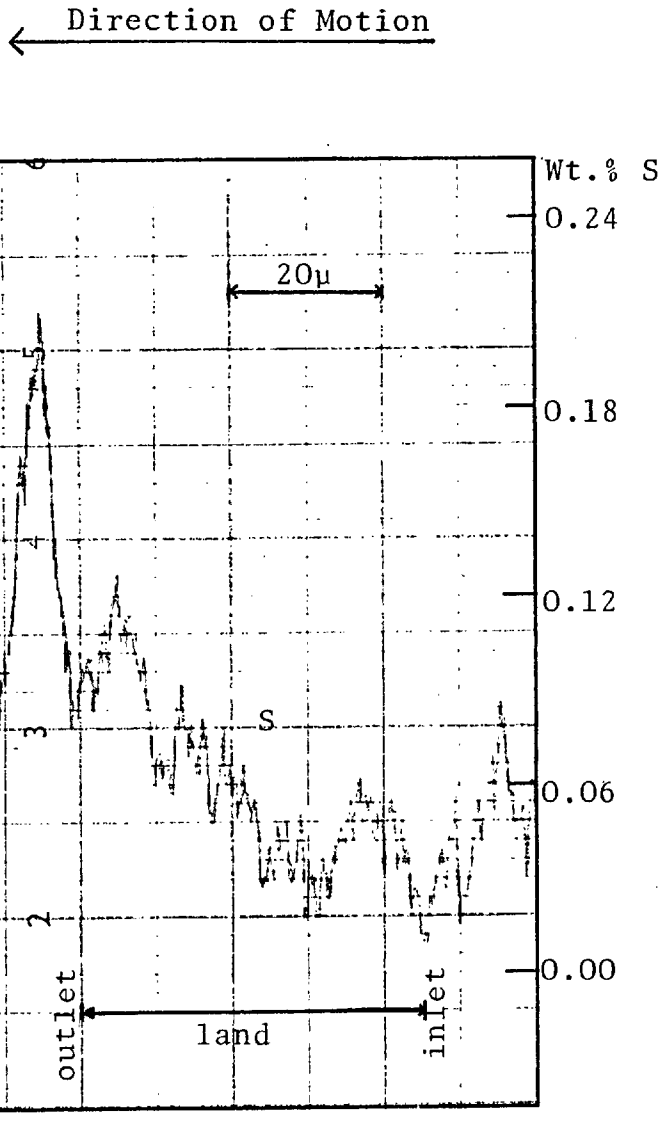

Fig. 5.16. Another EPMA trace along a land on the run-in porous surface

5.10.3. EP Additive

The phenomenon mentioned about is best understood from the theory of Boundary Lubrication. When the hydrodynamic film is not thick enough to separate the two surfaces, direct metal contact takes place and causes surface damage to both the bearing and the shaft. To reduce the amount of damage, most lubricating oils are fortified with additive chemicals which react with the metal surfaces to provide protective films. They are of several types and described as anti-wear, oiliness and extreme pressure additives. Under appropriate local temperature conditions the additives react with the metal surface to form soft, easily sheared inorganic or mixed organic/inorganic films on the surface, thereby preventing seizure and reducing wear.

EP additives are usually organic compounds of sulphur, chlorine or phosphorous. The reaction of these additives with the metal surfaces is affected by the presence of both the hydrocarbons and the normal environmental constituents such as air and water vapour. One of the special features is that they do not come into action until the temperature of the surface reaches a critical value, known as 'critical temperature'. For sulphur on steel it has been found[74] that the critical temperature is about 140°C. The longer the reaction time and the higher the temperature, the thicker is the deposited layer.

We may now construct a picture of what happens

during the operation of a porous bearing. The picture is exactly the same as that postulated in Chapter 5.9. The heat generated by the sliding friction raises the temperature of the bronze surface. At the same time the dam of oil cools down the front part of the land, thus creating a temperature gradient along each land, forming a wedge shape (by differential thermal expansion) which is more condusive to hydrodynamic lubrication. At some stage the rear of the land reaches the critical temperature and the sulphur additive in the oil comes into action and forms a layer of sulphide. This effect also provides a hint about the amount of the temperature difference between the front and the rear of a land. Assuming the additive comes into action at 120°C and that the oil in the dam is at the average running temperature of, say, 60°C, we would have a temperature difference of 60°C along the length of the land. As stated in Chapter 5.9, the differential expansion associated with this will be of the order of 8μin. The corresponding value of Kp would be 1 if h_0 was also 8μin.

It may be argued that the bearing in this case is only operating where E.P. reaction occurs. ~~in the boundary lubrication regime~~. Certainly it was, but the most significant result is that it demonstrates that a temperature gradient does exist. After all, the wedge-shaped sulphur layer will itself promote the hydrodynamic effect. Note that in Section 5.7 Kp was measured to be 0.05 approximately, instead of 1 as estimated here. This discrepancy is probably due to the fact that during the optical measurement the temperature was not high enough for Kp to achieve a larger value.

5.11. Literature Review of Parallel Surface Bearings

Parallel surface bearings have been used in industry for many years, yet their lubrication mechanism remained unclear until recently. Such bearings usually consist of a circular plate with several radial grooves leading to a central recess, into which the lubricant is supplied. The basic problem is that classical lubrication theory does not predict the formation of a stable hydrodynamic film for steady-state, isothermal, incompressible flow between two smooth parallel surfaces. Many ideas and models have been put forward to explain the working mechanism. Salama[75] studied the effect of surface waviness both experimentally and theoretically. The waviness was produced arbitrarily during the machining of the surface roughness. The effect of short wavelength roughness has been studied by Davies[76] and Burton[77]. Recent work concerning the surface micro-irregularities produced results which were related to the findings of this thesis. By photo-etching asperities onto a stator surface and running against a transparent rotor, Hamilton et al[78] observed that the film was not continuous but was interrupted by numerous long, narrow, cavitation streamers. A streamer began at the downstream side of an asperity and finished at a certain distance before the next asperity. The authors accounted for the load capacity by the presence of the cavitation, which truncated the negative part of the pressure profile associated with the asperity, which would otherwise counter-balance the positive part. Later, Anno et al[79] put forward the theory that there was a slight

tilt or taper on each asperity and they verified this theory experimentally. However, the cause of the tilt was not explained, by they indicated that the local thermal distortions of the asperity surface would be negligible.

Another model was suggested by Harrison[80] in which the small chamfer introduced by the grooves might produce a load capacity. Lewicki[81] proposed that the viscous oil dam at the leading edge of the thrust pad could account for a lifting pressure. Tønder[82] suggested that the presence of gas/vapour bubbles in the lubricant might cause a pressure build-up. He indicated that the presence of bubbles would not in themselves generate a positive pressure but that they would modify and inflate the pressure profile produced by other means. Fogg[83] proposed the 'thermal wedge' effect in which the decrease of the lubricant's density along the the direction of motion owing to the temperature gradient would result in hydrodynamic lift. Cameron[84] and Zienkiewicz[85] introduced the 'viscosity wedge' theory, in which the viscosity varied across the lubricant film (by the temperature difference of the two metal surfaces), and showed that a hydrodynamic pressure is generated.

The effect due to the thermal distortion of the bearing material was first suggested by Swift in the discussion of Fogg's paper[83]. However, the idea was discounted since Fogg reported that the bearing reacted immediately to the applied load. A great advance of this theory was due to Dowson[86] who included the variation of

relevant properties of the bearing material and the fluid to obtain a generalised form of Reynold's equation. Dowson and Hudson[87] applied this equation to a parallel surface bearing and found that the effect of thermal and viscosity wedge gave a negative pressure when realistic temperature boundary condition were used. Neal[88] showed in his experiments that the load capacity was due to a thermally induced convergent-divergent film shape. Ettles and Cameron[89] investigated the pressure generated in parallel surface bearings and found that when the film was thin enough the thermal distortion of the bearing surface produced a wedge shaped film sufficient to carry the load. The thinner the film the more the distortion and hence the greater the load capacity. Later, Robinson[90] and Taniguchi and Ettles[91] confirmed the thermal distortion theory both theoretically and experimentally. This model, known as 'thermal taper' is now recognised to be the main reason for the hydrodynamic lubrication of parallel thrust bearings. Note that these authors deal with large bearings of several inches in diameter. The thermal distortion of thrust pads as small as the lands in porous bearings has not been tackled before.

Seals are another kind of device which operate by two parallel surfaces sliding over each other. The majority of seals depend upon hydrodynamic lubrication for their satisfactory operation. All the models and effects mentioned above apply equally well to seals. For further information about this the reader is referred to Nau[92]. In summary, the effects, or models, mentioned above to explain

the operation of parallel surface bearings, all have a certain influence on the bearing. Some effects contribute to the load carrying, and some detract from it. The effects due to the waviness and the chamfer depend on how the bearing surface is produced during manufacture. The other theories deal with the thermal properties of the lubricant and of the bearing material. These are the 'viscosity wedge', the 'density wedge' and the 'thermal taper'. Ettles[89] gave a quantitative comparison of the load capacity of the three mechanisms and showed that the 'viscosity wedge' has a negative load capacity, and that the 'density wedge' effect is small compared with the 'thermal taper' effect.

CHAPTER SIX

NON-CONTACTING ZONES

In the last chapter we have seen what is happening in the load carrying zone of the bearing surface . For thoseparts of the porous surface which are not involved in the load carrying action, the story is entirely different. Under stable conditions most of the oil in the bearing system is held within the porous medium, so that the space in the clearance gap is filled up with air. Nevertheless, under some extreme conditions these zones exhibit several interesting phenomena which are worth mentioning.

6.1. Converging Zone

In the stationary condition the gap in this zone was filled up with oil. When the disc started moving, most of this oil flowed out of the gap, leaving it filled with air. In general, nothing very interesting happened in this zone. The oil remained substantially stationary within the pores in the bearing surface. However, under oil flooded conditions, e.g. at the beginning of the bearing's life, or when extra oil was added, interesting phenomena did happen. Oil was pumped out of the porous medium into the gap.

6.1.1. Definition of Pumping

Pumping is defined here as a process in which the oil in the pores is pushed out into the gap. When the oil leaving the pore touched the oil film on the moving glass disc, it coalesced with it and was carried downstream. This gives rise to a pulsating process, the frequency of which can range from several pulses per second to one pulse every several seconds.

6.1.2. Pumping Process

Since pumping is a pulsating process, we need only describe one cycle in detail. Consider a pore situated near the end part of Zone A, but in front of Zone B, (Fig.4.8), with a diameter of about 100μ. The depth of the pore would be about 40μ (although it might communicate with other pores deeper in the matrix). With each cycle of pumping the rise of the oil bubble commenced from just inside or just outside the pore and grew in size towards the glass disc. While it was still inside the pore the 'oil bubble' had a concave surface. As it grew towards the mouth of the pore, the radius of curvature decreased and as it emerged beyond the mouth of the pore the surface became convex. Up to this stage, the surface of the 'oil bubble' was spherically symmetrical. As the bubble came very close to the glass disc, say within 4μ to 5μ, its surface began to deform. It became flattened at the inlet and a 'spike' developed at the exit. Finally the 'spike' touched the glass plate and the oil was torn

away downstream. The meniscus then returned to its original low position and the process was repeated. This phenomenon happened within a fraction of a second or a few seconds. Fig.6.1 shows the interferogram representing different stages in the bubble growth, while their corresponding cross-sections are drawn in Fig.6.2. Other high speed interferograms of pumping are shown in Fig.6.3 and 6.4. Fig.6.5 records the trace of small patches of oil which have just been pumped out and are being carried away by the shaft.

6.1.3. Elasto-hydrodynamic Lubrication

The principle underlying the deformation phenomenon of the oil bubble can again be explained by the theory of elasto-hydrodynamic lubrication as has been demonstrated in Chapter 5.2.2. In the inlet zone, air is constantly being drawn into the gap by the motion of the glass plate. Therefore as the oil bubble approached the plate, it deformed elastically, causing a relatively flat surface at the top and a 'restriction' spike at the exits. The final stage of the pumping cycle is analagous to the 'spalling' effect in roller bearings in which the pressure is so high that a small piece of metal can be pulled out of the bearing surface.

The action of the air is to separate the oil bubble from the glass disc, and whether the pumping cycle can be completed or not becomes critical at this final stage of the cycle. If the pressure causing the bubble to rise is large enough, it will overcome the effect of the air

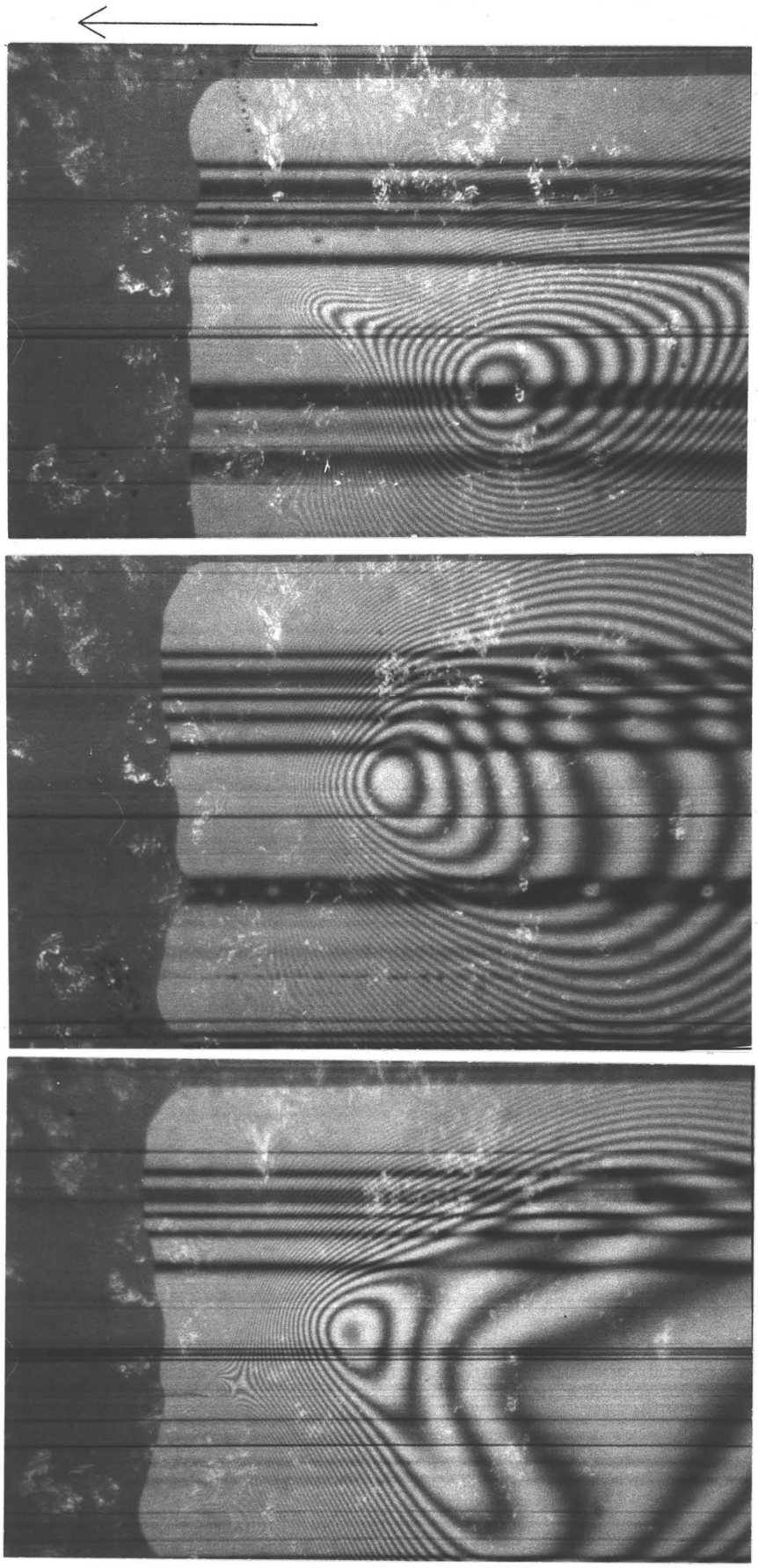

(a)
t = 0.25 sec.

(b)
t = 1 sec.

(c)
t = 1.8 sec.

Fig. 6.1 Interferograms of pumping, showing the growth of an oil meniscus, x 150.

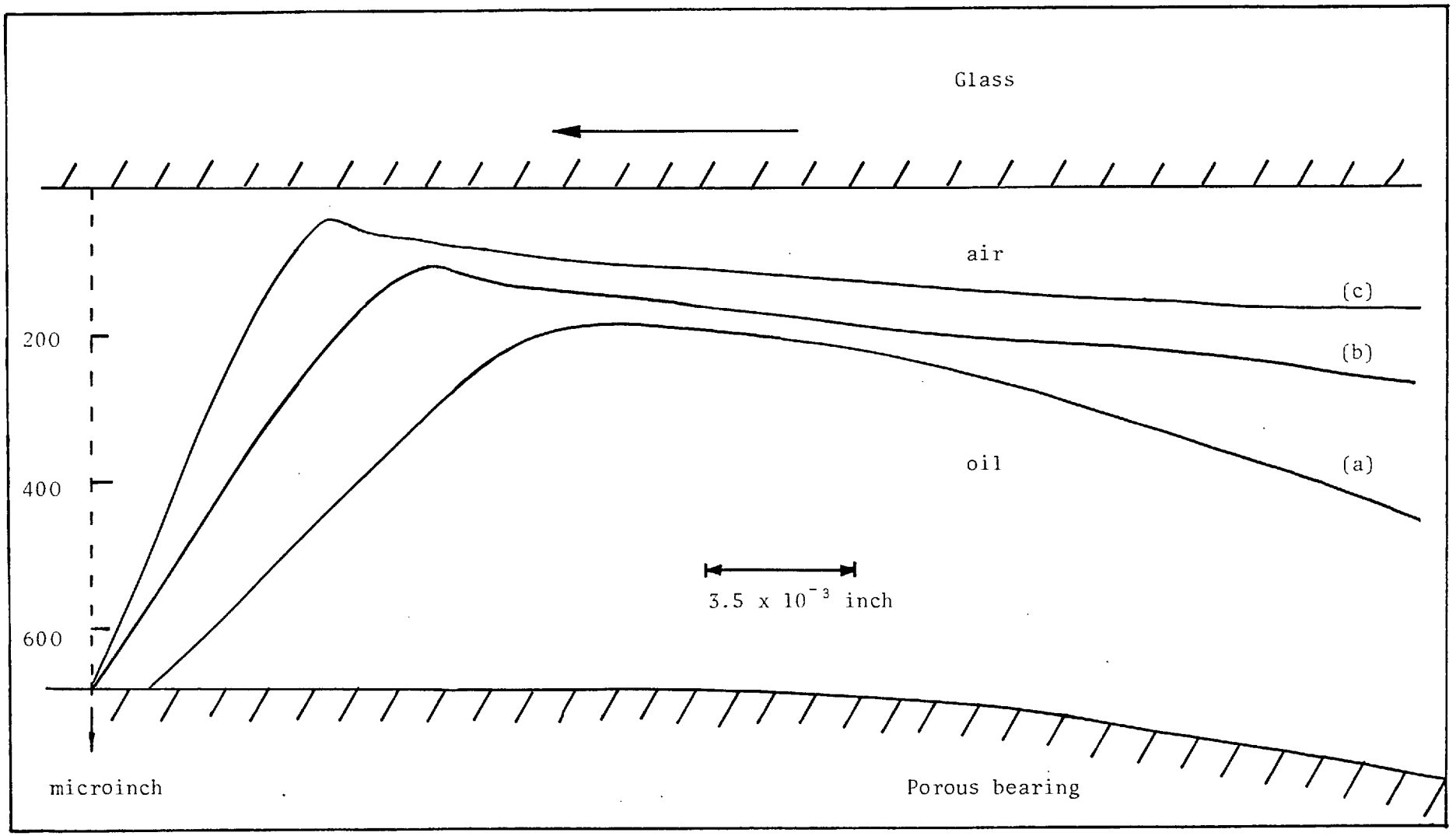

Fig. 6.2. Profile of the oil meniscus in Fig. 6.1

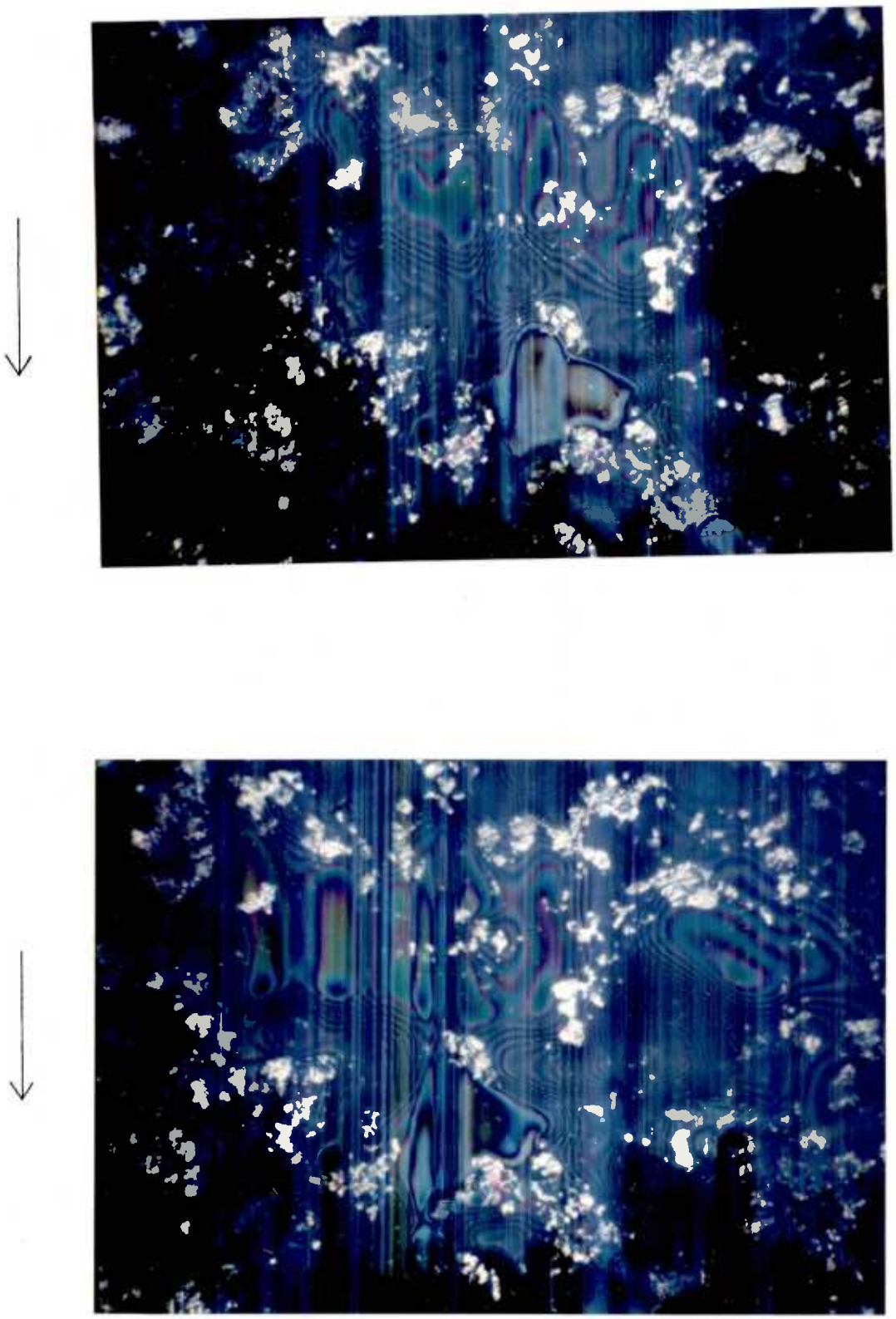

Fig. 6.3. Other interferograms of pumping, x 180

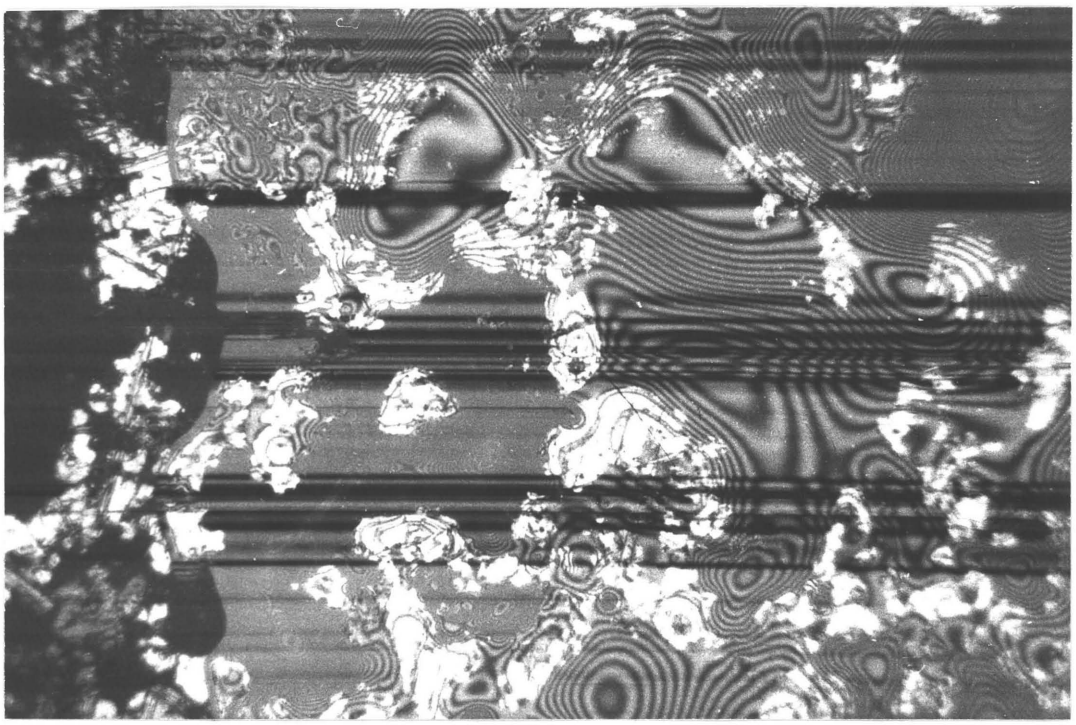

Fig. 6.4. Another interferogram of pumping, note the fringe pattern due to multiple beam interference, x 180.

Fig. 6.5 Trace of small patches of oil (arrows) which have just been pumped out and are being carried away by the glass disk, x 180.

being drawn in, will touch the glass plate and the pumping cycle will be complete. On the other hand, if this pressure is not large enough, the EHD effect of the air will prevent the bubble touching the shaft and the cylce will not be completed. In this case, the oil will just spread over the porous surface horizontally.

6.1.4. Factors that affect the rate of pumping

The frequency of pumping depends on several factors. For example, it increases with increasing oil content in the bearing, it decreases with the size of the pore from which it grows, and the geometry of the contact in the nearby region can also affect the pumping. Generally speaking, pumping only occurs when there is a surfeit of oil. When starvation was created by wiping away the oil attached to the glass disc, the pumping frequency decreased at the beginning and finally became zero. When an extra drop of oil was added into the inlet, the pumping increased instantaneously to a much faster value. Then it gradually decayed to a stable value.

6.1.5. Mechanism of Pumping

The pumping may be caused by extra oil flowing down into the porous matrix in nearby pores, causing a build up of pressure within the porous matrix. Hence, some lubricant is forced out of other pores to release the pressure. The places where the oil flows into the porous matrix will be seen when we discuss later the phenomenon which is

happening in Zone B. Those pores which are far away from the site where oil is flowing down share less effect of this pressure than those closer to it. This explains why pumping is concentrated in those pores which are near the end of Zone A , i.e. immediately in front of Zone B. It may also explain why a pore with a small diameter has a pumping rate which is higher than a larger one. This is because for a given amount of oil to be pumped out, the velocity would be greater when the pore diameter was small.

The frequency of pumping was also found to be synchronised with an uneven movement of the glass disc. This uneven movement was introduced deliberately by slightly tilting the plane of the disc with respect to the rotating axis. The synchronisation observed was apparently due to the pulsating flow of extra oil into the porous matrix. Some porous bearings are used at high speeds, in which a whirling of the shaft might occur. Therefore the observed synchronisation of the pumping frequency with that of the whirling of the shaft is likely to happen in practice.

6.1.6. Increase of Pumping by Closing the End Walls

There are two ways to increase the pumping rate. One is to add more oil into the bearing system, and the second is to close the end walls of the bearing. In experiments using porous samples whose end walls, except the working surface, were closed by lacquer, it was found that the pumping effect occurred in a very much more intensive way than if the end pores were left open. This effect is not difficult to understand since closing the end walls would

cause a greater build up of pressure within the porous matrix, leaving the only escape route the converging zone at the working surface.

6.1.7. The Role of Pumping in the Lubrication of Porous Bearings

In porous bearings the oil contained in the pores is used over and over again. The pumping action is an obvious means of oil-recirculation. Pumping is likely to be a dominant factor for oil recircluation at the beginning of the bearing's life, when the system is fully charged with oil. However, as oil is lost from the system, the pumping rate decreases and finally ceases, when the oil recirculation mechanism can only be by the wetting mechanism discussed in Chapter 5.3.4.

6.2. Oil Flooded Zone

Under flooded conditions the gap near the end of the converging zone is completely filled with oil. This is denoted as Zone B in Fig. 4.8. The length of this flooded region depends upon the clearance of the gap and the amount of oil rushing into it. This 'air-free' region was found to be mainly responsible for the pumping action. The film of oil adhering to the glass plate is brought into the end of the converging zone by the rotating disc. Since the forward movement of oil is restricted by Zone C, the oil has to accumulate in Zone B. Some of this oil flows downwards into the porous medium and generates the pressure

for the pumping action. In a solid journal bearing the accumulation of this oil in Zone B results in a build-up of sufficient pressure to lift the shaft, i.e. hydrodynamic lubrication. However, in a porous bearing this is not the case. The reasons are twofold. First, without an external supply of oil, the building up of a hydrodynamic pressure is greatly limited. Secondly, even if there was a hydrodynamic pressure in the converging wedge, it would easily be relaxed, as the oil leaked into the porous matrix, and might even be lost through the outside pores of the bearing wall.

6.2.1. Validity of Classical Theory

The length of Zone B depended strongly on the amount of oil in the system. If there was an external supply of oil into the inlet and if this supply was sufficient and continuous, the flooded area of Zone B would extend far upstream into the entire region of Zone A. In this case, the classical concept of lubrication of porous bearings would be correct at this particular part - the oil flooded part - of the surface. That means the macroscopic wedge of film is formed and the seepage of oil into the porous matrix behaves in accordance with Darcy's law. Under these conditions the oil film was thicker and the frictional torque was lower.

When the external supply was stopped, the oil in the bearing tended to leak away and the length of the flooded region decreased progressively to a short but stable value, leaving Zone A to be partially filled with air. When

starvation was deliberately created by wiping away the oil from the disc, the length of this flooded area decreased further and finally became virtually non-existent, e.g. it became the dam in front of the first set of lands in the load carrying zone.

6.2.2. Formation of the Flooded Zone

In the last chapter the oil dam in front of the lands was discussed. In fact, the flooded region can be regarded as an extension of this dam. Consider an arbitrary land situated at the front part of Zone C and assume that the system is extremely starved of oil. Obviously the dam corresponding to this land would be short. If the oil content of the porous matrix is increased, the length of this dam will also increase. The dam length would grow to an equilibrium condition in which the extra oil arriving at the dam would leak away down into the pores. As more oil was applied to the system, say by adding drops of oil into the inlet, more oil would flow down into the pores in front of the lands, and the length of the dam begins to increase, finally, filling up the pores and extending this effect to the lands and the pores upstream, thus forming the flooded region of Zone B (Fig.6.6).

This zone was found to be entirely responsible to the pumping action mentioned above. It was found that whenever Zone B was flooded with oil, there was pumping in Zone A, and vice versa. This is because the oil which passes into the pores in Zone B generates the pressure that pumps the oil out in the separation zones. Note that pumping never

occurs in the load carrying zone.

6. 3. Diverging Zone

Here there is the same separation as in Zone A. However, the oil in this region tended to remain deep inside the pores in the surface. That means we have a configuration that whilst the porous surface at the converging inlet was covered by a layer of oil, the oil in the diverging outlet remained deep in the bottom of the surface pores. However, some pumping also occurred in this zone, but with an intensity much less (about one-tenth) than that in Region A, i.e. less pores participate in the pumping and a slower pumping rate. Pumping here was restricted to a few pores of small diameter situated very close to the beginning of the region. Fig.6.7 shows the pumping of oil in this diverging zone.

6.4. Recirculation of Oil

The classical concept of the recirculation of oil in porous bearings is that the oil seeps into the porous matrix at the loaded region and comes out into the clearance gap in the unloaded region. Morgan [11] has demonstrated the recirculation of oil in the porous medium to be on a macroscopic scale and to be homogenous around the circumference of the bearing. Note that in his experiment the bearing was operated in an oil flooded condition in which a wool-felt soaked with oil was employed as an auxiliary reservoir.

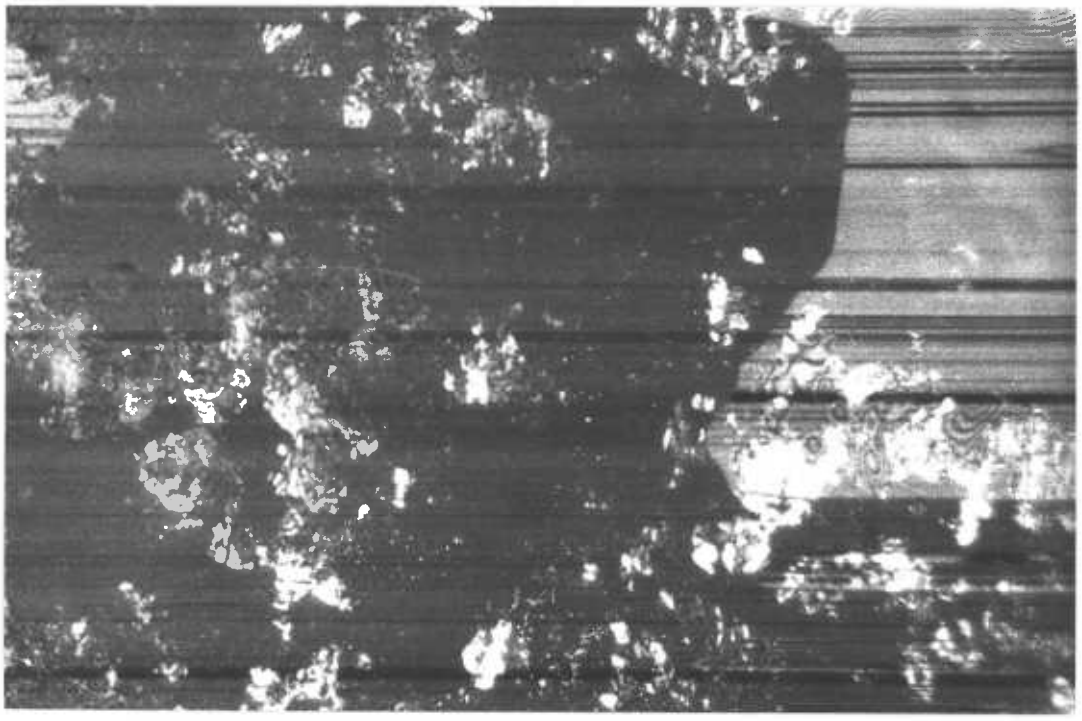

Fig. 6.6. Flooded region (zone B) interferogram, x 250.

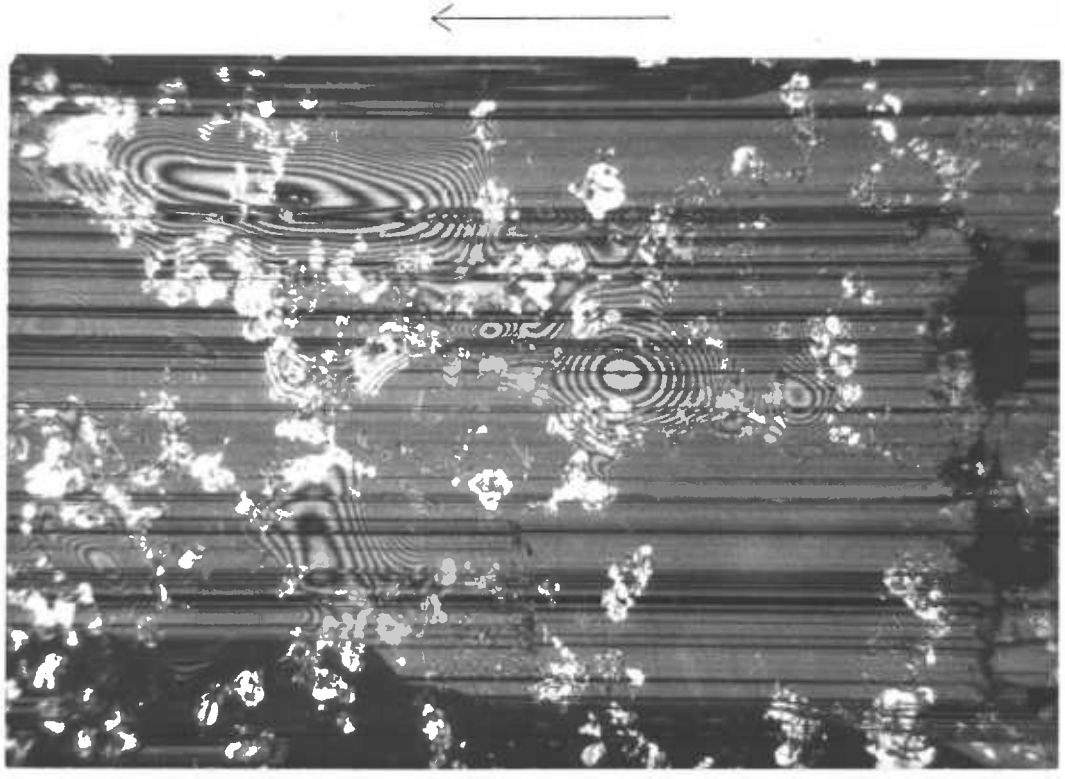

Fig. 6.7. Pumping in the diverging zone, x 180.

In the present experiments it was found that, first, in a starved or semi-starved condition the circulation of oil was on a microscopic scale. The action was concentrated in the load carrying zone, in which the oil came up to the contacting surface via the front wall of lands by means of the wetting mechanism. Also the extra oil in the dam probably flows down into the pores, to maintain the stable length of the dam. This means that the unit for the circulation of oil has the dimensions of a dam, which is only about 20μ. Secondly, when the system is flooded, a relatively large amount of oil flowed into the porous medium in Zone B, and the oil was pumped out into the gap in Zones A and D. Most of this pumping occurred in a small region immediately in front of Zone B. The ratio between the pumping action in Zone D and Zone A was about one-tenth.

It was considered whether any venturi effects might contribute towards the circulation of oil; that is, the action of the moving shaft producing a reduced pressure at the mouth of some surface pores, causing oil to be sucked out. However, judging from the observed EHD effects of the air, this hypothesis is unlikely to be true. Such suction forces may be able to get oil out of the pores, but they are not able to raise the oil sufficiently high for it to touch the running shaft, because as the oil comes close to the shaft, the air would tend to suppress it. Hence it is concluded that it is the internal positive pressure in the porous medium which gives rise to the pumping effect. However, suction can exist and the fact that the oil level is higher in the inlet convergent

zone than in the divergent outlet can be explained by the action of suction forces. Further evidence for the existence of suction forces is that immediately after the disc has stopped moving, the oil within pores in the separation zones was seen to fall downwards into the porous matrix. In short, it can be concluded that suction forces can contribute to the oil being drawn out of the pores, but it alone can never give rise to the phenomenon of pumping which has been observed.

CHAPTER SEVEN

ADDITIONAL EXPERIMENTS

7.1. Plane Thrust Porous Bearings

Besides being used as a journal bearing, porous metal is also used as a plane thrust bearing, either as a flange to the journal bearing, or as a separate thrust washer. The lubrication mechanism of this type of porous thrust bearing has not been studied before. By replacing the cylindrical domed porous specimen with a flat one, it is possible to study plane thrust porous bearings using the same interference experimental set-up mentioned previously. As might be expected, the phenomena occurring at the contact surface were similar to those of the load carrying zone described in Chapter 5, i.e. a cavitation and an oil dam associated with each land, and the load carried on the lands by the taper induced by differential thermal expansion and sulphur films. Fig. 7.1 shows a typical interferogram of the surface at work, and Fig. 7.2 plots the relationship between the film thickness and the square root of velocity. Fig. 7.3 shows a microscopic view of the surface after running continuously against a steel disc for 20 minutes, showing the same deposition of sulphur layer at the rear part of each land.

Just like the load carrying zone in a porous journal bearing, a plane parallel porous thrust bearing never exhibited the phenomenon of pumping. However, by tilting the thrust surface slightly, to produce a converging gap, the same phenomena to the converging zone of a porous

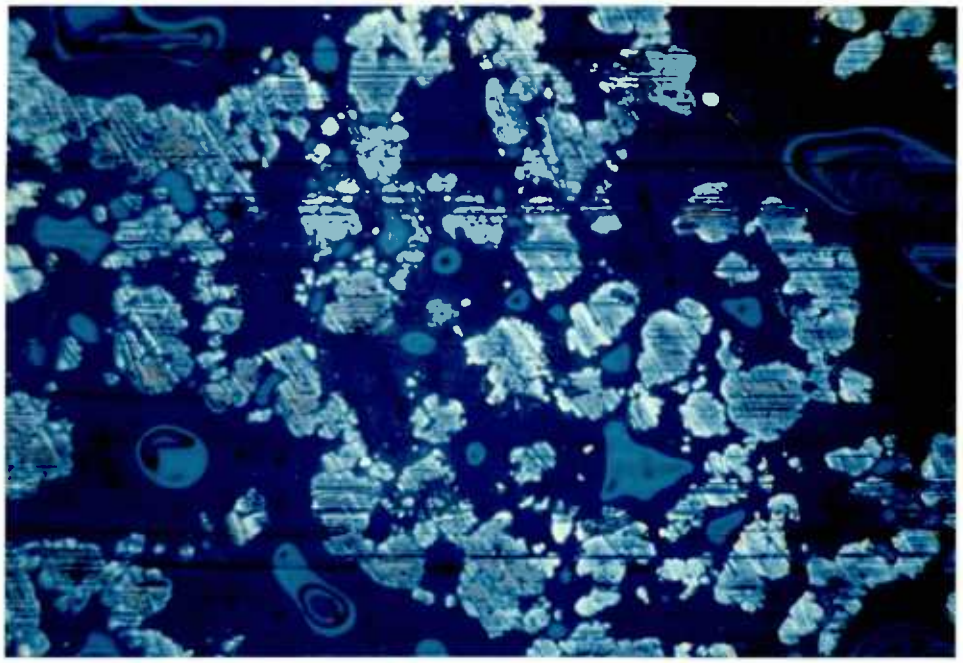

(a) $U = 0, \quad h \simeq 0$

(b) $U = 5\text{ft/min}, \quad h \simeq 2\mu\text{in}$

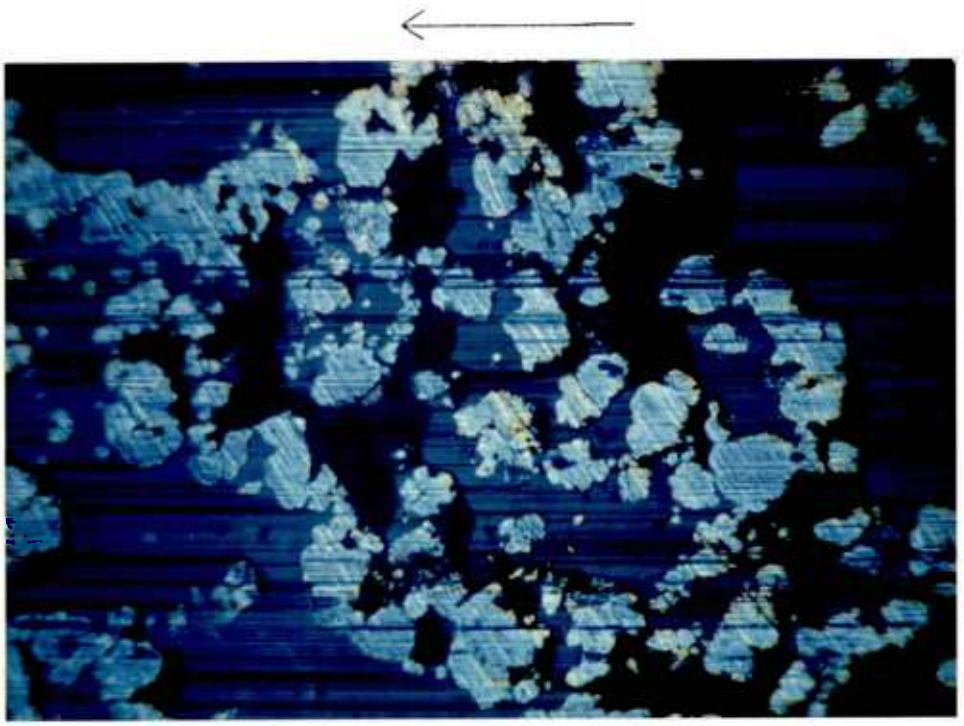

Fig. 7.1. Typical interferograms of a plane thrust porous bearing, showing the increase of film thickness as the speed increased, x 180, (continued on next page).

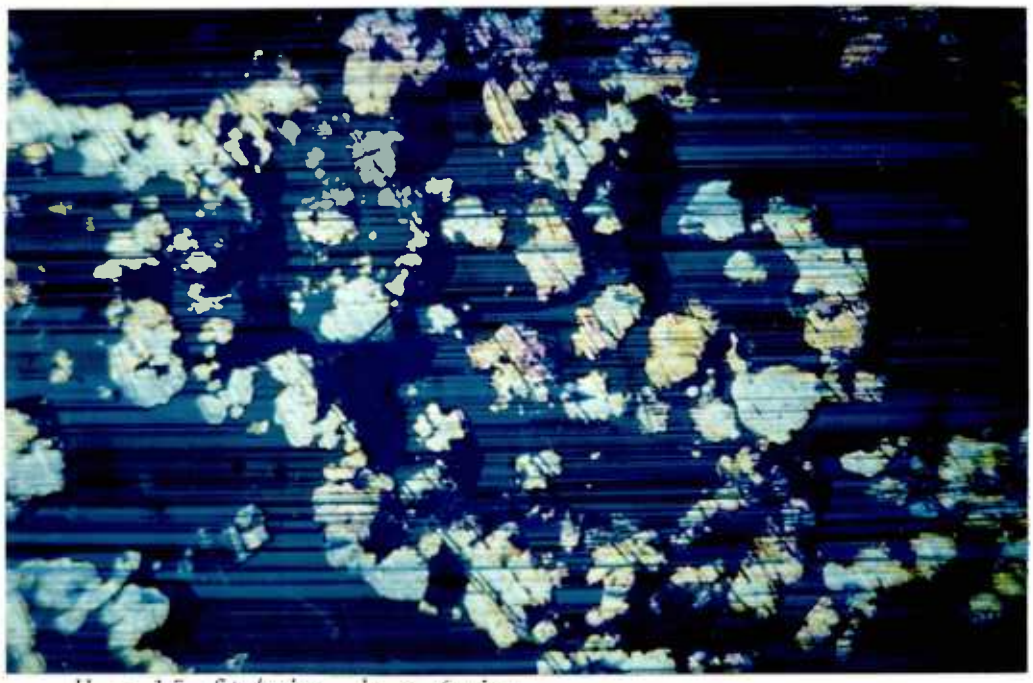

(c) U = 15 ft/min, h ≈ 6μin

(d) U = 30 ft/min, h ≈ 8μin

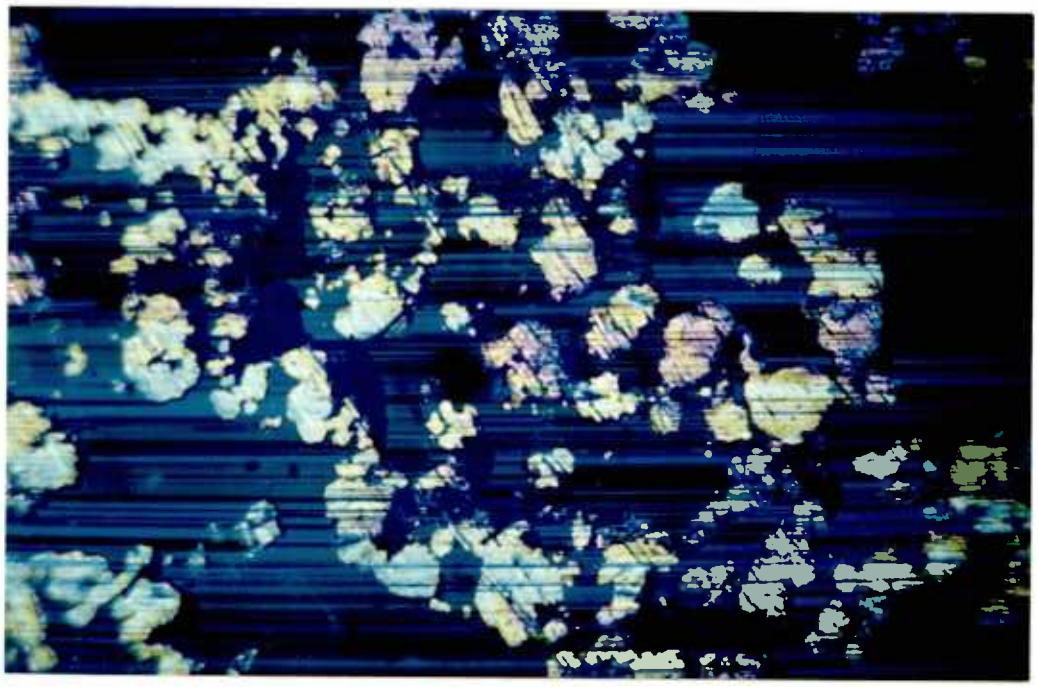

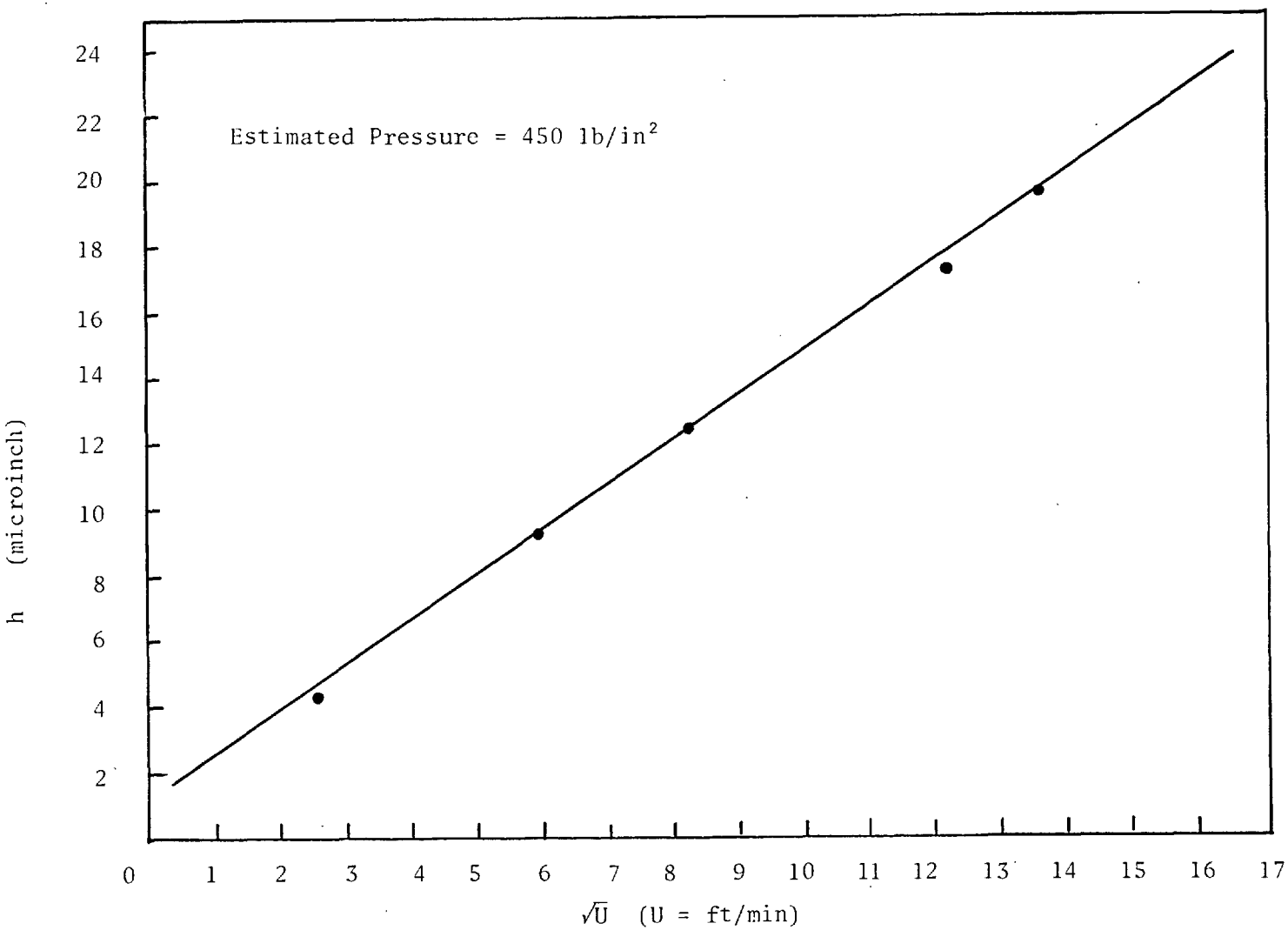

Fig. 7.2. Film thickness versus square root of speed.

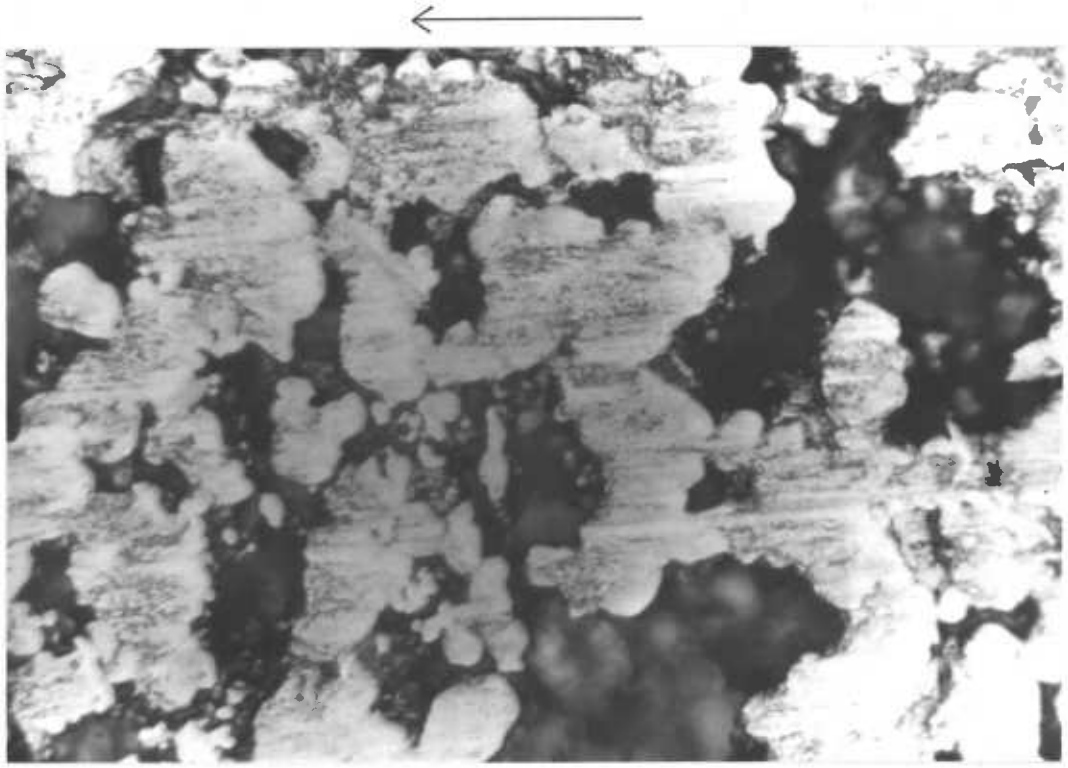

(a) x 200

(b) x 400

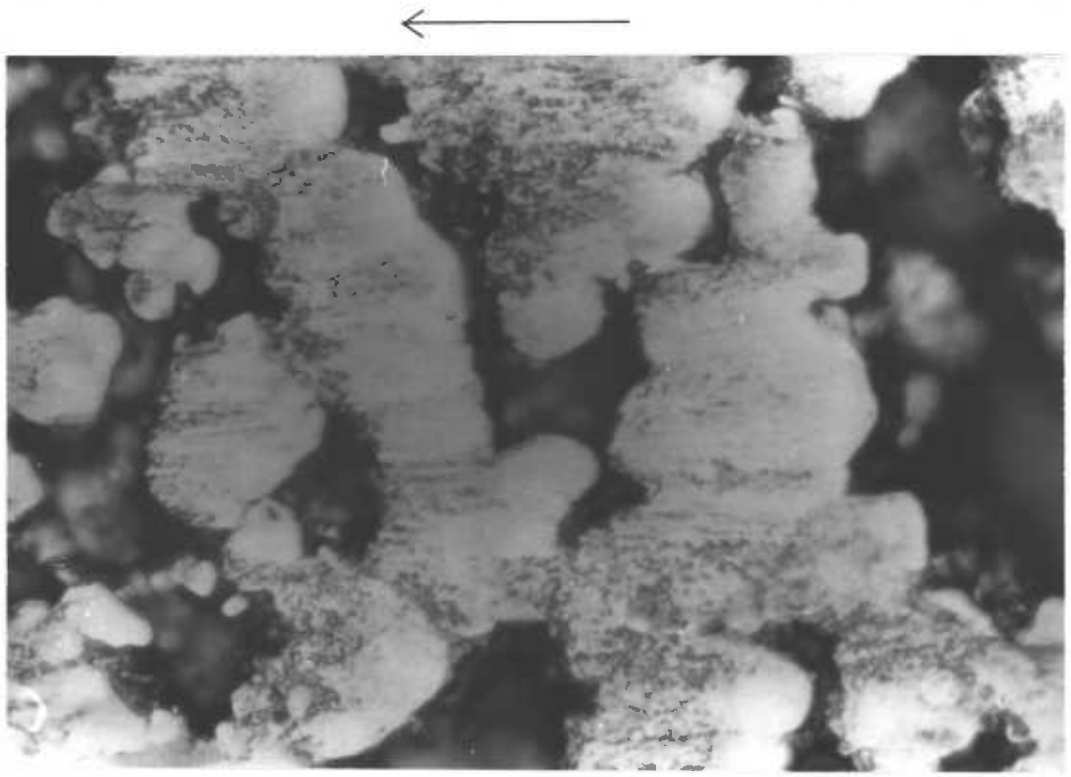

Fig. 7.3. Microscopic view of run-in surface of plane thrust porous bearing.

journal bearing occurred. Namely, because the applied load was now concentrated at the outlet edge of the specimen, intensive wear and metal smear occurred there; and immediately in front of the contact zone the same flooded zone occurred, and in front of the flooded zone the pumping of oil occurred. The principles underlying these phenomena have already been described in Chapter 6, so they will not be mentioned again.

In summary, the lubrication mechanism of a plane porous bearing is due to the formation of a micro-thermal taper on each land, over which hydrodynamic pressure is developed to carry the load.

7.2. Running-in Process

Porous metal bearings depend on the running-in process more than non-porous bearings. Fig.7.4 shows the effect of artificial asperities made by first running the porous specimen against a rough steel disc and then turning it through 90^{o} before testing it with optical interferometry. The hydrodynamic film is seen to be ruptured behind the asperities, as shown by the change of colour of the fringes (arrows) due to cavitation on the surface of the lands. Asperity contact results in a high local pressure. Although a porous metal bearing consists of about 70% of metal and 30% of pores, the amount of metal in actual rubbing contact is very much less than 70%, perhaps only about 20%. This fact was observed in the interference experiments. A typical interferogram of such a surface is shown in Fig.7.5. Note the same oil dam and

cavitation, but their corresponding 'lands' are so small and rough that they are hardly seen.

During the first few minutes of running, the area of real contact increases, rapidly to start with, but at a reducing rate as the process proceeds. After about an hour, the real area of contact settles to a steady value. This value depends on the design parameters such as porosity, load, velocity, quantity of oil, etc. Fig.7.6 shows a series of pictures of the bearing surface taken during running-in. The experiment was done by running the specimen against a steel disc, and after various periods of running, the surface was photographed. The increase in surface area is clearly seen. Fig.7.6d represents the final stage of the running-in process, after which this particular surface condition remains substantially unchanged (the experiment was terminated after 12 hours of running because no further change was noticed.) This increase of area took place in two ways. The first was by wear, in which metal is polished away from the top layer of the bearing and in so doing exposed more area of the particles in contact. The second was by metal smearing. Fig.7.7 compares the land areas in Fig. 7.6a and 7.6d. It is seen that the increase in area tends to follow the direction of sliding. This phenomenon arises with high local pressure and/or high local temperatures, in which the metal exhibits 'plastic' behaviour so that the top layers 'flow' along the direction of the shear forces. In doing so, some of the surface pores, especially the small ones, become closed. The amount of metal smearing was found to increase with increasing load.

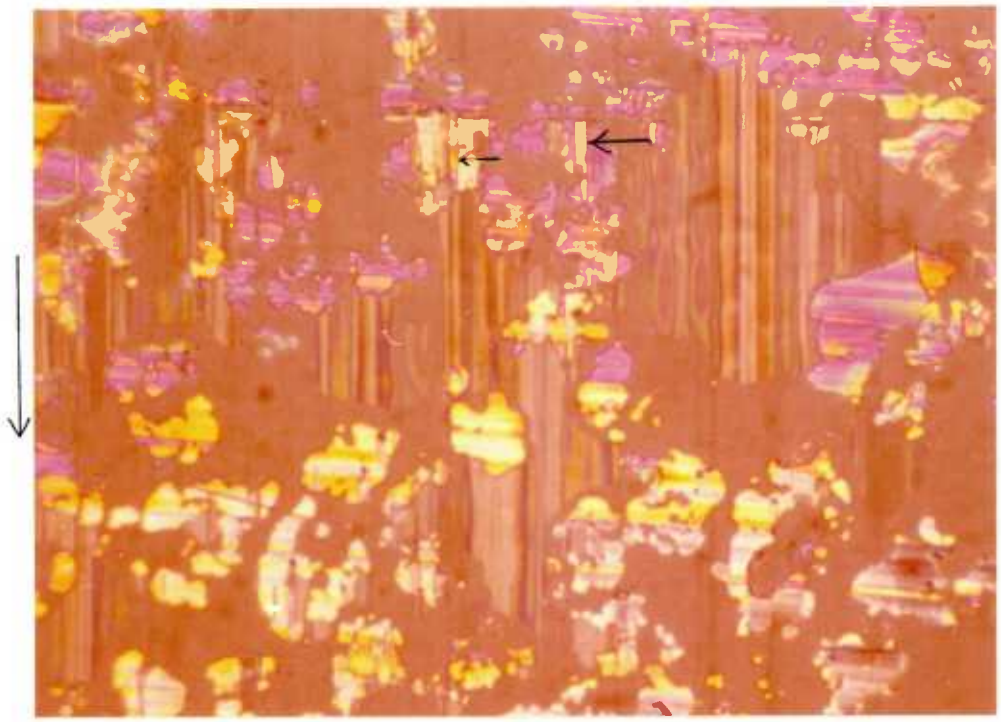

Fig. 7.4. Rupture of hydrodynamic film (arrows) due to asperities.

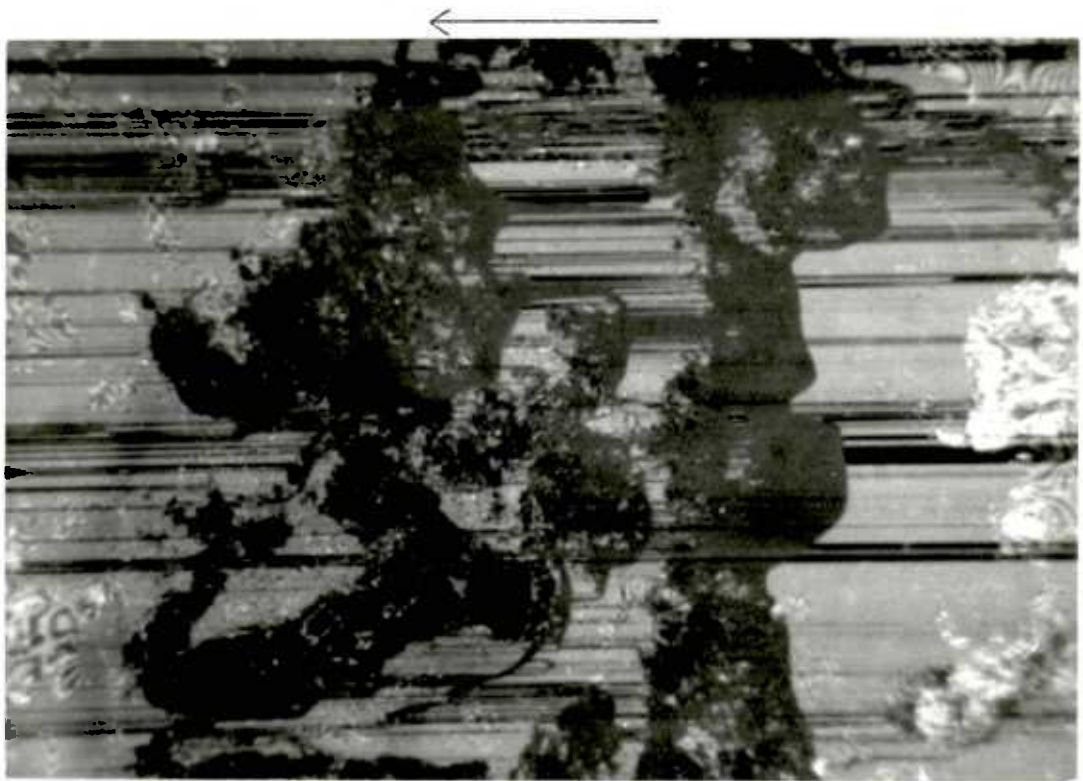

Fig. 7.5. Interferogram of a non-run-in porous surface, x 180.

(a) t = 0

(b) t = 40 min.

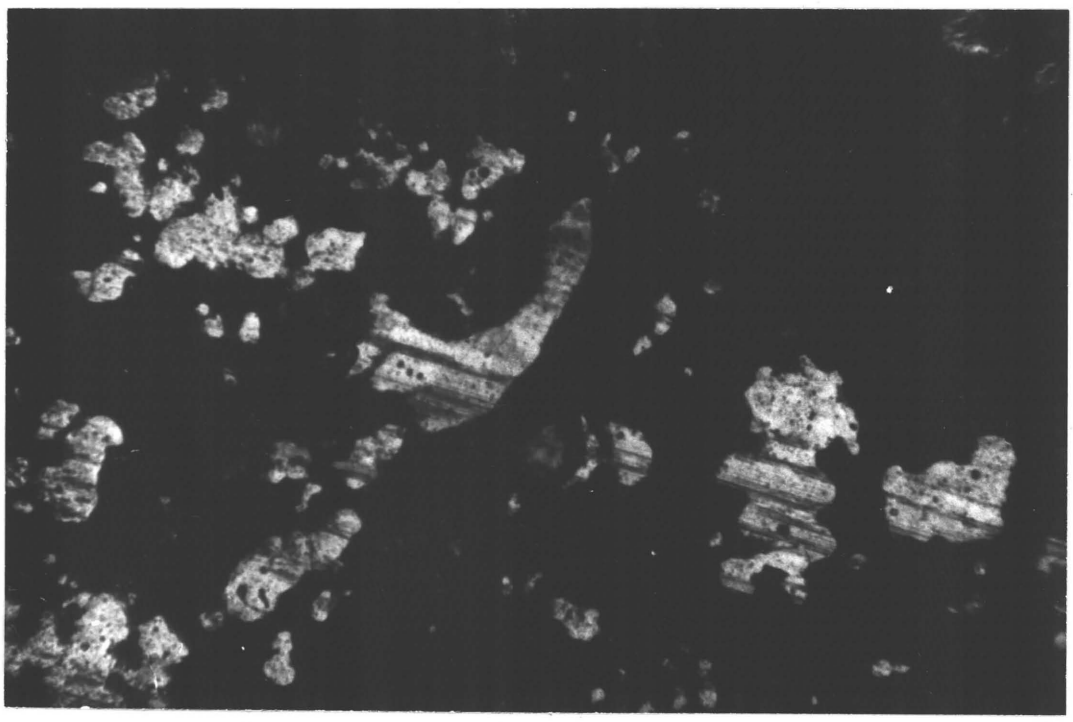

Fig. 7.6. Photomicrographs of porous surface at different times during running-in, x 300, (continued on next page).

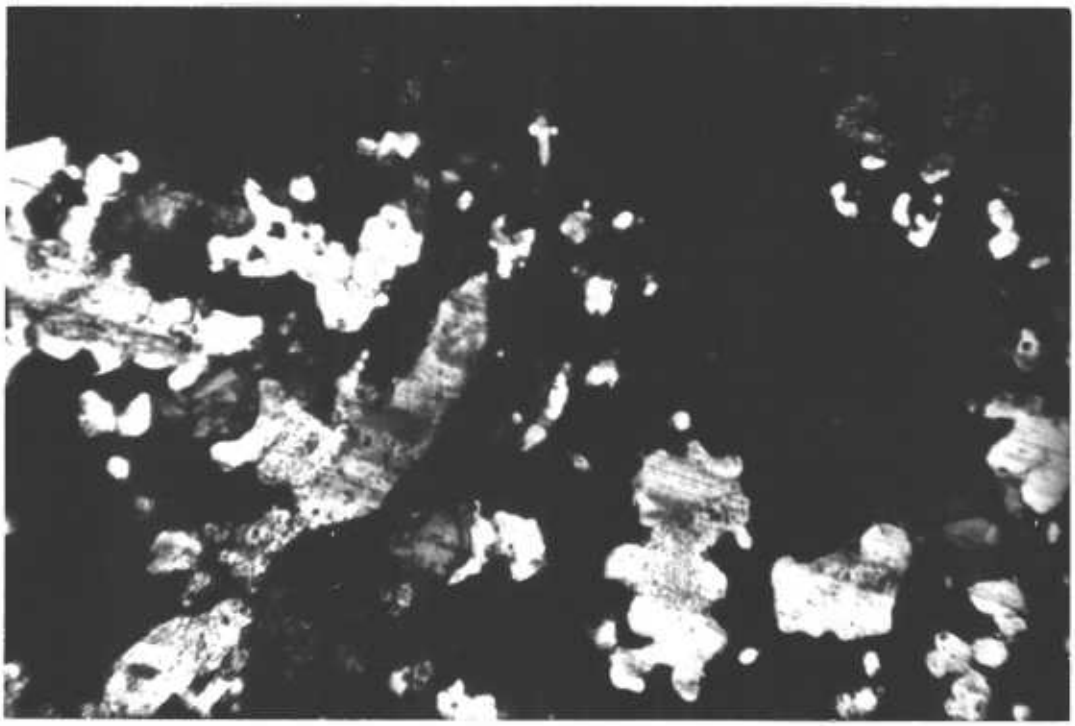

(c) t = 100 min

(d) t = 200 min

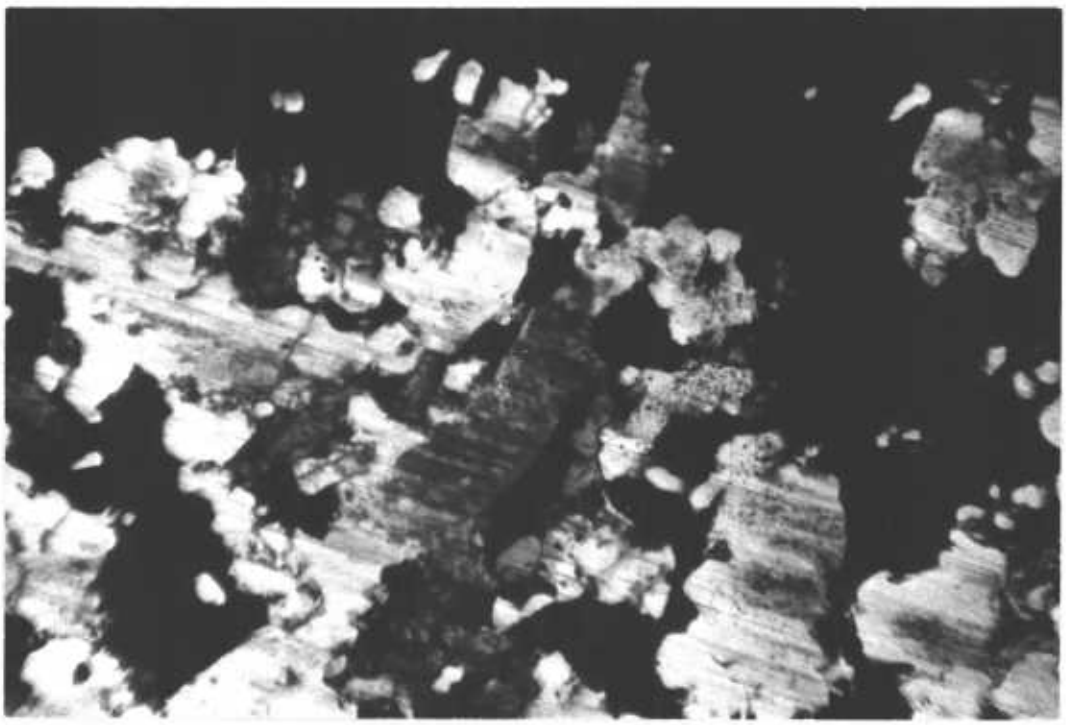

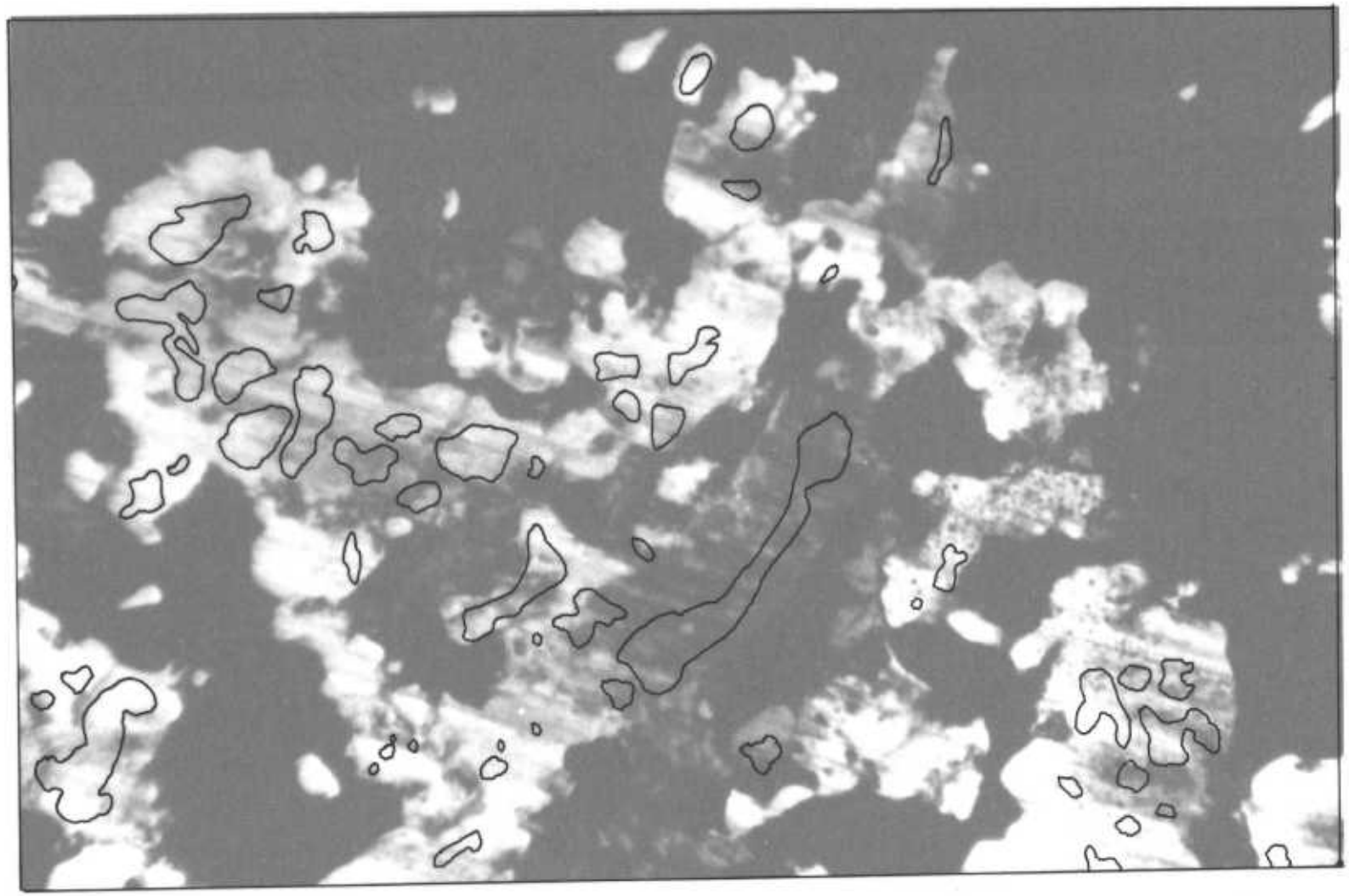

Fig. 7.7. Comparison of Fig. 7.6a and Fig. 7.6d, showing the effect of metal smearing and wear.

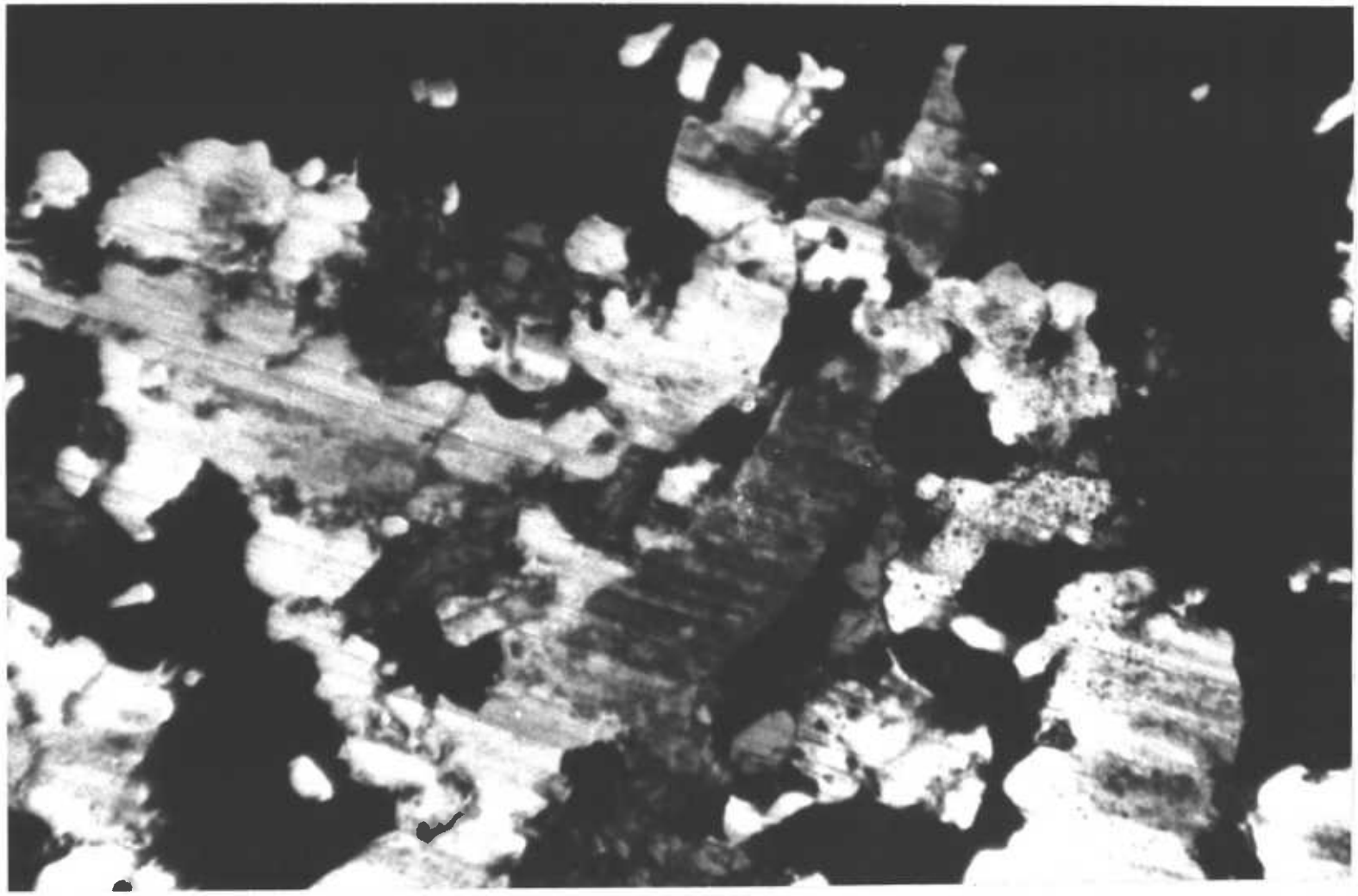

Fig. 7.7. Comparison of Fig. 7.6a and Fig. 7.6d, showing the effect of metal smearing and wear.

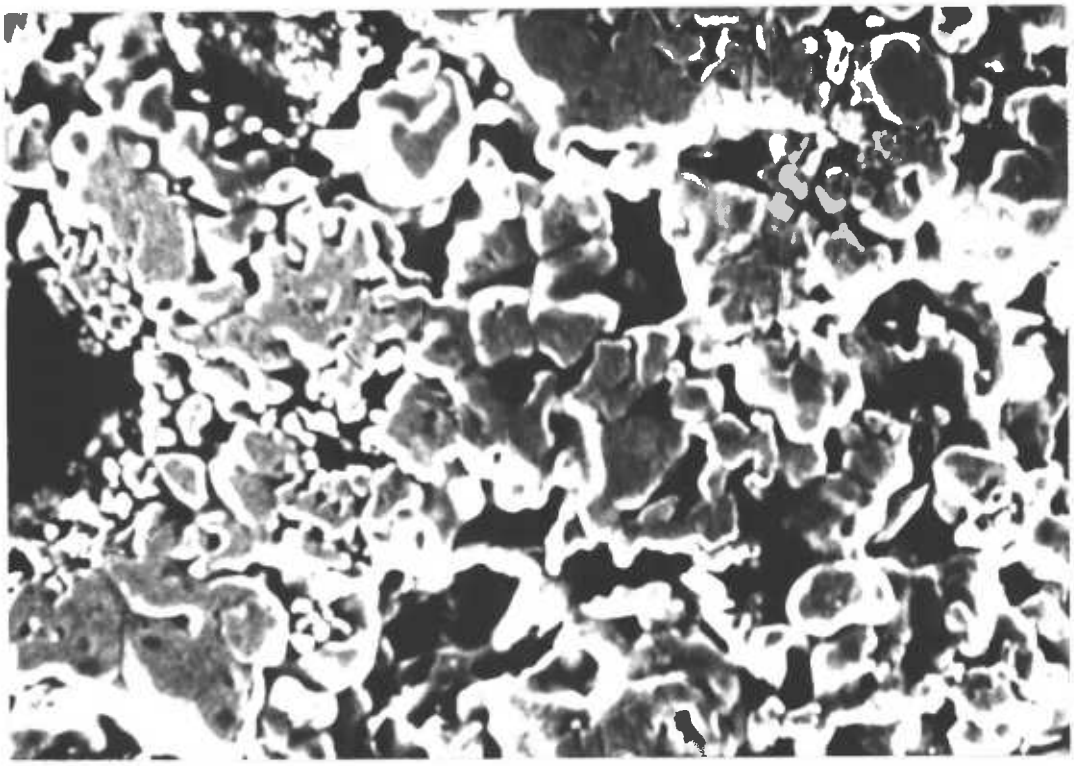

(a) Before

(b) After

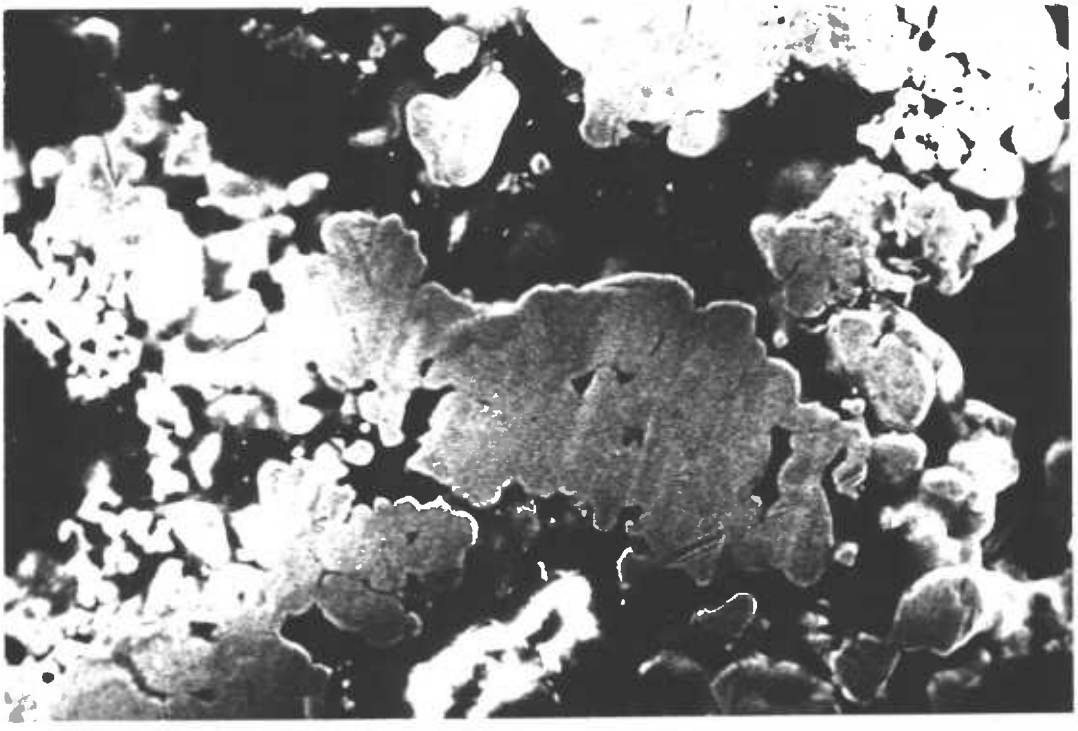

Fig. 7.8. Scanning electron micrographs of the same porous surface: (a) before and (b) after running-in, x 700.

Under normal conditions where the load is small and the velocity is high, the effect of metal smearing may be outweighed by the effect of wear. Further evidence of metal smearing and wear is shown in Fig.7.8. In short, the study of the running-in mechanism leads to the following conclusions:

1) The running-in process is a mixture of wear and metal smearing. Its ultimate effect is to create a sufficient area for the building up of a hydrodynamic film, when the process stops.

2) In general, the running-in process takes place within the first one to two hours.

3) Small lands which are close together tend to join up into a single large land.

4) 'A properly designed porous bearing' means one that after the running-in process still has enough pores left on the surface for the oil to come out of the porous matrix.

5) The most important consequence of the process is that it makes the two rubbing surfaces parallel (from a macroscopic point of view) regardless of the originally designed contact geometry.

7.3. Onset of Failure

The effect of wear and metal smearing during running-in causes the porous metal bearing to operate in the hydrodynamic regime. However, too much wear and metal smearing can lead to the premature failure of the bearing. The running-in process causes the area of the pores to decrease and the area of the lands to increase.

Remembering that in a non-flooded condition the only way for the oil stored within the porous matrix to come into the rubbing surface is by wetting, via the walls of the lands, reducing the pore area cuts down the supply rate of oil. Therefore there exists a critical value for the land to pore ratio, above which the porous bearing is doomed to fail early. This critical value depends upon many factors such as the quantity and quality of the oil, the load, the speed, the running temperature, etc. Morgan [44] indicated that a porous bearing starts to move towards the end of its useful life when the ratio is about one. His figure is based on an analysis of the surfaces of failed bearings.

This criterion for the onset of failure also applied to a properly designed porous bearing. During the running-in process, much debris will have been created (due to wear). Microscopic study has shown that the size of this debris ranges from 0.5μ to 2μ, and that it is suspended in the oil. This debris can act as a grinding or polishing media and, of course, creates more and more debris. That means that a run-in porous bearing operating in the hydrodynamic regime can be subjected to further wear if the film thickness is less than the size of the debris. It can cause local rupture of the oil film or may fill up the pores, both of which will adversely affect hydrodynamic lubrication. As oil is lost from the system, the hydrodynamic film thickness decreases and hence the land to pore ratio increases slowly but progressively. When this ratio reaches about one, the bearing approaches the end of its life at an increasing rate.

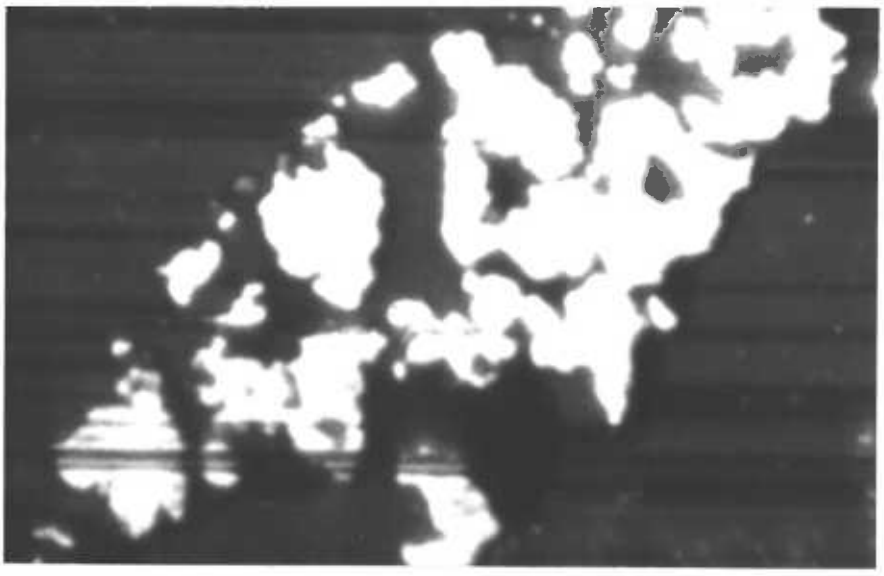

(a) Before running-in

(b) After running-in

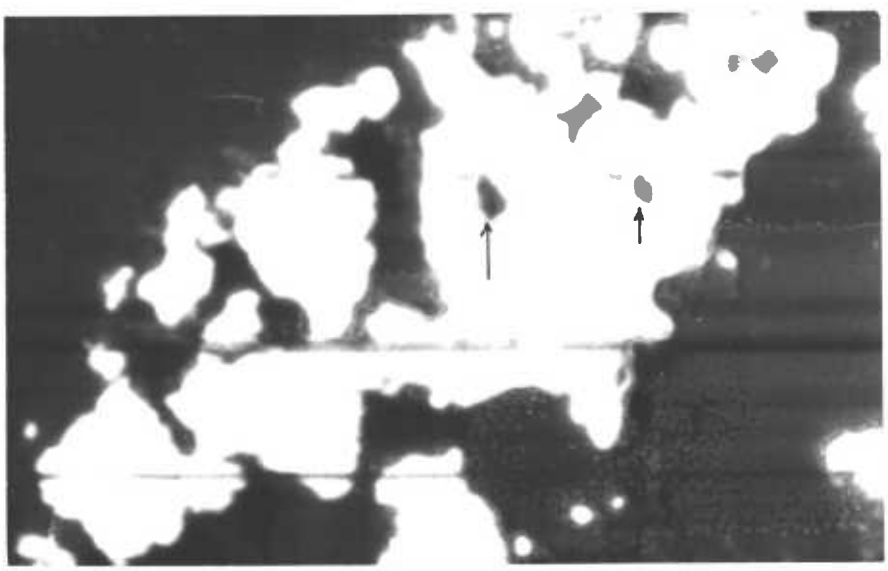

Fig. 7.9. Effect of pore closure on the formation of the oil dam (arrows), x 800.

During the final stages, the temperature rises, and if the differential thermal expansion of the bearing housing and shaft can cause a reduction in the running clearance, this may end in seizure.

Fig.7.9 shows how the supply of oil can be reduced by the closure of surface pores. Note that theoretically the load capacity of porous bearings increases with increasing pore closure, but in practice this is applicable only up to a certain extent, because the problem of oil supply is adversely affected.

7.4. Effects of Graphite

A solid lubricant - graphite - is usually present with porous bearings. This protects the bearing surfaces from direct metal to metal contact in conditions where the hydrodynamic oil film has not been formed. For example, in cases of 'stop-start' operation, the velocity may be so low that boundary lubrication is inevitable. Fig.7.10 shows the effect of a graphite particle on the lubrication of a porous bearing. The particle stood proud of the bearing surface such that it carried a large part of the load. There was no measurable hydrodynamic film formed over the graphite surface, probably because of the high local pressure. Its corresponding interference fringe appeared dark, and cavitation was developed behind the graphite. Bronze particles can be seen in the surrounding area well below the contact surface.

In another experiment, a porous sample with graphite was run against an uncoated glass plate for one hour. The

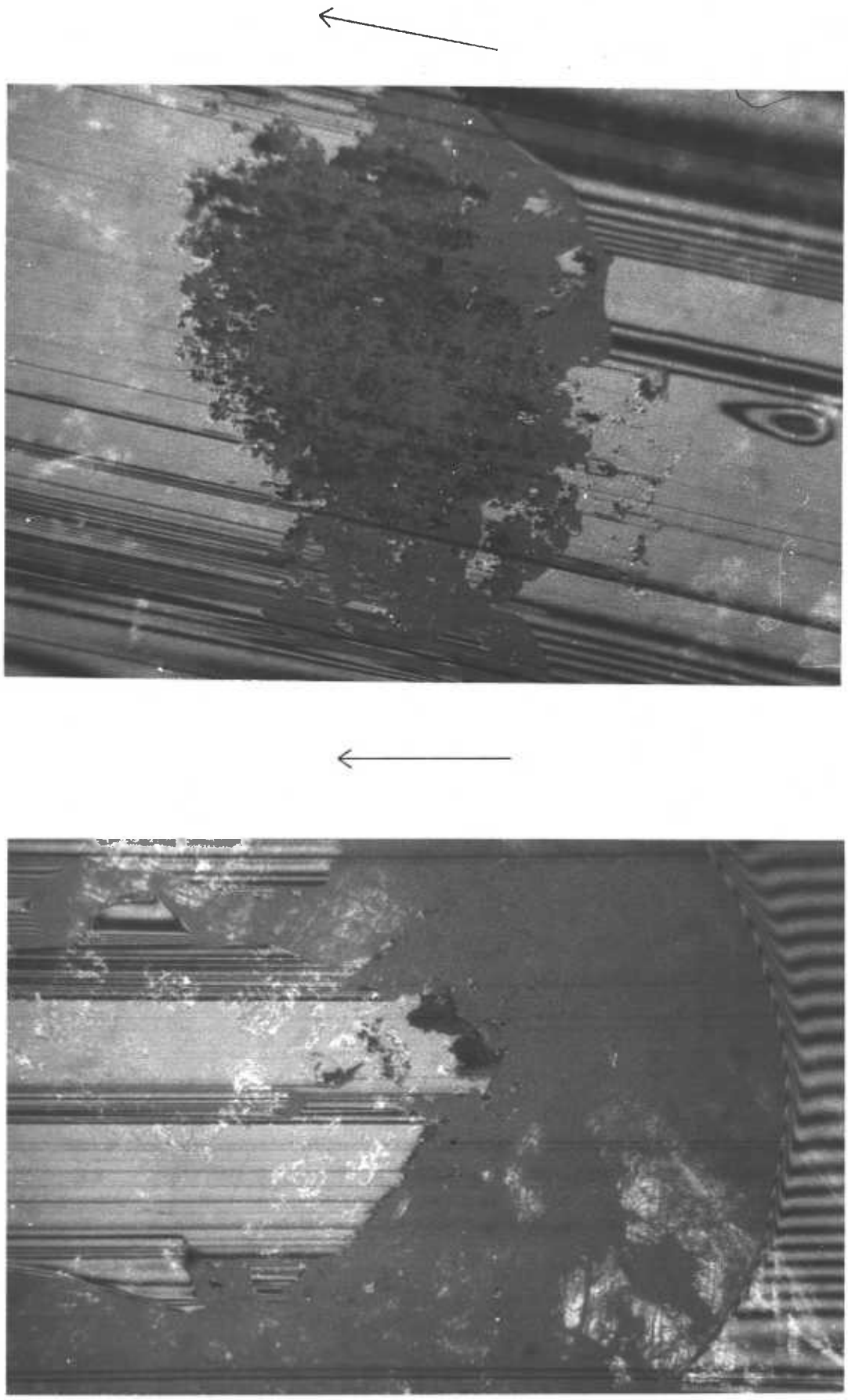

Fig. 7.10. Influence of graphite particles on the flow of lubricant, x 180.

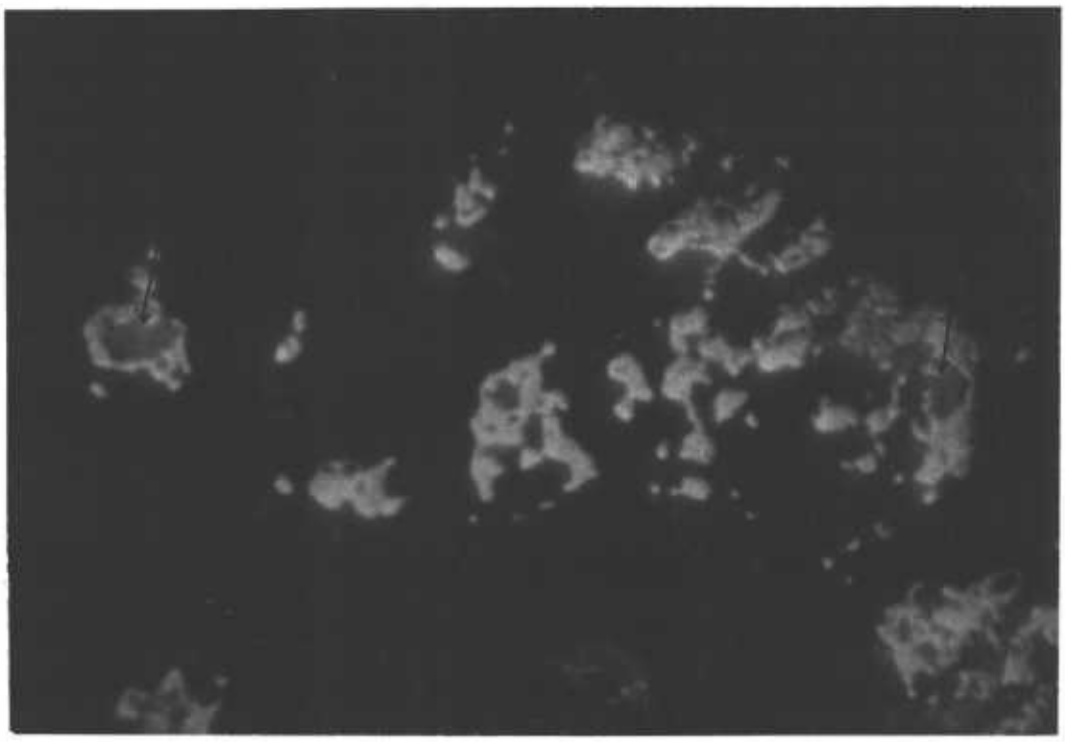

(a) Before running

(b) After running

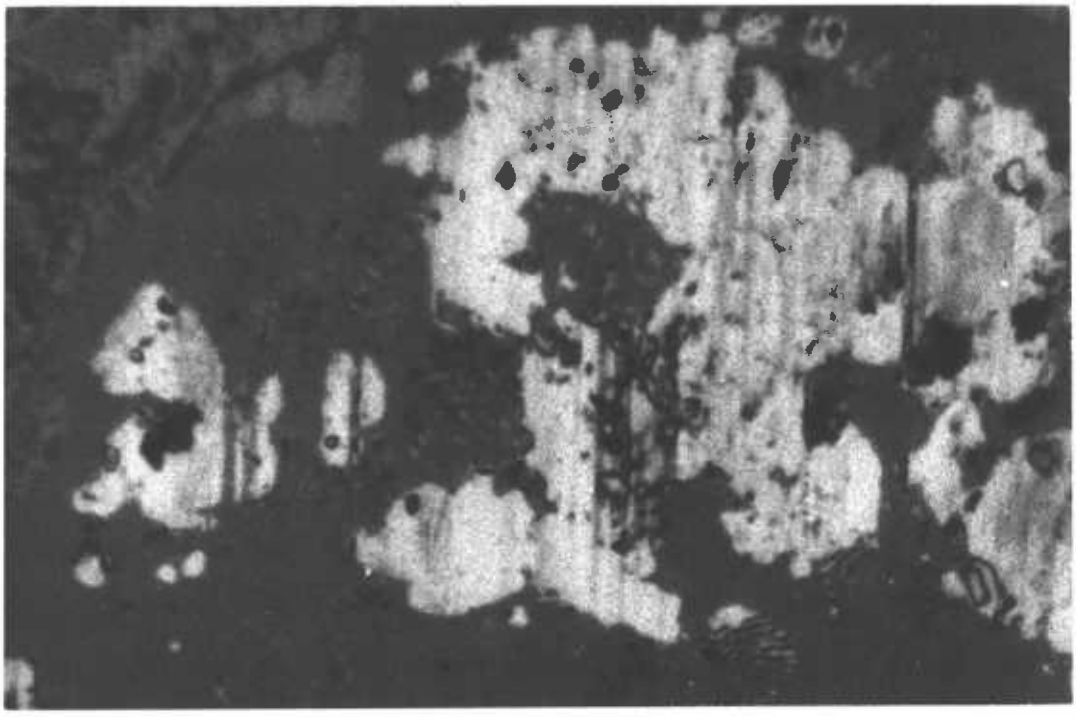

Fig. 7.11. Illustration of graphite particles (arrows) in boundary lubrication, x 800.

running conditions were designated such that the operation was entirely in the boundary lubrication regime. Fig.7.11a shows the original porous surface, with the graphite particles as indicated by the arrows. After running for one hour, considerable wear and metal smearing had occurred, and it seemed that the graphite had disappeared. However, when viewed with interference (using a coated glass disc), the presence of graphite particles was revealed, as is seen by their dark appearance in Fig.7.11b. The conclusion of these two experiments can be summarised into the following points.

1) In general, the graphite particles stand slightly higher (say, 0.5 microns to 1 micron) than the bronze particles.

2) Being a solid lubricant, this higher position at the surface is beneficial to the bearing. But in the sense of hydrodynamic lubrication, the graphite particles obstruct the bronze particles from participating in the load carrying action.

3) Under boundary lubrication conditions, the graphite particles remain in their original position, in spite of intensive wear and smearing.

7.5. Effects of Sulphur.

The sulphur additive in the oil was shown in Chapter 5 to be evidence that a thermal wedge existed on each land during the operation of the bearing. The tapering sulphide layer was very thin. After intensive running, the sulphide films are much thicker and Fig.7.12 shows the

photomicrograph of the surface of a porous journal bearing after running continuously for four hours at high speed under heavy load. It will be seen that most of the surface pores have been closed. Note the tail-shaped dark areas which have developed on the surface (like comets). Interferometric measurement showed the thickness of these dark areas to be higher than the neighbouring surface by 0.5 to 1 micron. Microhardness tests indicated that this dark material was softer than the neighbouring bright areas by a factor of two or more. Fig. 7.13 and Fig. 7.14 show the EPMA traces of the dark area, in a direction perpendicular to that of the tail. It is seen that the sulphur concentration increased dramatically in the wear scars (dark area). At the same time the concentration of tin in the wear scars decreased due to the covering effect of the sulphide layer. Note that the concentration of sulphur was also very high within the pores. It can be easily distinguished from that due to wear scars by the trace of the AEI which deflected slightly when the probe came across a pore. Note also that the concentration of tin also decreased in the pore.

Such tail-like sulphur spots were found to be distributed all over the bronze surface where the pores had been mostly closed. The reason they were formed in this way is not fully understood. One possible explanation is that the high local temperature at the point of asperity collision or local welding of the surfaces is sufficient to form a relatively large amount of sulphide

at these points. After that, the sulphide spot is smeared along the surface, making it look like a comet. The time during which these temperature fluctuations takes place may be very short, and their extent may be only on a microscopic scale [5].

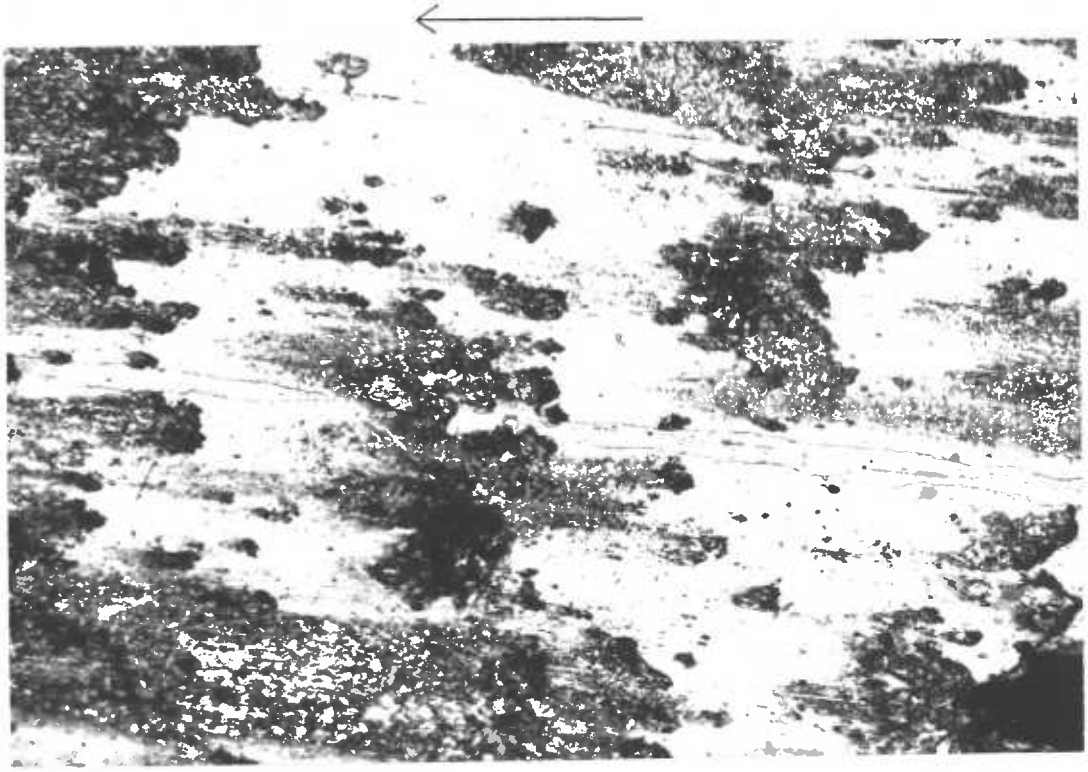

(a) x 200

(b) x 400

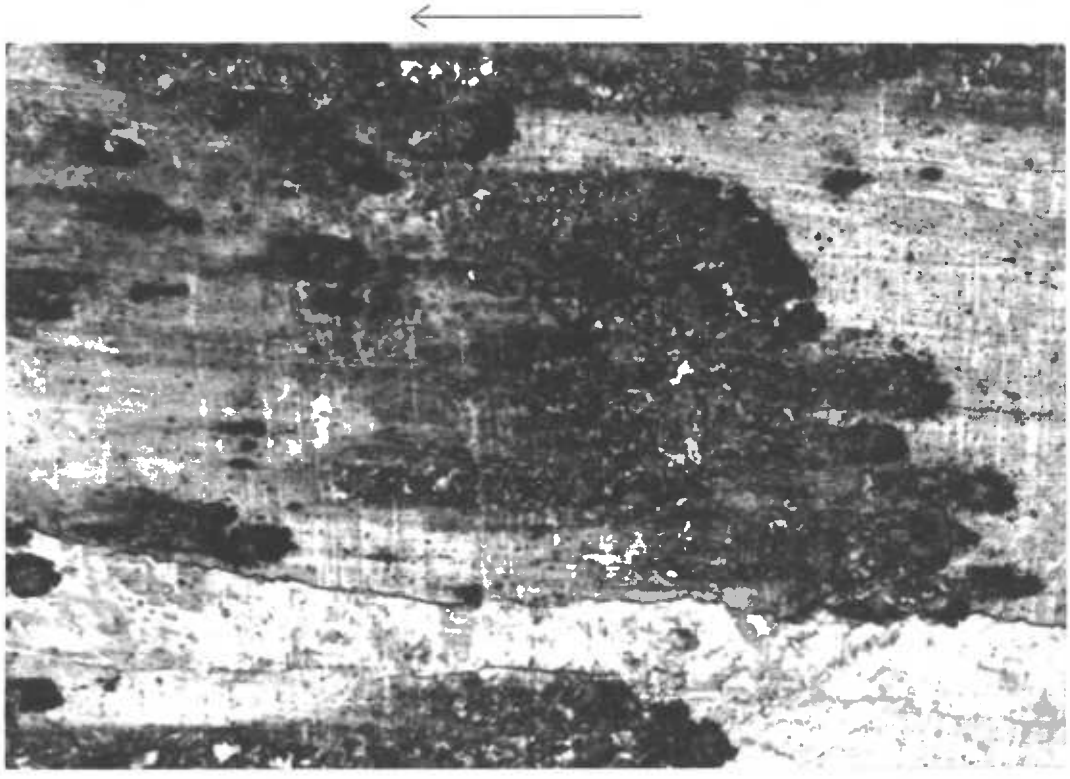

Fig. 7.12. Photomicrographs of porous surface after intensive running.

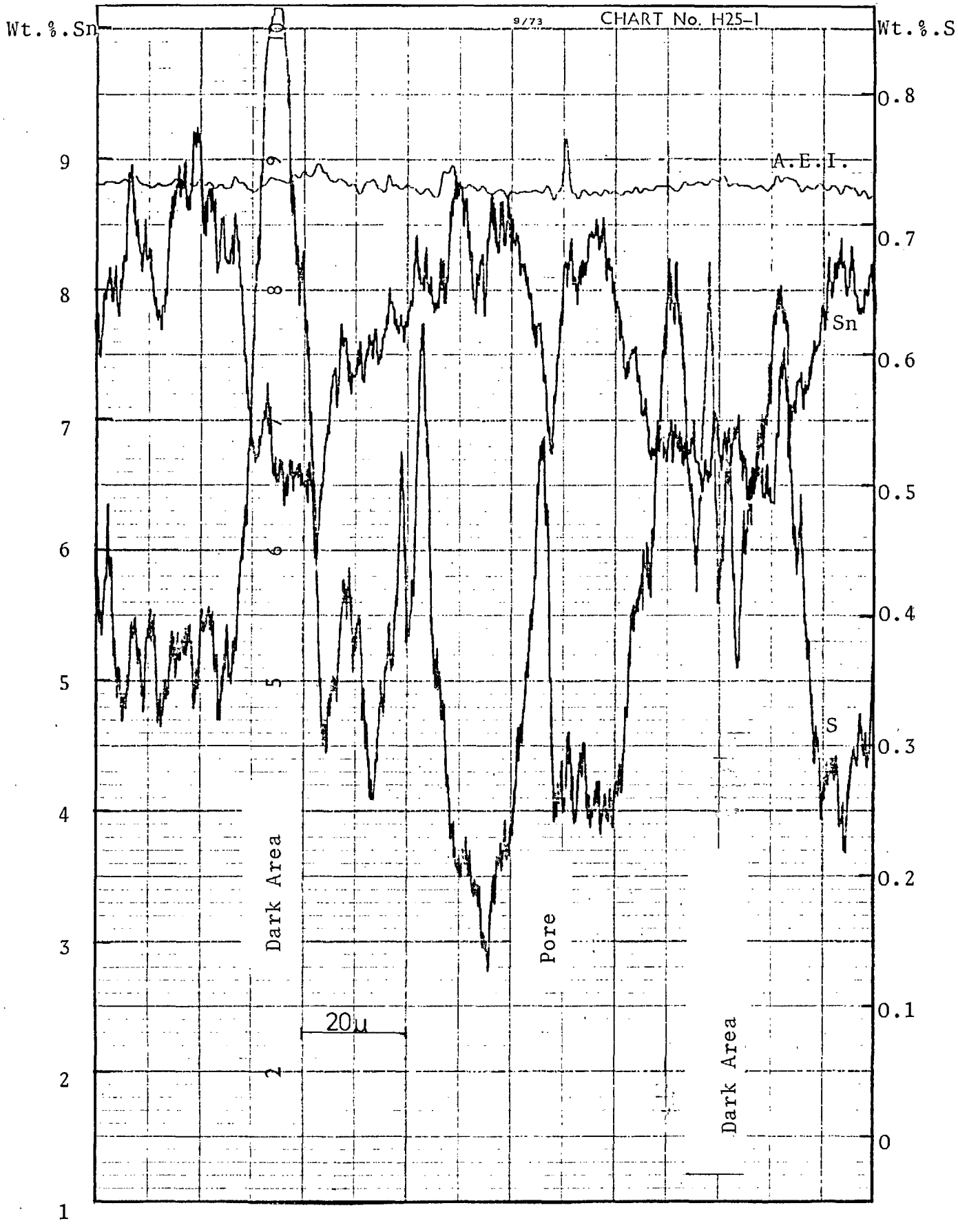

Fig.7.13. EPMA Trace across the wear scar (dark area) similar to that shown in Fig.7.12.

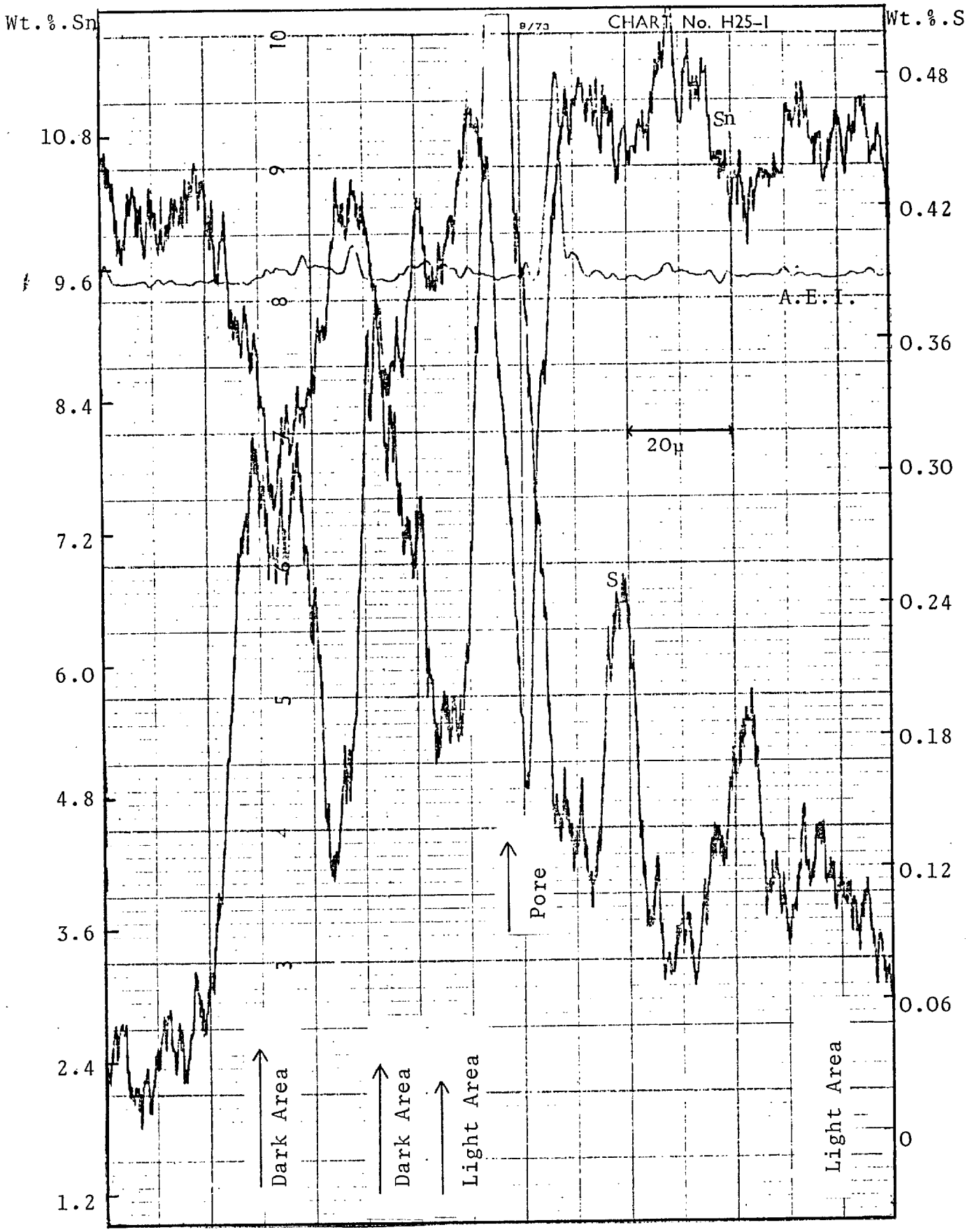

Fig.7.14. Another EPMA trace across the wear scar

CHAPTER EIGHT

DISCUSSION, CONCLUSION AND SUGGESTIONS FOR FUTURE WORK

8.1. Discussion

This thesis has investigated the mechanism of lubrication of porous metal bearings using optical interferometry,and metallurgical methods as subsidiary analysis. The results from these two independent physical techniques reinforce each other and give strong support to the new mechanism proposed. The optical technique has benefited from the two phase flow which occurs, without which it is almost impossible to tell which way the oil flows within the pores. Further, the validity of using the system employed here to represent a real journal bearing has been confirmed: the sulphur wedge effect found in porous journal bearings was also detected when the cylindrically domed porous specimen was run against a flat steel plate. This indicates that the same lubricating mechanism operated in both cases. Amongst the phenomena found in this project perhaps the most significant one is that of cavitation. Its presence immediately disproves the idea that the two surfaces are separated by a continuous film of oil. It also helps in the establishment of a thermal taper, which is crucial to the hydrodynamic lubrication. Other phenomena, such as the square root relationship between the velocity and

film thickness, and the deposition of sulphide films at the rear part of the land, have provided the framework within which the behaviour of the porous bearing is explained.

Under normal conditions, e.g., when no external supply of oil is available, the new mechanism proposed differs from the mechanism of operation of a non-porous (solid) metal journal bearing. For a non-porous bearing the film shape is determined by the clearance and eccentricity of the journal and the bearing. For a porous bearing, however, the film shape is 'created' by the operation of the bearing during running. The reason why the classical theory of journal bearing does not apply to porous bearings is that the oil in a porous bearing tends to leak into the porous medium and to stay there. Without enough oil, the macroscopic wedge cannot be established. Under these circumstances, most of the applied load is concentrated in a small area of closest approach of the two surfaces. The high pressure developed causes severe wear and plastic flow in the loaded region, creating and, hence, extending the area of contact over the bearing surface. In doing so the bearing preserves itself by generating a thermal taper on each land, over which a microscopic hydrodynamic oil film can be achieved.

8.2. Conclusions

The results of this study can be summarised in the following section.

8.2.1. Instrumentation

1. Optical interferometry has been proved to be a powerful tool in the investigation of porous metal bearings.
2. The power of the optical technique is increased by the presence of two-phase flow (cavitation).
3. Chromium or TiO_2 coatings of different thickness are required to match the variable reflectivity of the two-phase flow system.
4. The optical system employed here is virtually "blind" to objects about 20 microns below the contact surface. Hence only the surface features of the bearing are revealed. This is partly because of the presence of the reflecting coating on the glass disc, and partly because of the low reflectivity of the non-polished material within the pores.
5. The debris produced during the running-in of the specimen greatly reduces the time available for interference measurements.

8.2.2. Hydrodynamic Lubrication

1. Under normal conditions the macroscopic wedge of oil, similar to that of non-porous journal bearings, is not able to form.
2. The running-in process creates on the bearing surface a region which has substantially the same radius of curvature as the shaft (i.e. conformal).

3. The surface of lands after running-in is flat and has a very small taper around the edge.
4. The load capacity caused by this taper is small and cannot account for the satisfactory operation of the bearing.
5. The most likely mechanism is that differential thermal expansion causes each land in the contact region to act as a tilting pad thrust bearing.
6. The temperature gradient causing the differential expansion of the lands is enhanced by the cooling effect of the dam of oil in front of the land and the absence of cooling in the cavitation at the back of the land.
7. The load is carried by the sum of all the microscopic hydrodynamic films formed at each land.
8. The thickness of this hydrodynamic oil film increases linearly with the square root of the velocity.
9. The load capacity increases with increasing land area, but there exists a critical value for the land to pore ratio, above which the problem of reduced oil supply reduces the load capacity.

8.2.3. Self-lubricating Mechanism

1. Every land in the load carrying zone has a dam of oil at its upstream edge.
2. Under flooded conditions some of the oil in the dam may be flowing either into or out of the pores.

3. If the surface becomes starved of oil, oil will flow from the porous matrix into the dam.
4. The driving force of this upward flow is the interfacial tension.
5. Some of the oil in the dam leaks downstream around the sides of the land.
6. It is better to have a land shape which is elongated perpendicular to the running direction of the shaft, than elongated parallel.
7. A concave land (or group of lands) is better than a convex land.
8. In the flooded condition, the oil which flows into the pores reappears in the converging gap and to a lesser extent in the diverging gap, by a cyclic pumping action.
9. This pumping action is mostly concentrated in front of the flooded region in the converging gap.
10. This cyclic pumping action occurs because the rate of oil flowing out of the pore is less than the rate at which the moving shaft carries it away.
11. For a given amount of oil pumping small pores are better than large pores.

8.2.4. Boundary Lubrication

1. The running-in of the bearing is mainly in the boundary lubrication regime. During this period wear and metal smearing occur at the porous surface.

2. One of the consequences of the wear and metal smearing is an increase in the total land area available for load carrying, and hence the pore area decreases in proportion.
3. One result of the pore closure is a reduction in the supply of oil to the rubbing surface.
4. Before the establishment of hydrodynamic lubrication the solid lubricant graphite particles assist in the running-in process by providing additional boundary lubrication.
5. Under boundary lubrication conditions, the sulphur additives in the oil react with the bearing surface to form a protecting sulphide layer. This layer is formed at particular points, where the transient temperature is sufficiently high.
6. When the oil in the bearing is reduced such that it is operating only in boundary lubrication regime, it is close to the end of its life.
7. If, due to faulty design, excessive pore closure occurs during the running-in process, the oil stored within the porous matrix will be prevented from coming to the surface and premature failure may occur.

8.3. Suggestion for Future Works

Further experiments should be carried out to quantify (and correlate) the variable parameters such as load capacity, porosity, composition, hydrodynamic film

thickness, oil quality, etc., which are involved in the design of porous bearings. In addition, the effect of the running temperature on these parameters should also be studied. The debris created in the running-in process has to be separately considered. The advantages of an initially smoother surface should also be studied.

Finally, the realistic situation of a porous journal bearing should be employed in the same interferometry tests. This can be done by using a glass shaft with an image correction lens inserted into a window in the wall of the bearing opposite the loaded region.

APPENDIX I

CLASSICAL THEORY OF LUBRICATION OF POROUS METAL BEARINGS

Nomenclature

c	Radial clearance in journal bearing
e	Eccentricity
h	Film Thickness
H	Wall thickness
L	Length of journal bearing
p	Pressure
U	Surface velocity in x direction
u	Particle velocity in x direction
v	Particle velocity in y direction
w	Particle velocity in z direction
x	Coordinate in direction of motion
y	Verticle coordinate through film thickness
z	Coordinate perpendicular to direction of motion
ε	Eccentricity ratio = e/c
η	Absolute viscosity
Θ	Angular coordinate from max. film thickness
Φ	Permeability
Ψ	Permeability parameter = $\frac{H\Phi}{c^3}$

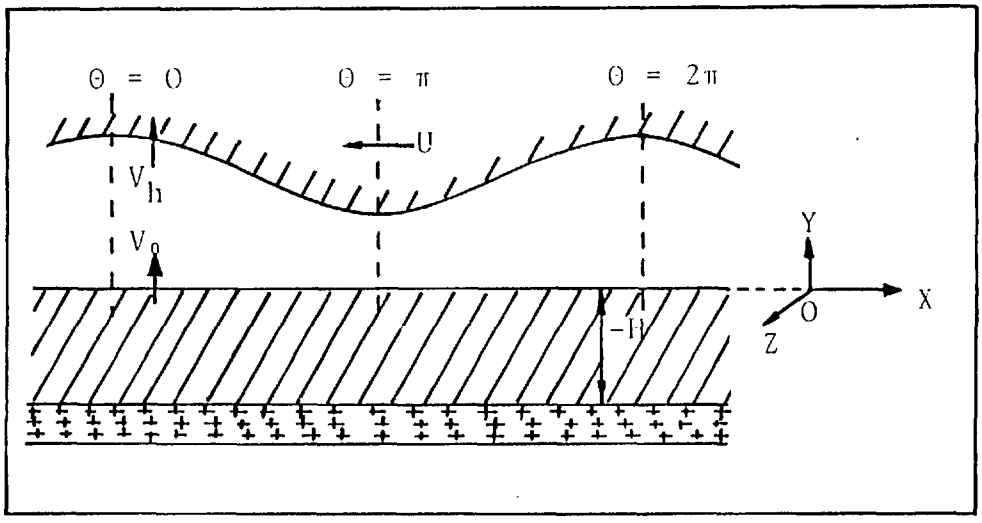

Fig. A.1.1 Geometry of Shaft and Sintered Bush opened up.

Reynolds equation in three dimensions is:

$$\frac{\partial}{\partial x}\left(h^3\frac{\partial p}{\partial x}\right) + \frac{\partial}{\partial z}\left(h^3\frac{\partial p}{\partial z}\right) = 6\eta\left[U\frac{dh}{dx} + 2(V_o - V_h)\right] \quad \ldots\ldots\ldots \text{(A.1.1)}$$

Where V_o and V_h are the y velocity components at $y = 0$ and $y = h$, respectively (Fig. A.1.1).

For a solid shaft $V_h = 0$; while V_o is governed by Darcy's law:

$$V_o = -\frac{\Phi}{\eta}\left(\frac{\partial p}{\partial y}\right)_o \quad \ldots\ldots\ldots \text{(A.1.2)}$$

The continuity of flow in the porous matrix requires:

$$\frac{\partial u}{\partial x} + \frac{\partial v}{\partial y} + \frac{\partial w}{\partial z} = 0 \qquad \text{..... (A.1.3)}$$

Again u,v,w are governed by Darcy's law:

$$u = -\frac{\partial p}{\partial x}\frac{\Phi}{\eta}$$

$$v = -\frac{\partial p}{\partial y}\frac{\Phi}{\eta}$$

$$w = -\frac{\partial p}{\partial z}\frac{\Phi}{\eta} \qquad \text{..... (A.1.4)}$$

Combining Eg. A.1.3 and Eq. A.1.4, we have,

$$-\frac{\Phi}{\eta}\left(\frac{\partial^2 p}{\partial x^2} + \frac{\partial^2 p}{\partial y^2} + \frac{\partial^2 p}{\partial z^2}\right) = 0 \qquad \text{..... (A.1.5)}$$

This is a Laplace equation, the solution of which gives the value of $(\frac{\partial p}{\partial y})_0$ in Eq. A.1.2.

The short bearing assumption of Dubois[12] is

$$\frac{\partial p}{\partial z} >> \frac{\partial p}{\partial x} \qquad \text{..... (A.1.6)}$$

Substituting Eq. A.1.2 and A.1.6 into A.1.1 gives

$$h^3\frac{\partial^2 p}{\partial z^2} = 6U\eta\frac{dh}{dx} + 12\frac{\Phi}{\eta}\left(\frac{\partial p}{\partial y}\right)_0 \qquad \text{..... (A.1.7)}$$

This leads to a parabolic pressure distribution in the z direction, which has the form

$$\frac{\partial^2 p}{\partial z^2} = k_1 \qquad \text{..... (A.1.8)}$$

where k_1 = constant.

Also from Eq. A.1.5 and A.1.6:

$$\frac{\partial^2 p}{\partial z^2} + \frac{\partial^2 p}{\partial y^2} = 0$$

Therefore $$\frac{\partial^2 p}{\partial y^2} = -\frac{\partial^2 p}{\partial z^2} = -k_1 \qquad \text{..... (A.1.9)}$$

so that $$\frac{\partial p}{\partial y} = -k_1 y + k_2$$

The boundary condition for this equation is:

$\frac{\partial p}{\partial y} = 0$ at $y = -H$ where the porous wall is in direct contact with the solid housing.

Thus $$\frac{\partial p}{\partial y} = -k_1(y+H) = -\frac{\partial^2 p}{\partial z^2}(y+H) \qquad \text{..... (A.1.10)}$$

and

$$\left(\frac{\partial p}{\partial y}\right)_0 = -\frac{\partial^2 p}{\partial z^2} H \qquad \text{..... (A.1.11)}$$

Combining A.1.7 and A.1.11 gives

$$h^3\frac{\partial^2 p}{\partial z^2} = 6U\eta\frac{dh}{dx} - 12\Phi H\frac{\partial^2 p}{\partial z^2}$$

or

$$\frac{\partial^2 p}{\partial z^2} = \frac{6U\eta\frac{dh}{dx}}{(h^3+12\Phi H)} \qquad \text{..... (A.1.12)}$$

Integrating this twice, using the boundary conditions $p = 0$ at $z = \pm\frac{L}{2}$ and $\frac{\partial p}{\partial z} = 0$ at $z = 0$ leads to

$$p = \frac{3U\eta\frac{dh}{dx}}{h^3 + 12\Phi H}\left(z^2 - \frac{L^2}{4}\right) \qquad \text{..... (A.1.13)}$$

To a first approximation the film shape in a journal bearing is $h = c(1 + \varepsilon\text{Cos }\Theta)$ where $\Theta = \frac{x}{R}$ and R is the reduced radius. Substituting this into Eq. A.1.13, and defining $\Psi = \frac{H\Phi}{c^3}$, gives

$$p = \frac{3U\eta\varepsilon \text{ Sin } \Theta}{Rc^2[(1 + \varepsilon \text{ Cos}\Theta)^3 + 12\Psi]}\left(\frac{L^2}{4} - z^2\right)$$

This is the pressure distribution for a narrow porous journal bearing.

APPENDIX II

ROUGH SURFACE INTERFEROMETRY

Nomenclature

A_r Surface area

H Central film thickness of EHL

h Height of local asperities measured from the mean plane of the surface

I Intensity of light

m Integer

n Refractive index of oil

V Fringes visibility

δ Optical path length

σ rms roughness of the bearing

λ Wavelength of light

In their studies of EHL of rough surfaces using optical interferometry, Wedeven[93] and Jackson[94] noticed that as the roughness of the ball bearing increased the interference fringes became broader and fainter until a rms roughness of 2.4μin was reached at which the fringes could not be distinguished at all. This phenomenon is analysed below and the result closely agrees with their observation.

Consider a steel ball of roughness σ which is running against a coated glass disk, as shown in Fig. A.2.1. For

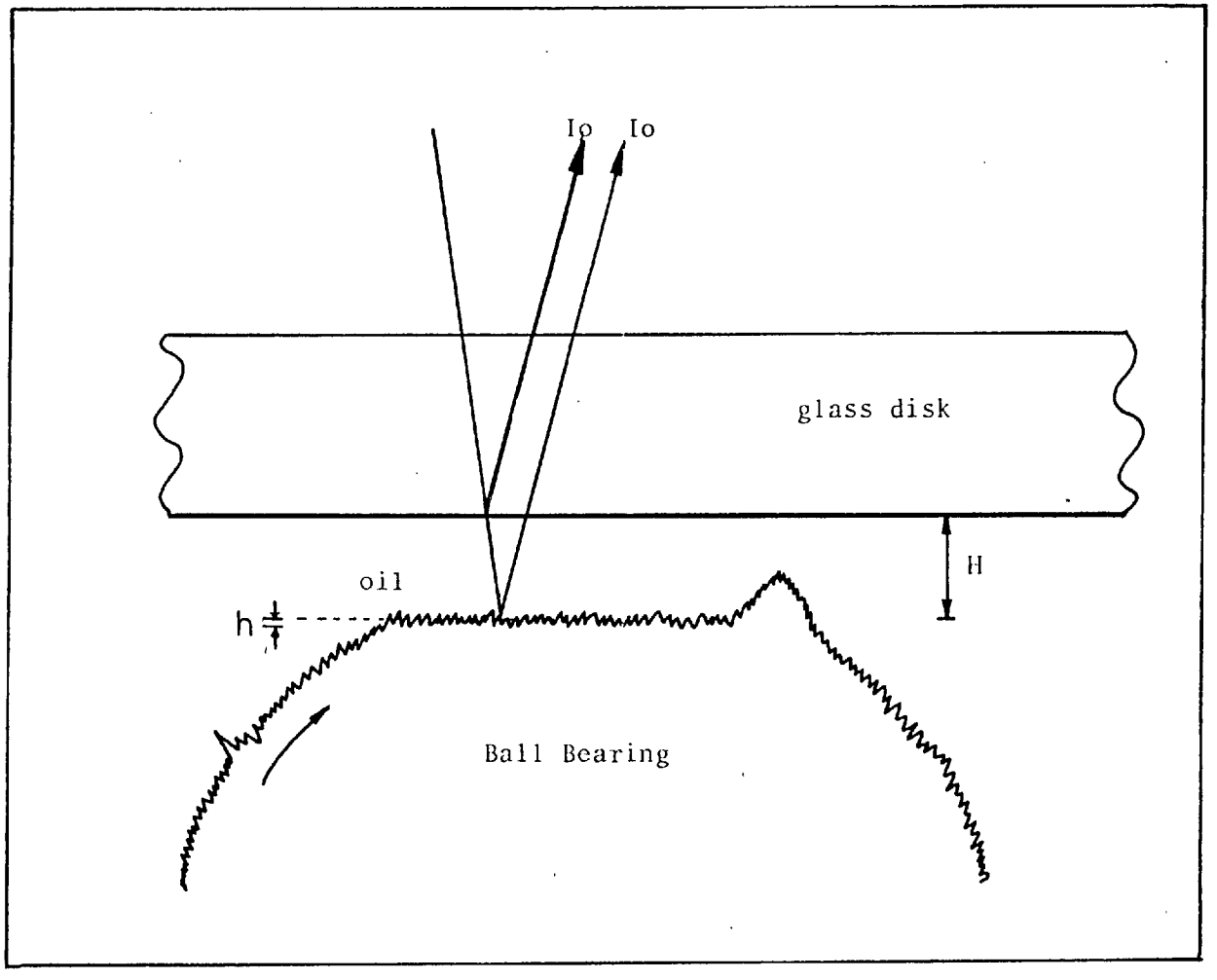

Fig.A2.1. Optical EHL of rough surface.

simplicity consider the ideal cases of two beam interference in which the intensities of the beams are equal and that the light is monochromatic. From the theory of interference[55], the resulting intensity at a particular point of the surface is given by

$$I' = 4I_0 \cos^2 \frac{\delta}{2} \qquad \text{..... (A.2.1)}$$

where $\delta = \frac{4\pi}{\lambda} n(H+h)$ ..... (A.2.2)

On the other hand the fraction of area at a given height 'h' above and below the mean plane is[95]:

$$A_r = 1 - \frac{1}{\sqrt{2\pi}} \int_{-\infty}^{t} e^{-\frac{s^2}{2}} ds \qquad \text{..... (A.2.3)}$$

where $t = \frac{h}{\sigma}$ ..... (A.2.4)

Thus the infinitismal area at a certain height h is:

$$\Delta A_r = \frac{-1}{\sqrt{2\pi}} e^{-t^2/2} \Delta t \qquad \text{.....(A.2.5)}$$

Assuming the amount of light reflected from a certain level of the rough surface is proportional to its area, we have, from Eq. A.2.1 and Eq. A.2.5,

$$\Delta I = 4I_0 \cos^2 \frac{\delta}{2} \cdot \Delta A_r \qquad \text{..... (A.2.6)}$$

If the rotating speed of the ball is fast enough, all that can be observed is the sum of the intensities corresponding to the infinitismal areas distributed over the bearing surface, that is

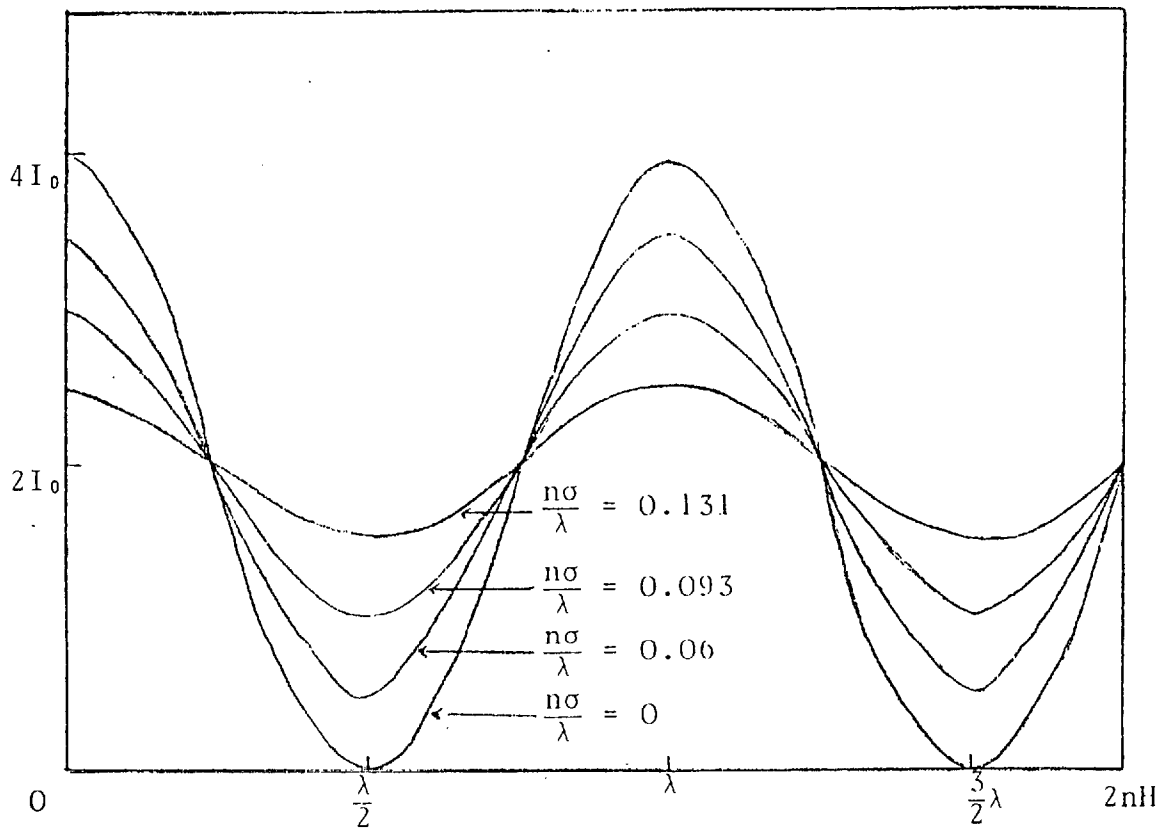

Fig.A.2.2. Intensity versus Film Thickness

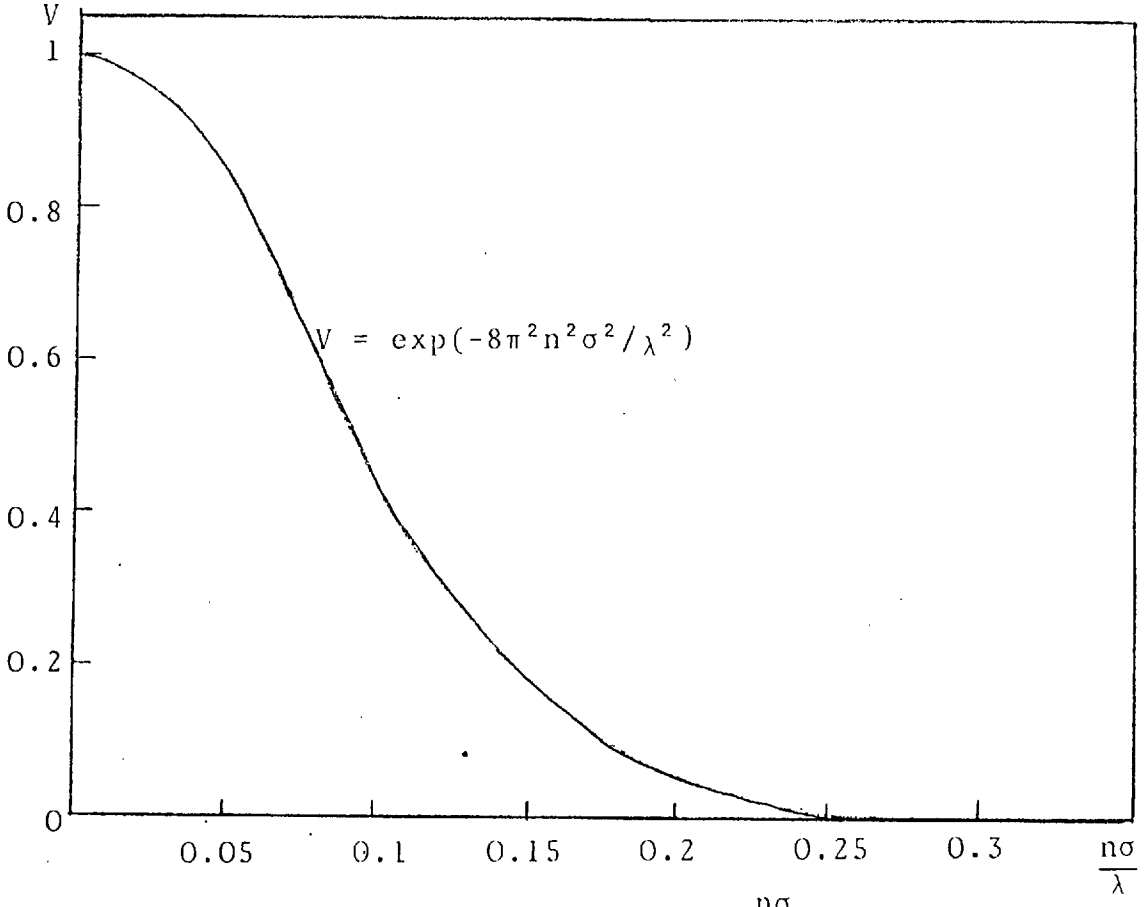

Fig.A.2.3 Visibility versus $\frac{n\sigma}{\lambda}$

$$I_{total} = \int \Delta I$$

$$= \frac{4I_0}{\sqrt{2\pi}} \int_{-\infty}^{\infty} e^{-t^2/2} \cos^2 \frac{\delta}{2}\, dt$$

$$= 2I_0 (1 + e^{-8\pi^2 n^2 \sigma^2/\lambda^2} \cos \frac{4\pi}{\lambda} nH) \qquad \ldots\ldots\ldots \text{(A.2.7)}$$

By varying the value of H, bright and dark fringes can be obtained (Fig.A.2.2). I_{total} becomes maximum and minimum when 2nH is equal to $m\lambda$ and $(m + \frac{1}{2})\lambda$, respectively. Therefore

$$I_{max} = 2I_0 (1 + e^{-8\pi^2 n^2 \sigma^2/\lambda^2}) \qquad \ldots\ldots\ldots\ldots \text{(A.2.8)}$$

$$I_{min} = 2I_0 (1 - e^{-8\pi^2 n^2 \sigma^2/\lambda^2}) \qquad \ldots\ldots\ldots\ldots \text{(A.2.9)}$$

The visibility is:

$$V = \frac{I_{max} - I_{min}}{I_{max} + I_{min}} = e^{-8\pi^2 n^2 \sigma^2/\lambda^2} \qquad \ldots\ldots\ldots\ldots \text{(A.2.10)}$$

The value of V versus $\frac{n\sigma}{\lambda}$ is plotted in Fig. A.2.3. It is seen that the visibility becomes very small when $\frac{n\sigma}{\lambda}$ is larger than 0.15. For example, if a yellow light source (λ= 0.59μ) is used and n is equal to 1.5, the roughness of the ball which can still provide distinguishable fringes is limited to less than 0.059μ (2.4μin), as has been found by Wedeven and Jackson.

Eq. A.2.10 can be extended further to determine the surface roughness of the bearing. This is done by measuring the visibility at two different wavelengths, using a photo-detector:

$$V_1 = e^{-8\pi^2 n^2 \sigma^2 / \lambda_1^2}$$

$$V_2 = e^{-8\pi^2 n^2 \sigma^2 / \lambda_2^2}$$

Therefore

$$\sigma^2 = \frac{1}{8\pi^2 n^2}\left(\frac{1}{\lambda_2{}^2} - \frac{1}{\lambda_1{}^2}\right) \ln \frac{V_1}{V_2} \qquad \ldots\ldots\ldots\ldots \text{(A.2.11)}$$

Thus the rms roughness of the bearing can be obtained.

REFERENCES

1. Tsukerman, S.A.
"Powder Metallurgy"
Pergamon, London (1965)

2. Roberts, A.G.
"The Role of Tin in the boundary lubrication of bronze"
Ph.D. Thesis, London University (1974)

3. Morgan, V.T.
"Permeability of Porous Metals"
Symposium sur la Metallurgie des Poudres, Paris (June 1964), La Societe Francaise de Metallurgie pages 419 to 430 (In English)

4. Scott, J.J.
"Selection of lubricated oils for porous bronze bearings"
Progr. Powder Metal (1963), 19, P.127

5. Bowden, F.P. and Tabor, D.
"The friction and lubrication of solids"
Oxford University Press, Oxford, London (1950)

6. Reynolds, O.
"On the theory of lubrication and its application to Mr. Beauchamp Tower's experiment including an experimental determination of the viscosity of olive oil"
Phil.Trans. (1886), 177(i), P.157

7. Beauchamp Tower

"1st Report on Friction Experiments"

Proc.Inst.Mech.Eng. (Nov. 1883), P.632

"Second Report" ibid (1885), P.58.

"3rd Report" ibid (1888) P.173

"4th Report" ibid (1891), P.111.

8. Sommerfeld, A.

"Zur hydrodynamischen Theorie der Schmiermittelreibung"

Zeits. f. Math. U. Phys. (1904), 40, P.97

9. Christopherson, D.G.

"A new mathematical method for the solution of film lubrication problems."

Proc.Inst.Mech.Eng. (1941), 146, P.126

10. Cameron, A. and Wood, Mrs. W.L.

"The full journal bearing"

Proc.Inst.Mech.Eng. (1949), 161, P.59

11. Morgan, V.T. and Cameron, A.

"Mechanism of lubrication in porous metal bearings"

Conference on lubrication and wear, Institution of Mechanical Engineers (1957), London, P.151.

12. Ocvirk, F.W. and Dubois, G.B.

"Analytical derivation and short bearing approximation for full journal bearings"

N.A.C.A. Report (1953), P.1157.

13. Cameron, A., Morgan, V.T. and Stainsby, A.E.

"Critical conditions for hydrodynamic lubrication of porous metal bearings"

Proc. Inst.Mech.Eng. (1962), 176, P.761

14. Rouleau, W.T.
"Hydrodynamic lubrication of Narrow Press Fitted Porous Metal bearings"
J. of Basic Eng. (1963), P.123

15. Rhodes, C.A. and Rouleau, W.T.
"Hydrodynamic lubrication of narrow porous bearings with sealed ends"
Wear (1965), 8, P.474

16. Shir, C.C. and Joseph, D.D.
"Lubrication of a porous bearing - Reynolds Solutions"
J. of Appl. Mech. (1966), P.761.

17. Murti, P.R.K.
"Lubrication of narrow porous bearings with arbitrary wall thickness"
J. Lub. Tech. (1973), Paper No. 73-Lub-G

18. Carson, R.W.
"A special reveiw of all self lubricated bearings"
Product Engineering, April 13 (1964), P.79

19. Morgan, V.T.
"Porous Metal Bearings"
Trilology (1969), 2, P.107

20. Murti, P.R.K.
"Lubrication of narrow porous bearings with arbitrary wall thickness"
Trans. ASME, J. of Lub. Tech. (1973), P.511

21. Singh, D.V.
"Stability and relative stability of porous journal bearing system with axes skewed"
Trans. ASME, J.Lub. Tech. (1974), P. 621

22. Chang-Yi Wang

"Heat generated by Couette flow with porous wall"

Trans. ASME. J. Lub. Tech. (1973), P. 538

23. Reason, B.R.

"A numerical solution for the hydrodynamic lubrication of finite porous journal bearings"

Proc. I. Mech. Eng. (1973), 187, P.71

24. Cusano, C.

"Lubrication of porous journal bearings"

J. Lub. Tech. (1972), 94(1), P.69

25. Cusano, C. and Phenlan, R.M.

"Experimental investigation of porous bronze bearings"

Trans. ASME. J. Lub. Tech. (1973), P.173

26. Capone, E.

"Lubrication of Axially undefined porous bearings"

Wear (1970), 15, P.157

27. Rhodes, C.A.

"Hydrodynamic Lubrication of Partial Porous Metal Bearings"

J. Basic Eng. Trans. ASME. (1966), P.53.

28. Shir, C.C.

"Lubrication of a porous bearing - Reynolds solution"

J. Appl. Mech. (1966), P.761

29. Joseph, D.D., and others

"Lubrication of a porous bearing - Stroke's Solution"

J. Appl. Mech. Trans. ASME, (1966), P.753

30. Sneck, H.J.
"A mathematical analogy for determination of porous metal bearings' performance and characteristics"
J. Lub. Tech. (1967), 89, P.222

31. Joseph, D.D. and Tao, L.N.
"The effect of permeability on the slow motion of a porous sphere in a viscous liquid"
ZAMM. (1964), 44, P.361

32. Beaver, G.S. and Joseph, D.D.
"Boundary conditions at a naturally permeability Wall"
J. Fluid Mech. (1967), P. 197

33. Murti, P.R.K.
"Effect of slip flow in narrow porous bearings"
Trans. ASME., J. of Lub.Tech. (1973), P.518

34. Rouleau, W.T. and Stainer, L.T.
"Hydrodynamic porous journal bearing; Part I - Finite full bearing"
J. Lub. Tech. (1974), 96, P. 346

35. Murti, P.R.K.
"Squeeze film behaviour in porous circular disks"
Trans. ASME. J. Lub. Tech. (1974), P.206

36. Murti, P.R.K.
"Squeeze films in full porous metal bearings"
Wear (1974), 30, P.257

37. Murti, P.R.K.
"Dynamic behaviour of pure squeeze film in narrow porous bearings"
Trans. ASME. J. Lub. Tech. (1974), P.360

38. Hai Wu
"Effect of velocity slip on the squeeze film between porous rectangular plate"
Wear (1972), 20, P.67.

39. Youssef, H. and Eudier, M
"Production and Properties of a new porous bearing"
Powder Metallurgy Conf. (1965) Paper 5.3

40. Marshall, P.R. and Morgan, V.T.
"Review of porous metal bearing developments"
Proc.Instn. Mech. Engrs. (1965-66), Paper 7, P. 154

41. Cusano, C
"Analytical investigation of an infinitely long, two layer porous bearing"
Wear (1972), 22, P.59

42. Morgan, V.T.
"Hydrodynamic porous metal bearings"
Lubrication Engineering (1964), P.448

43. Morgan, V.T.
Triliology (1970), 3, P.111

44. Morgan, V.T.
Private Communications, (1974-77).

45, Hardy, W.B.
"Collected scientific papers of Sir William Bate Hardy"
Cambridge University Press. London (1936), P.609

46. Skinner, S.
"On the occurrence of cavitation in lubrication"
Phil. Mag. (1904), 7, P.329

47. Stone, W.

"A proposed method for solving some problems in lubrication"

Commonwealth Engineer, Australia (1921), P.115

48. Kirk, M.T.

"Hydrodynamic lubrication of perspex"

Nature (1962), 194, P.965.

49. Archard, J.F. and Kirk, M.T.

"Lubrication at point contact"

Proc. Roy. Soc. A (1961), 261, P.532

50. Gohar, R. and Cameron, A

"Theoretical and experimental studies of the oil film in lubricated point contact"

Proc. Roy. Soc. A (1966), 291, P.520

51. Ettles, C. and Cameron, A

"The action of the parallel surface thrust bearings"

Proc. 4th Lubrication and Wear Conference, I.M.E. Scheveningen 180, Pt. 3k, Paper 17, P.61, (1966).

52. Foord, C.A., Wedeven, L.D., Westlake, F.J. and Cameron, A.

"Optical elastohydrodynamics"

Proc. Inst. Mech. Eng. (1969-70) Vol. 184 I

53. Wedeven, L.D., Evans, D. and Cameron,A.

"Optical analysis of ball bearing starvation"

ASLE/ASME Joint Lubrication Conference, Cincinnati, Ohio (Oct. 1970), ASME Paper No. 70-Lub-19.

54. Wymer, D.G. and Cameron, A.

"Elastohydrodynamic lubrication of a line contact, I: Optical analysis of a roller bearing"

Inst. Mech. Engrs. London (1974).

55. Born, M. and Wolf, E.
"Principle of Optics"
Fourth Edition, (1970)

56. Francon, M.
"Optical Interferometry"
Academic Press, New York (1966)

57. Richardson, E.G.
"Dynamics of real fluid"
Edward Arnold Ltd., London (1961), 2nd Edition.

58. Hall, J.W.
"An effect of air content on the occurrence of cavitation"
J. Basic. Eng. (1960), P.941

59. Ward, C.A. and others
"On the thermodynamics of nucleation in weak gas-liquid solution"
Trans. ASME. J. Basic Eng. (1970), P.695

60. Hall, J.W. and Slicenus, G.F.W.
"Scale effect on cavitation"
J. Basic. Eng. (1961), P.365

61. Smith, R.A.
"A photographic study of the effect of an air bubble on the growth and collapse of a vapour bubble near a surface"
J. Basic Eng. (1972), P.933

62. Syamala Rao, B.C. and others
"Cavitation erosion studies with venturi and rotating disk in water"
J. Basic Eng. (1970), P.563

63. Kling, L.L.
"Photographic study of spark induced cavitation bubble collapse"
J. Basic Engr. (1972), P.825

64. Thiruvengadam, A.
"A united theory of cavitation damage."
J. Basic Engr. (1963), P.365

65. Plesset, M.S.
"Effect of explosion time on cavitation damage"
J. Basic Eng. (1966), P.697

66. Hall, J.W.
"Cavitation hysteresis"
J. Basic Eng. (1966), P.199

67. Cameron, A.
"Principle of lubrication"
Longmans (1966).

68. Hall, J.W.
"The inception of cavitation on isolated surface irregularities"
J. Basic Eng. (1960), P.163

69. Dowson, D and Higginson, G.R.
"A numerical solution to the EHD problem"
J. Mech. Eng. Sci. (1959), 1, P.6

70. Dowson, D. and Higginson, G.R.
"The effects of material properties on the lubrication of elastic rollers"
J. Mech. Eng. Sci. (1960), 2, P.188.

71. Archard, G.D., Geir, F.C. and Airst, W.
"The EHL of roller"
Proc. Roy. Soc. A (1961), 262, P.57.

72. Paul, G.
"Optical determination of the high pressure refractive index and viscosity of liquids entrapped in point contact"
Ph.D. Thesis, London University (1971)

73. Ettles, C.
"The development of a generalized computer analysis for sector shaped tilting pad thrust bearings"
Trans. ASLE, (1975), Vol.9, 2, P. 153.

74. Spike, H.
"Physical and Chemical Adsorption in Boundary Lubrication"
Ph.D. Thesis, London University, (1972).

75. Salama, M.Z.
"The effect of macro-roughness on the performance of parallel thrust bearings"
I.M.E. Proc. (1950), 163, P.147.

76. Davies, M.
"The generation of pressure between rough, fluid lubricated moving deformable surfaces"
Lubr. Eng. 19 (1963), P.246

77. Burton, R.
"Effect of two dimensional sinusoidal roughness on the load support characteristics of a lubricant film"
J. Basic Eng. (1963), 84D, P.258

78. Hamilton, D.B. and others
"A theory of lubrication by micro-irregularities"
Trans. ASME., J. Lub. Tech. (1966), 88, P.177

79. Anno, J.N. and others

"Micro-asperity lubrication"

J. Lub. Tech. (1968), P.251.

80. Harrison, W.J.

"The hydrodynamic theory of the lubrication of a cylindrical bearing under variable load, and a pivot bearing"

Trans. Cambridge Philos. Soc., (1919), 72, P.373

81. Lewicki, W.

"Theory of hydrodynamic lubrication in parallel sliding"

The Engineer, (1955),200, P.939

82. Tønder, K.

"Parallel surfaces lubricated by a bubbly oil"

Wear, (1975), 35(1), P.23

83. Fogg, A.

"Fluid film lubrication of parallel surface thrust bearings"

Proc. Instl. Mech.Eng. (1946), 155, P.49

84. Cameron, A.

"Hydrodynamic lubrication of rotating discs in pure sliding. A new type of oil film formation"

J. Inst. Pet. (1951),37, P.471

85. Zienkiewics, O.C.

"Temperature distribution within the lubricating films between parallel bearing surfaces and its effects on the pressure developed"

Inst. Mech. Eng. Conf. Lubr. (1957), P.135

86. Dowson, D.
"A generalised Reynolds equation for fluid film lubrication"
Inst.Mech.Sci. (1962), 4, P.159

87. Dowson, D. and Hudson, J.D.
"The hydrodynamic analysis of the infinite slider bearing, Part II, The parallel surface bearing"
Lubr. Wear Conv., I.Mech. Eng. (1963), P.42

88. Neal, P.B.
"Film lubrication of plane-faces thrust pads"
Lubr. Wear Conv., I.Mech. Eng. (1963), P.69

89. Ettles, C. and Cameron, A.
"Thermal and elastic distortion in thrust bearings"
Proc. Conf.Lub. Wear ZME. Paper 7 (1963).

90. Robinson, C.J.
"Thermal and Elastic distortion in thrust bearings"
Ph.D. Thesis, London University, (1971)

91. Taniguchi, S. and Ettles, C.
"A thermo-elastic analysis of the parallel surface thrust washer"
Trans. ASLE Paper 74LC-5C-2

92. Nau, B.S.
"Hydrodynamics of face seal films"
British Hydromechanics Research Association,
Second International Conference of Fluid Sealing,
April, 1964.

93. Wedeven, L.D.
"Optical measurement in elastohydrodynamic rolling contact bearings"
Ph.D. Thesis, London University, (1970).

94. Jackson, A.J.

"Optical elastohydrodynamics of rough surfaces"

Ph.D. Thesis, London University, (1973).

95. Thomas, T.

(Teeside Polytechnic), Private Communication,(1975)